

RICE UNIVERSITY

Advancing Higher Level Control of Nanoparticle Assemblies Through Ligands

By

David Michael Marolf

A THESIS SUBMITTED  
IN PARTIAL FULFILLMENT OF THE  
REQUIREMENTS FOR THE DEGREE

Doctor of Philosophy

APPROVED, THESIS COMMITTEE



Matthew Jones (Chair)

Assistant Professor of Chemistry  
Assistant Professor of Materials Science and  
NanoEngineering



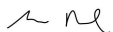
Peter Rossy

Harry C. & Olga K. Wiess Chair in Natural Sciences  
Professor of Chemistry  
Professor of Chemical & Biomolecular Engineering

  
Angel Marti (Aug 9, 2023 20:31 PDT)

Angel Marti-Arbona

Professor of Chemistry  
Professor of Bioengineering  
Professor of Materials Science and NanoEngineering  
Chair, Department of Chemistry



Sibani Lisa Biswal

William M. McCardell Professor in Chemical Engineering  
Professor of Materials Science and NanoEngineering  
Senior Associate Dean of Engineering

HOUSTON, TEXAS

August 2023

## ABSTRACT

### **Advancing Higher Level Control of Nanoparticle Assemblies Through Ligands**

by

**David Michael Marolf**

The nanoscale size regime is full of potential for the study and development of new functional materials. Many biological materials exist on the nanoscale and can assemble into a variety of complex machinery capable of performing the functions necessary for life to continue. Human-made materials are still far behind what exists naturally, however, over the past few decades, nanoparticles have emerged as a synthetic class of material with intriguing properties making them capable of a large variety of potential applications. One such property is their ability to self-assemble under certain conditions, potentially paving the way to better mimic the high functionality of biological materials. In this thesis, I present research into self-assembling systems of particles that will bring the community closer to true biomimetic materials, primarily through careful use and control of the ligands at the nanoparticle surface.

In chapter 1, I detail how ligands affect nanoparticles on multiple levels. First, I discuss how ligands are crucial for the synthesis and growth of a variety of nanoparticles of various compositions and morphologies. Then, I detail how ligands are used to impart functionality to nanoparticles in a variety of different applications.

Finally, I discuss how ligands are used to assemble particles, paying special attention to how ligands can be used to assemble nanoparticles in more complex ways such as “lifelike” dissipative self-assembly. In chapter 2, I discuss my findings applying the community’s understanding of functionalization to the functionalization of ultrathin gold nanowires, the highest aspect ratio gold nanoparticle morphology currently known. Through functionalization with a stimuli-sensitive ligand, dynamic systems of nanowires that assemble and disassemble in response to specific stimuli can be obtained. These nanowires can also be assembled into macroscopic fibers, demonstrating preliminary work that could be continued to develop fibers of nanowires as functional materials. In chapter 3, I present my work exploring the study of DNA-functionalized gold nanoprisms and their sharp transitions between an assembled and disassembled state. I explore the origins of these sharp transitions that cannot be explained by contemporary models of similar DNA-functionalized nanoparticles. Finally, in chapter 4, I discuss the challenges the community faces developing synthetic, out-of-equilibrium, dissipative nanoscale self-assembling systems. To characterize such systems even if they can be successfully designed and synthesized, careful consideration must be given to the spatial and temporal resolution available with current analytical techniques along with the inherent advantages and drawbacks of these techniques. Furthermore, as spatial and temporal resolution continues to be improved, the amount of raw data produced per experiment increases at a high rate necessitating the adoption and development of more advanced data analysis techniques.

This thesis furthers the field of self-assembly, such that future researchers will be closer to developing synthetic systems with high degrees of complexity capable of precise function that can be targeted towards a variety of applications.

# Acknowledgments

When I started my PhD, I knew to expect it to be a time of educational growth for me, but I hadn't correctly anticipated how difficult and at times painful that growth process might be and how much grad school might push me to grow more than just as a scientist. And to be fair to my younger self, I don't think anyone could have anticipated the timing of my PhD to coincide with so much external chaos and upheaval. During my tenure, I have endured a global pandemic, a handful of hurricanes (including Hurricane Harvey during my first summer at Rice), nationwide police brutality protests that were often responded to with even more violence, multiple extremely troubling political shifts in this country (including the overturning of *Roe v. Wade*), and probably at least a dozen more "historic" events that, quite frankly, sucked. All of that is too much for any person to deal with by themselves, and that is why I am so eternally grateful that I didn't go through all that alone and instead had a myriad of people in my life to help and support me. It's now my privilege to highlight as many of those people as I can and thank them dearly for their kindness and support. (I also apologize if I have neglected anyone due to the frazzled state of my brain as I attempt to write up six years' worth of work into one document. If I did, please know that your contributions were still deeply appreciated!)

I would like to start by thanking my advisor, Matt Jones. He remains the most brilliant scientist I have ever worked with and an excellent teacher. However, I don't really want to spend the time highlighting those particular contributions to my PhD work as, to a certain extent, that is to be expected of any worthwhile PI. I instead

would like to thank him for his contributions that I truly believe went above and beyond his professional obligations. During my very storied time at Rice, there were many times when the situation I found myself in was deeply uncertain, and Matt was the anchor that held me in place and allowed me to continue my work as best as I was able. I almost left the program during the pandemic as I didn't have faith in Rice's systems at place to control the pandemic, but I stayed because I trusted Matt. And I'm happy to report that trust was well placed. In a separate time when Rice slashed my pay in half without warning (long story), Matt not only offered whatever professional clout he had to help me fix that issue with Rice but also offered to personally cover the rest of my stipend to make sure I could afford living expenses while this situation was being fixed. Thankfully, it never came to that, but it helped me immensely to have that level of support during a time of increased inflation where I truly could not afford my living expenses on half an income. I always tell new grad students to find an advisor that won't just help you scientifically but is also a good person who you can trust during this formative and often vulnerable time in your life. I truly don't know how my life would have looked in another lab and I am extremely grateful that I was lucky enough to find myself in Matt Jones' lab all those years ago.

Speaking of joining the Jones lab, I also want to thank all my labmates, past and present, who have been so excellent both as collaborators but also even more as friends. The work was much easier sharing it with you all. I've enjoyed all the long discussions (sometimes when we should have been working; sorry Matt!) and fun times we've had and I am excited to see where we all go in the future. I would like to give a special shoutout to my friend and partner on the nanowires project, Theo

Gerrard-Anderson. I met Theo seven years ago as we worked as summer interns in a lab in Mainz, Germany and I never imagined that would be the start of such a long friendship. It was an honor to work together on the nanowires and I am grateful at how well we complemented each other in our work styles. We joked that we took turns carrying the project when the other was burnt out or dealing with various life crises, and while I can only say that I hope I was able to carry Theo when he was down, he certainly carried me. I think the memories I will carry most closely from working on our project together will be our complex and somewhat deranged bits we would fall into inevitably during labwork or meetings. May Yawgroth devour you last, brother.

I would now like to thank my family, my longest-running supporters. I'm not sure any of us were quite prepared what my time in grad school would look like, but I am very grateful to have always known that you were behind me supporting me. Whether that support was emotional (as you listened to me vent many, many times about failed experiments) or financial (as you paid for meals when we were together and fed this hungry, poor grad student), it was well appreciated. During the uncertainty of these years, it was unfathomably helpful to have a collection of supporters who always had my back no matter what. I will say my young nephew, Axel Marolf, born on January 15, 2023, didn't do as much of the heavy lifting as the rest of my family, but considering he is still working hard at developing object permanence, I will give him a pass this time, but am still expecting a major turnaround in the near future.

I now want to thank the other members of the Sorority: Arzeena Ali, Sarah Hulan, and Rachael Kress. When we all met on visitation weekend, I didn't recognize that I was meeting some of the dearest friends of my life. We've shared so many laughs, tears, and impotent screams of rage, and I can't imagine better people to have been through it with. Our nights spent eating Aga's, or going to the Renn Faire, or playing Castle Panic will be some of my fondest grad school memories.

I now would like to thank three more people who experienced a bit of the grad school chaos before me and so were instrumental in helping guide me through it: Logan Bishop, Thomas Heiderscheit, and Christian Jacobson. I owe you many drinks for all the time you spent talking me off ledges especially during those early years. I'm not sure I would have made it through my first CHEM 600 or my QE without you all there constantly reminding me it was going to be fine. I also need to thank you all for ruining my productivity by introducing me to D&D and a myriad of other board games and video games. Having that consistent escape in my life was crucial to my survival. And above all else... Thanks for the Glorious Combat, Family. Rock and Stone.

Jessie, James, and Sean are three of my oldest friends and I am grateful that they put up with all my grad school concerns for six years. I know none of you have personal experience with grad school currently, but you have all been such excellent empathetic listeners and supporters throughout the whole thing. You've always been ready to celebrate with me, hype up my accomplishments, and be shoulders to cry on during less pleasant times. And I also am grateful that you were willing to be my first guinea pigs as I learned to DM! Escaping into made up worlds with you three has been



an immense amount of fun and a well-needed break from a sometimes difficult reality and I look forward to continuing that for many more years to come.

I would also like to thank all the members of the D&D group I played with at Rice: Theo Gerrard-Anderson, Sarah Hulkan, Rachael Kress, Tim Robertson, Joe Swain, and Zhi Yang. It was an honor to procrastinate with you and watch as you defeated the Cult of Myrkul and the dreaded dragon of Icespire Peak. Completing that campaign with you all is honestly one of the accomplishments I am most proud of during my time at Rice, and I am so grateful to have shared all that time with you.

I have spent a lot of time mentioning how difficult my tenure was, and I would be remiss if I didn't highlight perhaps the group most responsible for getting me through those times: the Rice University Counseling Center. (For my labmates, as a final reminder, it is fully functional in person and over the phone or on Zoom!) Mental health is a common struggle for grad students and I am no exception. The RUCC was instrumental in helping guide me through my anxiety and other mental health struggles to both survive grad school but also to be a better person. In particular, I would like to thank Gabe Ramirez, who I spent around four years working with. You guided me through so much change and struggle in my life, and I honestly believe the wisdom you helped guide me to is the thing I'll hold on to most tightly as I move on to the next stage of my life.

I also owe a lot to some of the best people at Rice, who I think deserve a lot more recognition for the work they put in: the administrative staff and teaching faculty, particularly, Kristi Kincaid, Krista Kobylanskii, Ruxin Feng, Caroline McNeil,

Pam On, and Anita Walker. The work and care you show to the students that cross your paths is one of the best parts of the department.

I have thanked all the humans my frazzled brain can remember to thank but there are still two individuals who need credit, and those are the two cats I have had during grad school. I first would like to thank Alfred, who put in the most on-site hours supporting me. I can't express how helpful it was to come home and have that furball there waiting for me, who was always just happy to see me home and truly couldn't care less about whether or not my experiments worked that day. You got me through the darkest part of the pandemic, Alf, and I wish there was more I could do to thank you. Sadly, Alfred passed away late October 2022, and that was by far the hardest part of my time in grad school. But thankfully, despite having very big shoes to fill, a worthy successor came into my life December of that year. Pippin, you're an absolute psychopath, but you have been instrumental in helping me get through this hard last year. In Alfred's memory and in hope of affording Pippin a cat tree with PhD money, I'm happy to complete this journey.

# Contents

<b>Acknowledgments</b> .....	<b>iv</b>
<b>Contents</b> .....	<b>x</b>
<b>List of Figures</b> .....	<b>xiii</b>
<b>List of Tables</b> .....	<b>xviii</b>
<b>List of Equations</b> .....	<b>xix</b>
<b>Nomenclature</b> .....	<b>xx</b>
<b>Introduction</b> .....	<b>1</b>
1.1. Ligands as Capping Agents .....	2
1.2. Ligands as Growth Directors .....	4
1.3. Ligands for Nanoparticle Functionality .....	7
1.4. Ligands for Self-Assembly.....	10
1.5. Ligands for Dynamic Self-Assembly.....	12
1.6. Ligands for Complex Self-Assembly.....	14
1.7. Conclusion .....	18
<b>Controlling the Assembly State of Ultrathin Gold Nanowires Through Stimuli-Responsive Ligands</b> .....	<b>19</b>
2.1. Introduction.....	19
2.2. Results and Discussion .....	22
2.2.1. AuNW Functionalization with HS(CH <sub>2</sub> ) <sub>11</sub> (EG) <sub>6</sub> OCH <sub>2</sub> COOH .....	22
2.2.2. AuNW Assembly Using Ca <sup>2+</sup> .....	24
2.2.3. AuNW Assembly in Acidic Conditions.....	28
2.2.4. AuNW Fiber Extrusion .....	34
2.3. Conclusion .....	37
2.4. Materials and Methods .....	38
2.4.1. Ultrathin Gold Nanowire Synthesis .....	38
2.4.2. Ultrathin Gold Nanowire Functionalization with HS(CH <sub>2</sub> ) <sub>11</sub> (EG) <sub>6</sub> OCH <sub>2</sub> COOH .....	39
2.4.3. Ultrathin Gold Nanowire Assembly .....	39

2.4.4. Ultrathin Gold Nanowire Fiber Extrusion .....	40
2.4.5. SAXS Measurements.....	40
2.4.6. Materials.....	41
<b>Investigating Thresholding Behavior in Equilibrium and Nonequilibrium Nanoparticle Assemblies .....</b>	<b>42</b>
3.1. Abstract .....	42
3.2. Introduction.....	43
3.3. Background.....	45
3.4. Results and Discussion .....	52
3.5. Methods .....	65
3.5.1. Nanoparticle Synthesis and Purification.....	65
3.5.2. DNA Functionalization .....	66
3.5.3. DNA Assembly.....	67
3.5.4. $T_m$ and FWHM .....	67
3.5.5. van 't Hoff Analysis .....	68
3.6. Conclusion .....	68
<b>Measuring Challenges in Dynamic and Nonequilibrium Nanoscale Systems.....</b>	<b>70</b>
4.1. Abstract .....	70
4.2. Introduction.....	71
4.3. Why Nano? .....	74
4.4. Perspective .....	77
4.5. Techniques .....	78
4.5.1. In Situ Atomic Force Microscopy .....	82
4.5.2. Light Scattering .....	86
4.5.3. Super-Resolution Microscopy.....	89
4.5.4. Liquid-Phase Transmission Electron Microscopy .....	94
4.6. Data Analysis, Deep Learning, and Multiscale Modeling .....	100
4.7. Conclusion .....	105
<b>Conclusion, or There and Back Again .....</b>	<b>107</b>
<b>References .....</b>	<b>110</b>



# List of Figures

**Figure 1.1 Ligands Direct NP Growth.** A schematic showing the same seed particle being driven down two hypothetical growth directions depending on the presence of either a capping agent (ligand) that preferentially binds (100) facets (red) or a capping agent that binds (111) facets. Reprinted with permission from ref. 15. Copyright 2015 American Chemical Society. .... 6

**Figure 1.2 Ligands Control Nanoparticle Catalyst Selectivity.** TEM images of a) 3.5 nm Pt nanoparticles and b) 4.5 nm CoPt<sub>3</sub> nanoparticles used as catalysts for alkyne hydrogenation reactions. c) The percentage of products formed from 4-octyne hydrogenation using unfunctionalized Pt and CoPt<sub>3</sub> nanoparticle catalysts and Pt and CoPt<sub>3</sub> nanoparticles in the presence of 0.13 M 1-octylamine. Reprinted with permission from ref. 26. Copyright 2012 American Chemical Society ..... 9

**Figure 1.3 Surface-Ligand Interactions Cause Patchy Particles.** The titration of carboxylic acid presenting nanodumbbells. The same molecule has a different effective pK<sub>a</sub> when bound to the surface due to the difference in radius of curvature across the particle. Reprinted with permission from ref. 38. Copyright 2013 Nature Publishing Group. .... 12

**Figure 1.4 Stimuli-Responsive Ligands Enable Stimuli-Responsive Assembly.** Schematic demonstrating the assembly of particles through irradiation of UV light and the resultant formation of “nanoflasks” before being disassembled through irradiation of visible light and the release of the resulting product. Reprinted with permission from ref. 44. Copyright 2016 Nature Publishing Group. .... 14

**Figure 1.5 Dissipative Assembly Explores Significantly Different Phase Spaces than Equilibrium and Metastable Assemblies.** a) A schematic showing the consumption of energy used to activate a hypothetical self-assembly process. b) A comparison of the energy landscape of equilibrium states, kinetically trapped or metastable states, and dissipative states. Reprinted with permission from ref. 48. Copyright 2017 Royal Society of Chemistry. .... 16

**Figure 2.1 Nanowire Functionalization.** a) Pictures of the functionalization mixture at different stages. The dark color is due to the presence of nanowires. b) An illustration of the oil-in-water emulsion formed upon mixing the nanowire-containing hexane phase with the ligand-containing aqueous

phase. Presumably, a Pickering emulsion forms with the nanowires resting at the interface before thiol-Au bonds form, ultimately pulling the nanowire into the aqueous phase. c) TEM image of the nanowires as-synthesized. d) TEM image of the nanowires after functionalization. .... 24

**Figure 2.2 Nanowire Assembly Through  $\text{Ca}^{2+}$  Chelation.** a) SAXS spectra of three samples of AuNWs varying  $\text{CaCl}_2$  and pH. Dotted vertical lines are added to guide the eye. b) An illustration of the HCP structure formed from bundled nanowires. The nanowires are viewed from the tips for ease of viewing. c) An illustration of the  $\text{Ca}^{2+}$  chelate linkages between nanowires. .... 28

**Figure 2.3 Nanoparticle Assembly Under Acidic Conditions.** a) SAXS spectra of three samples of AuNWs varying pH through HCl or NaOH addition. b) An illustration of the hydrogen bond linkages between nanowires. c) SAXS spectra of five samples of varying pH through use of buffers. d) An illustration of the possible lamellar structure formed from AuNWs assembled under acidic conditions using buffers. .... 30

**Figure 2.4 The Effect of Salt Concentration on Acidic Assembly, and Reversibility of the Acidic Assembly.** a) SAXS spectra of three samples of AuNWs at pH 2 varying KCl. Dotted vertical lines are added to guide the eye. b) SAXS spectra of AuNWs demonstrating reversibility. AuNWs can be assembled through addition of acid and disassembled through addition of base. This process is reversible upon addition of more acid. .... 32

**Figure 2.5 Macroscopic Fibers Formed From Nanowires.** a) Frames of a video showing the extrusion of fibers into a coagulant bath containing 100 mM HCl and 300 mM NaCl. b) Images of fibers collected from the acidic coagulant bath. c) Frames of a video showing the extrusion of fibers into a coagulant bath containing 100 mM NaOH and 100 mM  $\text{CaCl}_2$ . d) Images of fragments of fibers collected from the  $\text{Ca}^{2+}$ -containing coagulant bath. Larger fibers could not successfully be removed from the bath due to their brittle nature. .... 37

**Figure 3.1 Cooperativity and Multivalency.** a) A model of a cooperative system. b) A model of a multivalent system. c) A model of a cooperative and multivalent system. .... 45

**Figure 3.2 Self-Assembling Prisms through Single-Stranded and Double-Stranded DNA.** a) UV-Vis extinction spectra showing differences in binding with ssDNA and dsDNA-functionalized prisms. Inset: TEM image of a Au nanoprism (scale bar: 50 nm). b) A model demonstrating the flexibility of

ssDNA conformational change before and after binding along with the DNA design. c) A model demonstrating the rigidity of ssDNA on the surface of prisms before and after binding along with the DNA design..... 54

Figure 3.3 Assemblies with ssDNA Yield Sharper Transitions. A bar graph comparing the average FWHM of disassembly for both ssDNA-functionalized prisms and dsDNA-functionalized prisms..... 56

Figure 3.4 Potential Mechanisms Leading to Enhanced Thresholding Behavior of ssDNA-Functionalized Prisms. a) A model illustrating the hypothesis that an array of cations organized to the phosphate backbone of a hybridized sticky end encourages the hybridization of neighboring strands. b) A model illustrating the hypothesis that the formation of intraparticle loops preorganize the DNA such that the formation of sticky end interactions between particles is encouraged..... 57

Figure 3.5 Cation Size Affects the Observed  $T_m$  in Assembled Nanoprisms. Melting curves of ssDNA-functionalized nanoprisms and dsDNA-functionalized prisms utilizing different-sized prisms and cations..... 59

Figure 3.6 van 't Hoff Analyses of Prism Disassembly. . a) An illustration of a van 't Hoff plot. b) The enthalpy of disassembly of various systems of self-assembled DNA-functionalized prisms. determined through van 't Hoff plots. c) The entropy of disassembly of various systems of self-assembled DNA-functionalized prisms. determined through van 't Hoff plots. .... 64

Figure 4.1 The Advantage of Dissipative Processes. a) A simplified, hypothetical energy diagram indicating the difference between global equilibrium, metastable kinetically trapped, and energy-dependent out-of-equilibrium states. In this framework, the out-of-equilibrium state has the unique property of being able to explore a wide range of reaction coordinate space with a relatively small input of energy. (b) Illustration of the difference between passive diffusive behavior of individual nanoparticles and the collective emergent behavior of a hypothetical nanoparticle assembly driven by the input of energy..... 73

Figure 4.2 Understanding How Spatial and Temporal Resolutions of Instrumentation Limit Systems Able to Be Effectively Studied. (a-c) Simulated image of an assembly of 50 nm cubes imaged at (a) 2.5 nm, (b) 20 nm, and (c) 200 nm spatial resolution. (d-f) A simulation of 50 nm cubes assembling at (d) 5 ms, (e) 50 ms, and (f) 500 ms temporal resolution. Three particles of interest



have been labeled (1, 2, and 3) to help track the assembly process. (g) A spatiotemporal map of the single-particle imaging techniques covered in this perspective; data collected from references 162 163 164 165 166 167 168 169 170 171 172 173 174 175 176 177 178 179 180 181 182 183 184 185 186 187 188..... 79

**Figure 4.3 Capacity for In Situ AFM to Probe Dissipative Nanoparticle Assembly.** a) Illustration of nanoparticle assembly measured through in-situ AFM. The physical interaction between the cantilever and the particles generates image contrast. (b-d) In-situ AFM images demonstrating the growth of zeolite crystals over time. Adapted with permission from ref. 186. Copyright 2018 Nature Publishing Group. (e-f) In-situ AFM images demonstrating the fusion of lipid-nanodiscs in solution. Adapted with permission from ref. 185. Copyright 2018 American Chemical Society..... 82

**Figure 4.4 Capacity for Light Scattering to Probe Dissipative Nanoparticle Assembly.** a) Illustration of the imaging of diffusing nanocubes in solution through light scattering. Particles that approach within a diffraction limit of one another (~100 nm) cannot be differentiated. b) Frames from a video utilizing nanoparticle tracking analysis to observe the movement and growth of transition metal oxide nanoparticles. Adapted with permission from ref. 204. Copyright 2011 American Chemical Society. c) Size distributions of two batches of maltoheptaose-*block*-polystyrene nanoparticles formed under different synthetic conditions. Adapted with permission from ref. 205. Copyright 2013 American Chemical Society..... 87

**Figure 4.5 Capacity for SR Microscopy to Probe Dissipative Nanoparticle Assembly.** a) Illustration of the imaging of nanocubes using super-resolution microscopy. Particles must be labeled with fluorophores that emit individually and thus can be mapped to a single point spread function and localized below the diffraction limit. b) Comparison of a diffraction-limited confocal image of assembled polystyrene beads and the same assembly imaged using a super-resolution microscopy technique (stimulated emission depletion, STED).<sup>174</sup> Reproduced with permission from ref. 174. Copyright 2010 American Chemical Society. c) Super-resolved images of the formation of a microtubule (purple) forming from a mitochondrion (green) over time.<sup>162</sup> Reproduced with permission from ref. 162. Copyright 2018 Cell Press. .... 92

**Figure 4.6 Capacity for Liquid Phase TEM to Probe Dissipative Nanoparticle Assembly.** a) Illustration of a sealed TEM liquid cell, allowing the imaging of spherical nanoparticle assembly. Heating elements and the inflow of new

reagents to the cell are indicated as methods to initiate a reaction. b) Liquid-phase TEM images showing the assembly of gold nanoprisms over time.<sup>221</sup> Reproduced with permission from ref. 221. Copyright 2017 Nature Publishing Group. c) Spatially-mapping the dynamic motion of nanorods leads to a color-coded count of the total number of nanorods in each 5 nm by 5 nm pixel. d) Plots of the radial distribution function and the pairwise interaction potential of nanorods, extracted from the trajectories in part c).<sup>227</sup> Reproduced with permission from ref. 227. Copyright 2015 American Chemical Society..... 95

# List of Tables

<b>Table 3.1 Average <math>T_m</math> of DNA-Functionalized Nanoprism Assemblies Under Various Conditions. ....</b>	<b>58</b>
<b>Table 3.2 Average FWHM of Melting of DNA-Functionalized Nanoprisms .....</b>	<b>59</b>

# List of Equations

Equation 3.1 Hill Equation.....	46
Equation 3.2 Thresholding Behavior Caused by Multivalency .....	47
Equation 3.3 Thresholding Behavior Caused by Cooperativity .....	48
Equation 3.4 Thresholding Behavior Cause by Both Multivalency and Cooperativity .....	48
Equation 3.5 Chaikin Model for Determining FWHM from $T_m$ .....	61
Equation 3.6 Linear Form of the van 't Hoff Equation .....	62
Equation 3.7 Correlation Between Singlet Fraction and Collective Equilibrium Constant.....	63

# Nomenclature

AFM	atomic force microscopy
AuNWs	ultrathin gold nanowires
CTAB	cetyltrimethylammonium bromide
dsDNA	double-stranded DNA
FWHM	full width at half maximum
HCP	hexagonal close packed
NPs	nanoparticles
SR	super-resolution
ssDNA	single-stranded DNA
TEM	transmission electron microscopy
$T_m$	melting temperature

# Chapter 1

## Introduction

For nearly half a century, scientific interest in the research and use of colloidal metal nanoparticles has exploded. The development of the electron microscope has allowed metal nanoparticle research to flourish as groups all over the world study various ways to synthesize, control, and develop nanoparticles for use in a variety of applications.<sup>1</sup> A variety of papers can be found discussing the properties of Al nanocubes,<sup>2</sup> Au nanorods,<sup>3</sup> Ag nanoplates,<sup>4</sup> and more. But it is noteworthy that in the nomenclature used to describe these nanoparticles, the ligands bound to the nanoparticle surface are often ignored, typically focusing only on composition and morphology. However, it is often the case that the ligands used are crucial for the success of metal nanoparticle synthesis, growth, functionality, or application under study.<sup>5, 6</sup> This chapter seeks to explore the crucial role ligands play in the development of metal nanoparticles. We will first discuss the role ligands play in the synthesis and growth of various nanoparticles before exploring how ligands affect the properties

and function of nanoparticles. We will then explore deeper how ligands are used in nanoparticle self-assembly before finishing with how ligands can be used to achieve higher levels of self-assembly behavior from hierarchical self-assembly to dynamic self-assembly and finally to dissipative self-assembly. It should be noted that while it was Faraday's work in 1857 reducing gold salt to make gold colloid that started the path towards modern nanoscience, it is the ligands passivating the surface of the gold colloid that allows them to remain colloidally stable all these years later.<sup>1, 7</sup>

### **1.1. Ligands as Capping Agents**

Wet synthesis methods to produce metal nanoparticles are one of the most common methods seen in modern nanoscience today. This method involves taking a metal salt and reducing it with some form of reducing agent to form the metal that composes the nanoparticle core. However, if this is performed without some sort of capping agent (or a ligand to stabilize the surface of the nanoparticle), bulk metal will be formed rather than individualized particles. The reason for this is simple. Nanoparticles have incredibly high surface area compared to more typical macroscopic structures metals can form. A capping agent, whether that is a surfactant or some other kind of ligand, is required to kinetically trap the metal atoms and prevent them from reaching the thermodynamic minimum of a macroscopic metal structure. To this end, in nearly every wet synthesis method, capping agents will be present when the reducing agent is added to solution. The variety of capping agents used are as numerous as the number of kinds of nanoparticles that exist. However, there are a few common ones seen.<sup>6</sup>

For aqueous phase syntheses, surfactants (molecules with a hydrophobic portion and a hydrophilic portion) are extremely common. The most famous of these surfactants is cetyltrimethylammonium bromide (CTAB).<sup>6</sup> With the use of this ligand, numerous particles can be formed including Au nanopsheres,<sup>8</sup> Au nanoclusters,<sup>9</sup> and Au nanorods.<sup>10</sup> CTAB stabilizes the particles primarily by providing them with a charged surface, as CTAB is a cationic ligand. As a result, electrostatic repulsion will inhibit the nanoparticles' ability to fuse back together or aggregate and precipitate out of solution.<sup>11</sup>

For organic phase syntheses, small molecule ligands that can provide a steric barrier to prevent particle aggregation are seen more frequently.<sup>11</sup> One of the most common ligands seen in a variety of syntheses is oleylamine. With the use of oleylamine, a large variety of organic-phase nanoparticles of various compositions and morphologies can be formed, including magnetic "polypod-like" Co nanoparticles,<sup>6</sup> bimetallic Au-Pd nanoparticles with "windmill" morphologies,<sup>12</sup> and ultrathin Au nanowires.<sup>13</sup>

Ligands are crucial for stabilizing particles during synthesis, but that is not their only use in the production of nanoparticles. Ligands can also be used to guide nanoparticle nucleation or growth to form nanoparticles of particular anisotropic shapes.



## 1.2. Ligands as Growth Directors

To understand how we can control nanoparticle synthesis to synthesize nanoparticles of specific anisotropic shapes, certain fundamentals of nanoparticle synthesis must first be discussed. Nanoparticle synthesis is often divided into two separate steps. The first of which is known as nucleation. This step occurs immediately as the first metal ions are reduced to small particles composed of metal(0) atoms known as nuclei. The second step, known as growth, occurs directly after nucleation. During this step, metal atoms are added to collections of pre-existing nuclei. There are two reasons we conceptualize synthesis this way. The first is that there is a difference in energy between reducing a metal ion to form a nucleus (homogeneous nucleation) and reducing a metal ion to add onto an existing nucleus (heterogeneous nucleation). Generally, homogeneous nucleation is higher energy than heterogeneous nucleation. This leads us to the second reason we conceptualize synthesis as these two distinct steps. By taking advantage of the difference in energy required to achieve homogeneous and heterogeneous nucleation, we can further separate the nucleation and growth steps. We can optimize the conditions to achieve the highest quality and least polydisperse nuclei (sometimes called seed particles) and then add those “seeds” to a growth solution composed of additional metal salt, ligands, and a reducing agent that is not strong enough to cause homogeneous nucleation but is strong enough to cause heterogeneous nucleation onto the added nuclei. This extra step allows researchers to chemically tailor the growth solution to encourage nanoparticles to grow in ways that might not be ideal for nucleation. As an

example, this method is used in the synthesis of triangular nanoprisms. Spherical “seed” particles are synthesized through fast addition of  $\text{NaBH}_4$ , a powerful reducing agent, to a solution of  $\text{HAuCl}_4$  and sodium citrate. The  $\text{Au(III)}$  is quickly reduced to  $\text{Au(0)}$  since  $\text{NaBH}_4$  is a powerful enough reducing agent to cause homogeneous nucleation, leading to the formation of small, citrate-capped seed particles. These particles can then be added to a growth solution consisting of  $\text{HAuCl}_4$  and ascorbic acid (among other chemicals that stabilize the particles and dictate growth towards the formation of nanoprisms as discussed later). Before the seed particles are introduced, ascorbic acid reduces the  $\text{Au(III)}$  to  $\text{Au(I)}$ , but is not a strong enough reducing agent to cause homogeneous nucleation by reducing  $\text{Au(I)}$  to  $\text{Au(0)}$ . Once the seeds are added, heterogeneous nucleation is possible since there is a pre-existing  $\text{Au}$  surface, and as a result, ascorbic acid is able to reduce the  $\text{Au(I)}$  to  $\text{Au(0)}$  leading to the growth of the triangular prism particles.<sup>14</sup> But how does the growth solution direct the growth of triangular nanoprisms rather than the formation of lower surface area spherical particles? One of the main ways scientists can tailor the growth solution is by controlling what ligands are present.<sup>6</sup>

Bulk metal is composed of atoms in a specific crystal structure. Nanoparticles will typically match the crystal structure that they form when in bulk. Due to this desired atomic packing, atoms will be added preferentially in specific locations and directions, resulting in faceted objects. Ligands bind to different facets with different strengths. As a result, specific ligands can passivate specific facets encouraging growth in directions that expand those facets (Fig. 1.1).<sup>15</sup> This can result in nanoparticles with different morphologies. Returning to the example of the synthesis

of Au nanoprisms, iodide is present in the growth solution. Iodide preferentially binds to the Au {111} facet. As a result, these facets are stabilized and it is less energetically favorable for Au atoms to be added to those surfaces rather than other available surfaces.<sup>14</sup>

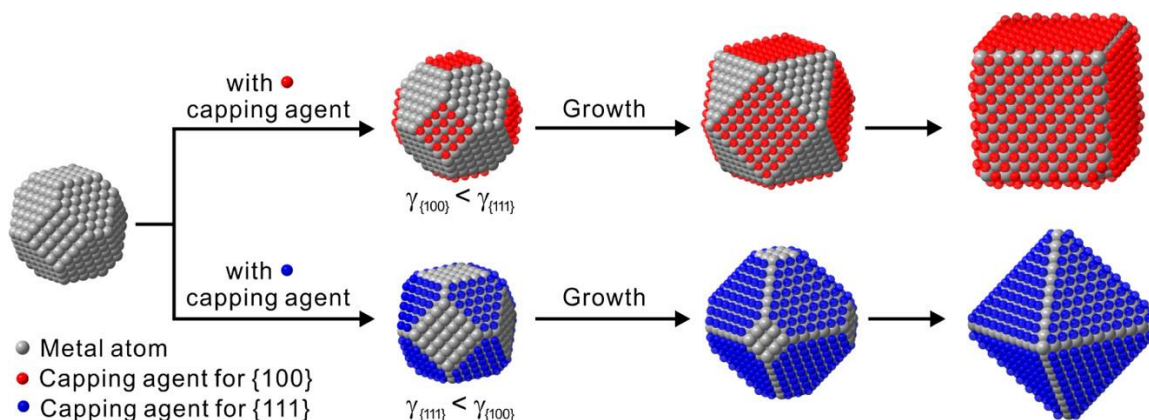


Figure 1.1 Ligands Direct NP Growth. A schematic showing the same seed particle being driven down two hypothetical growth directions depending on the presence of either a capping agent (ligand) that preferentially binds {100} facets (red) or a capping agent that binds {111} facets. Reprinted with permission from ref. 15. Copyright 2015 American Chemical Society.

The reason scientists might want to develop nanoparticles with different morphologies is that many properties of nanoparticles rely on their specific structures.<sup>16 17</sup> As a result, to achieve specific behaviors, nanoparticles of particular morphologies must be used. A full breakdown of how morphology affects various properties is beyond the scope of this work, however, controlling morphology is not the only way to achieve a specific function with a system of nanoparticles. Controlling their ligand chemistry is also effective.

### 1.3. Ligands for Nanoparticle Functionality

Nanoparticles show potential in a large number of fields, including optics,<sup>18</sup> medicine,<sup>5, 19, 20</sup> catalysis,<sup>21</sup> and electronics.<sup>22</sup> For all of these applications, the ligands are crucial even if it is merely to stabilize the particles themselves. To illustrate how ligands influence nanoparticles' properties and as a result, their usefulness in specific applications, here are a few specific examples.

Nanoparticles are being considered for a variety of medicinal functions from improved contrast agents for diagnostic techniques to scaffolds for targeted photothermal therapies.<sup>23</sup> However, a major challenge in the use of nanomaterials in medicine is their biocompatibility. Nanoparticles are often cleared from the body quickly due to the natural immune response. Some success has been observed functionalizing nanoparticles with the hydrophilic polymer poly(ethylene glycol) (PEG). While this surface chemistry shows some improvements, upon repeated treatments of PEG-functionalized nanoparticles, the immune system often responds to their presence through the production of anti-PEG antibodies, which ultimately cause clearance of the nanoparticles. Jiang *et al* discovered that by using the superhydrophilic zwitterionic poly(carboxybetaine) as ligands, functionalized particles demonstrate a prolonged circulation time in the body without a major increase in the rate of clearance in subsequent treatments. It is thought that this is due to the superhydrophilic nature of the poly(carboxybetaine) making it more difficult for proteins to adsorb to the surface.<sup>24</sup>

Moving away from medicine to the field of optics, nanoparticles can interact with light in numerous ways, such as gold and silver nanoparticles being able to fluoresce. The degree to which these particles fluoresce can be influenced by their ligand chemistry. Jin *et al* have demonstrated that the intensity of fluorescence of gold nanoclusters can be enhanced through functionalization with ligands containing electron-rich atoms (such as N or O) and functional groups (such as carboxylic acids and amines). These electron-rich species are better able to donate electron density to the gold core, thus increasing its ability to fluoresce.<sup>25</sup>

Finally, another major area of interest for the use of nanoparticles is catalysis. Metal catalysts are extremely common for use in a large variety of commercial chemical reactions. Metal nanoparticles are of major interest due to their characteristically high surface-to-volume ratio, allowing for a much lower use of total metal mass to achieve the same surface area as a macroscopic metal catalyst. One of the major goals of much catalysis research is to discover catalysts with a high degree of selectivity, so as to be able to synthesize a desired product with minimal waste. One way selectivity can be altered is through control of the ligands functionalizing the particles as evidenced by work performed by Shevchenko *et al*. In their work, they use Pt and bimetallic Co/Pt nanoparticles (Figure 1.2a and b) to perform hydrogenation reactions on alkynes. These reactions typically cause complete hydrogenation of alkynes to alkanes, making them undesirable if instead the desired product is an alkene. However, if the nanoparticles have been functionalized with primary alkylamines prior to the reaction, the nanoparticles can catalyze the reaction and form alkenes with over 90% selectivity (Figure 1.2c). The reason for this is that

for the reaction to commence, the alkyne must bind to the nanoparticle, which is possible because of its high electron donating ability. However, upon hydrogenation to an alkene, the binding energy of the molecule is weakened and is unable to compete with the high level of alkylamines present, thus causing it to desorb and leaving the alkene as the final product.<sup>26</sup>

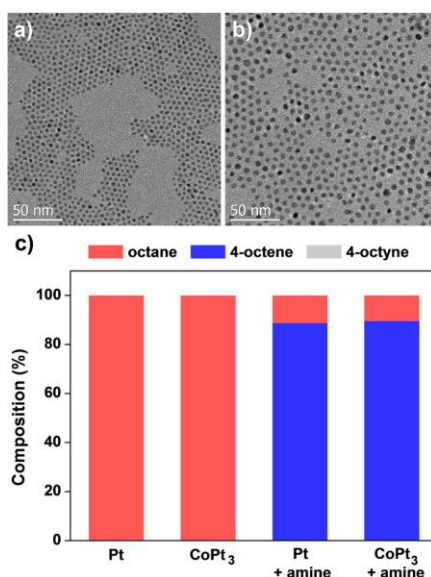


Figure 1.2 Ligands Control Nanoparticle Catalyst Selectivity. TEM images of a) 3.5 nm Pt nanoparticles and b) 4.5 nm CoPt<sub>3</sub> nanoparticles used as catalysts for alkyne hydrogenation reactions. c) The percentage of products formed from 4-octyne hydrogenation using unfunctionalized Pt and CoPt<sub>3</sub> nanoparticle catalysts and Pt and CoPt<sub>3</sub> nanoparticles in the presence of 0.13 M 1-octylamine. Reprinted with permission from ref. 26. Copyright 2012 American Chemical Society

The ability for ligand chemistry to impact nanoparticle properties cannot be understated. However, of particular interest is ligands' ability to assemble nanoparticles.

### 1.4. Ligands for Self-Assembly

One of the functions ligands can mediate in nanoparticles is their ability to form aggregates and assembled structures.<sup>16, 27-30</sup> This topic is being highlighted for greater discussion as the self-assembly of nanoparticles can lead to even greater and higher level functionality such as dynamic systems of nanoparticles, including “life-like” systems of nanoparticles that assemble through dissipative self-assembly methods. It should be noted that not all nanoparticle self-assembly is ligand-driven (as evidenced by such cases as magnetic-driven self-assembly<sup>31</sup> or self-assembly caused by other driving forces such as drying effects<sup>32</sup>). However, ligand-controlled self-assembly methods can be very powerful and precise.

The specifics of how ligands mediate self-assembly depend highly on the particular system, but as a general statement, ligands mediate self-assembly by affecting the attractive and/or repulsive forces acting between nanoparticles and the system they reside in.<sup>29</sup> For instance, as discussed previously, charged ligands cause electrostatic repulsion between nanoparticles allowing them to maintain colloidal stability. However, if two systems of nanoparticles with oppositely charged ligands are introduced, there will be attractive electrostatic interactions between the particles from the opposite systems. As a result, supercrystals of nanoparticles can be obtained. This methodology was utilized by Grzybowski *et al* to assemble Ag and Au particles into a diamond-like lattice. The Ag particles were functionalized with the positively charged  $\text{HS}(\text{CH}_2)_{11}\text{NMe}_3^+$  molecule and the Au particles were functionalized with the negatively charged  $\text{HS}(\text{CH}_2)_{10}\text{COO}^-$  molecule.<sup>33</sup>

Electrostatics are simply one force of many available to nanoscientists. Other forces generated from control of nanoparticle ligand chemistry that can be leveraged include hydrogen bonding,<sup>34</sup> dipole-dipole interactions,<sup>35</sup> and even covalent bonding through functionalization of multiple particles using polyvalent ligands.<sup>36</sup> Choosing a single particular ligand to utilize a particular intermolecular force to assemble particles is also not the only tool available for the design of complex assembling systems. It has been demonstrated that particles can be functionalized such that multiple ligands are added to the nanoparticle surface in specific “patches.”<sup>37</sup> Alternatively, anisotropic particles can display different local chemical environments due to the non-consistent radius of curvature, resulting in areas with different ligand chemistry.<sup>38</sup> These patches can control the valency of nanoparticle-nanoparticle interactions allowing for more complex interactions.<sup>37</sup> For example, Grzybowski *et al* has demonstrated that due to the non-consistent curvature of Au “nanodumbbells,” the effective  $pK_a$  of carboxylic acid presenting ligands change based on what area of the nanoparticle the ligand is bound to (Fig. 1.3). As a result, through careful control of pH, certain areas on the nanoparticle surface can be rendered negatively charged while other areas are neutrally charged. This enables the formation of previously unreported self-assembled “cross-stack” structures.<sup>38</sup>

The discussion thus far has been focused simply on the formation of assemblies. However, a higher degree of complexity can be obtained when the ligand interactions that cause assembly are reversible.



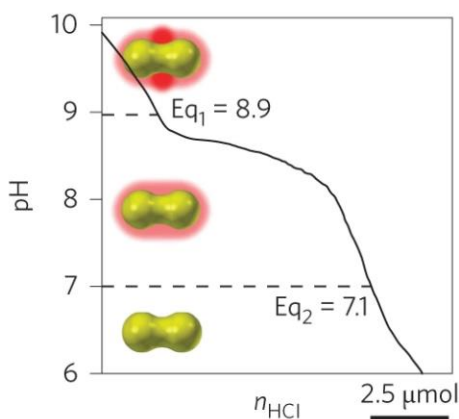


Figure 1.3 Surface-Ligand Interactions Cause Patchy Particles. The titration of carboxylic acid presenting nanodumbbells. The same molecule has a different effective  $\text{pK}_a$  when bound to the surface due to the difference in radius of curvature across the particle. Reprinted with permission from ref. 38. Copyright 2013 Nature Publishing Group.

### 1.5. Ligands for Dynamic Self-Assembly

One of the primary reasons ligand-driven self-assembly is of interest is the ability to have dynamic systems rather than static systems. Many ligands are highly responsive to various stimuli (including light,<sup>35</sup> heat,<sup>39</sup> pH,<sup>40</sup> other chemical impetuses,<sup>41</sup> etc.), and when bound to the surface of a nanoparticle, that responsiveness can be translated to the nanoparticle as a whole. If those stimuli-responsive ligands are involved in self-assembly, the nanoparticles will be able to responsively assemble and even disassemble in response to those stimuli.<sup>42, 43</sup> For instance, DNA-functionalized nanoparticles can assemble through DNA base-pair interactions. These interactions are labile and sensitive to heat. As a result, assemblies can be disassembled through heating and then re-assembled upon further cooling.<sup>39</sup> The ability to reversibly assemble nanoparticles opens the door for even further potential applications. For instance, Klajn *et al* demonstrated that the

nanosized-pores inside of assemblies of spherical particles can be used as “nanoreactors” where trapped molecules undergo chemical reactions at an increased rate. While this has been observed using other porous materials such as zeolites, there is a major challenge to release the products from such nanoreactors. To solve this challenge, Klajn *et al* functionalized nanoparticles with ligands terminating in a *trans*-azobenzene moiety. Upon irradiation with UV light, the molecule undergoes *trans-cis* isomerization, forming *cis*-azobenzene. Due to the polar nature of this isomer, dipole-dipole interactions cause assembly of the nanoparticles. However, upon irradiation with visible light, these azobenzene moieties undergo *cis-trans* isomerization, changing the polarity, and as a result, disassembling the nanoparticles and releasing the molecular products trapped in the pores. This process can be repeated as needed until the reaction goes to completion (Fig. 1.4).<sup>44</sup>

The transition between the assembled and disassembled state can also be highly sensitive in certain systems.<sup>39</sup> This sensitivity opens the door for a variety of potential applications, including sensing.<sup>43</sup> Understanding how to instill dynamic responsiveness in nanoparticles and ideally increasing their ability to respond sharply with a degree of sensitivity continues to be a major goal for the field of dynamic self-assembly (and is discussed more thoroughly in Chapter 3). It’s possible that by being able to control the sharpness of the assembly transition, higher levels of complexity can be obtained in self-assembled systems.

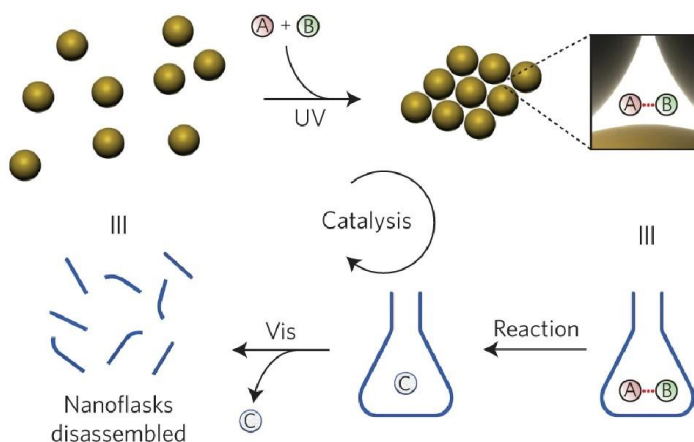


Figure 1.4 Stimuli-Responsive Ligands Enable Stimuli-Responsive Assembly. Schematic demonstrating the assembly of particles through irradiation of UV light and the resultant formation of “nanoflasks” before being disassembled through irradiation of visible light and the release of the resulting product. Reprinted with permission from ref. 44. Copyright 2016 Nature Publishing Group.

## 1.6. Ligands for Complex Self-Assembly

Utilizing ligands to control the assembly states of nanoparticles is a powerful tool. However, the more sophisticated the assemblies of the nanoparticles, the greater potential they have. The field of self-assembly has progressed greatly over the decades, but as of yet, the most complex types of assembly have so far only been consistently achieved sporadically. Greater understanding of the necessary design principles are required before such systems can become common.

One such type of complex self-assembly is hierarchical self-assembly. This type of self-assembly involves the sophisticated assembly of components into ordered structures at multiple length scales.<sup>45</sup> This is analogous to amino acids being assembled into functional proteins. The amino acids are assembled into a linear

sequence that is then folded to form secondary and tertiary structures that enable the function of the protein. To fully understand the structure of the protein, the protein must be examined on each of these levels.<sup>46</sup> While not nearly as sophisticated as the complex structure of proteins, there have been advancements in the formation of nanoparticle assemblies with analogous hierarchical structure. One of the most consistent methods to produce these hierarchical structures is through use of a template or mold. By using techniques such as electron-beam lithography, substrates can be patterned with nanoscale precision and chemically treated to tailor particular nanoparticle-substrate interactions. Commonly, the interactions tailored utilize the chemical nature of the ligand bound to the nanoparticle.<sup>45</sup> As an example, Reinhard *et al* developed a hierarchical assembly of Au nanoparticles onto a substrate for the development of a material designed to perform surface-enhanced Raman spectroscopy (SERS). These “nanoparticle cluster arrays” were formed by first using electron-beam lithography to form nanoscale wells that could then be functionalized with a positively charged ligand. Nanoparticles with negatively charged ligands were introduced to the system resulting in the formation of small clusters nanoparticles assembling in the wells. This enables the formation of a hierarchical assembly where the assembly must be characterized on both the level nanoparticle level (such as how many particles are in each cluster and their relative degree of order) as well as the cluster level (such as the order and spacing with which the wells were patterned onto the substrate).<sup>47</sup> Hierarchical assemblies such as these have arisen due to the high level of understanding achieved by the self-assembly community. This push for greater complexity in self-assembled systems will continue to demonstrate more

powerful avenues for nanoparticles to be applied to many more challenges faced in science.

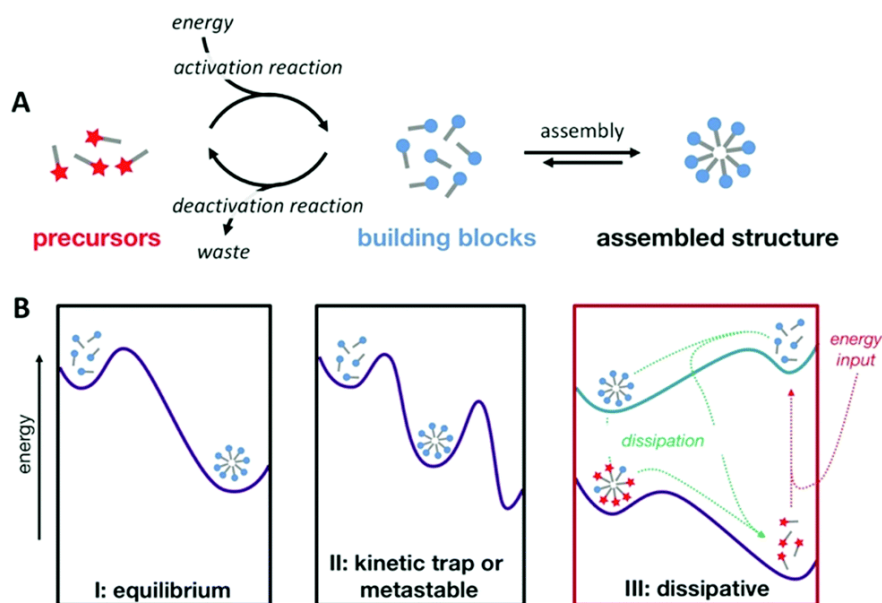


Figure 1.5 Dissipative Assembly Explores Significantly Different Phase Spaces than Equilibrium and Metastable Assemblies. a) A schematic showing the consumption of energy used to activate a hypothetical self-assembly process. b) A comparison of the energy landscape of equilibrium states, kinetically trapped or metastable states, and dissipative states. Reprinted with permission from ref. 48. Copyright 2017 Royal Society of Chemistry.

The various types of self-assembly that have thus far been discussed have immense potential. However, it is the opinion of this author that the true pinnacle of self-assembly is dissipative self-assembly. This method of self-assembly requires the input of energy. This may seem like a limitation, but since these assemblies exist often far out of equilibrium, extremely nuanced and interesting properties are possible. This energy-intensive type of self-assembly is after all, how many biological systems operate, allowing them to perform extremely complex tasks necessary to sustain life.

This topic is explored more thoroughly in Chapter 4, but briefly, dissipative self-assemblies are able to access thermodynamic states vastly different from equilibrium or kinetically trapped states due to the constant influx of energy exciting them (Fig. 1.5).<sup>48</sup> As a result, these assemblies demonstrate the potential for properties not possible for more traditional assemblies. Dissipative self-assemblies can demonstrate adaptability, being able to respond to changes in the environment by changing themselves. They can also demonstrate a somewhat opposite behavior: responding to perturbations by returning to their original state, otherwise known as self-healing. And finally, they have the potential to self-replicate.<sup>49</sup> We know these properties to be true, although mostly from observing naturally-occurring dissipative assemblies, rather than perfectly being able to develop these systems synthetically. There have been few examples of dissipative self-assembly on the nanoscale due to the challenge of designing such systems. However, some examples do exist, including the previously discussed work by Klajn *et al.* The *cis*-azobenzene isomer is not stable and will over time or with perturbations (such as visible light or heat) revert to the more stable *trans*-azobenzene isomer. The nanoflasks are an example of dissipative self-assembly, requiring the constant input of energy in the form of UV light to remain stable.<sup>44</sup>

It is my view that these out-of-equilibrium techniques are the next step for self-assembly and nanoscience as a whole. However, a much greater understanding of the design principles to synthesize such materials must be obtained. As a result, more work studying higher level ligand behaviors is necessary to achieve this. Developing greater synthetic control is not the only hurdle. More powerful analytical

tools are necessary to probe the behaviors of these systems that need to be studied at extremely high spatial and temporal resolutions.<sup>50</sup>

## **1.7. Conclusion**

Understanding ligands is crucial to understanding systems of metal nanoparticles. Ligands are essential to the stability of metal nanoparticles and clever use of functional ligands enables a high degree of control over the properties and behaviors of nanoparticles. It should be noted that many proteins and other high-functioning biological materials exist on the nanoscale. These biological materials are responsible for the complexity of life, and there's no fundamental reason these same attributes couldn't be instilled in synthetic systems. With further understanding and precise control over ligand chemistry, someday people will be able to develop synthetic nanoparticle-based systems on the same order of complexity.

## Chapter 2

# **Controlling the Assembly State of Ultrathin Gold Nanowires Through Stimuli-Responsive Ligands<sup>1</sup>**

### **2.1. Introduction**

Ultrathin gold nanowires (AuNWs) are a class of one-dimensional nanomaterial which display a unique array of structural and physical properties. With

---

<sup>1</sup> This work was produced as a collaboration between David Marolf, Theo Gerrard-Anderson, Rohan Pillai, and Joe Khoury. Material in this chapter is being prepared into a manuscript with Marolf and Gerrard-Anderson as cofirst authors that will be submitted to a peer-reviewed journal. This research used resources of the Advanced Photon Source, a U.S. Department of Energy (DOE) Office of Science user facility operated for the DOE Office of Science by Argonne National Laboratory under Contract No. DE-AC02-06CH11357.



lengths greater than 1  $\mu\text{m}$  while being only  $\sim 2$  nm in diameter, ultrathin gold nanowires are exceptionally anisotropic with an aspect ratio in excess of 10,000.<sup>51, 52</sup>

While several groups were developing AuNW syntheses simultaneously,<sup>53-55</sup> a simple room temperature protocol involving the sonication of an  $\text{HAuCl}_4$  solution in oleylamine (OLAM) from Peidong Yang's group became the basis for further improvements.<sup>13</sup> In 2009, Feng H. et al developed a synthetic protocol which could be carried out at room temperature and completed within a day due to the addition of triisopropylsilane as a reducing agent.<sup>56</sup> This protocol and minor modifications of it would go on to become the standard in the field and now AuNWs can be synthesized rapidly and in large quantities with minimal impurities.<sup>57</sup> AuNWs as synthesized possess a unique tetrahedrally close packed gold lattice with a structure identical to that of the structure of bulk manganese,<sup>58</sup> and their surfaces are coated with OLAM bound via the amine.<sup>59</sup>

The high aspect ratio of AuNWs grants them an unparalleled flexibility among noble metal nanostructures, having a calculated persistence length of 758 nm,<sup>60</sup> and bending with a radius of curvature as low as 20 nm without fracture.<sup>61</sup> This flexibility in combination with their electrical conductivity makes AuNWs appealing for applications in flexible electronics and mechanical sensing.<sup>52, 61-64</sup>

The interactions of AuNWs in solution, by their nature as colloidal nanoparticles, are mediated by the ligands or surfactants bound to their surfaces. To be able to fully control AuNW fabrication and assembly, attempts have been made to

control their surface interactions. As synthesized, AuNWs undergo bundling owing to an attractive depletion-driven interaction caused by unbound OLAM in solution, and it has been shown that the level of bundling can be controlled via OLAM concentration, nanowire concentration, and temperature.<sup>59, 65</sup> AuNWs have also been subjected to surface ligand exchanges to produce nanowires coated with phosphines, thiols, and amines. For example, El Said A. Nouh *et al* were able to control the inter-nanowire distance in bundles of AuNWs by exchanging oleylamine for shorter trioctylphosphine.<sup>66</sup> Because AuNWs undergo decomposition into spheres over time due to Rayleigh instability,<sup>67</sup> attempts have been made to further stabilize the AuNWs through ligand exchanges with varying degrees of success.<sup>68-70</sup> Research has begun exploring the effects of ligand exchange to control the assembly state of nanowires, but the field is yet to see an attempt to functionalize AuNWs with a ligand capable of undergoing switchable supramolecular interactions (either responding to temperature, light or, a chemical stimulus) enabling dynamic control of assembly state, such as those seen in work involving the assembly of less anisotropic nanoparticles.<sup>71, 72</sup> These typically involve ligands that can utilize hydrogen bonding, metal ion chelation, dipole-dipole interactions, electrostatic interactions, or some other switchable supramolecular force to initiate assembly. The ability to dynamically trigger assembly and exercise control over the assembly's energy landscape using carefully designed supramolecular ligand systems would allow an unprecedented level of control over materials fabricated from AuNWs.

In this work we demonstrate the functionalization of AuNWs with a carboxylic-acid-terminated ligand and their subsequent phase transfer from hexane into water. We also demonstrate the ability to control nanowire assembly via controlling the pH and the presence or absence of divalent metal cations. The structure of the resulting AuNW assemblies is elucidated via small angle X-ray scattering (SAXS). Additionally, we demonstrate preliminary work using these assembly techniques to form fibers composed of AuNWs.

## 2.2. Results and Discussion

### 2.2.1. AuNW Functionalization with $\text{HS}(\text{CH}_2)_{11}(\text{EG})_6\text{OCH}_2\text{COOH}$

As mentioned above, as-synthesized AuNWs are capped with OLAM in a solution of hexane and form bundles of varying sizes..<sup>59</sup> For the goal of controlling assembly state, it is desired to begin with the AuNWs in an individualized state rather than already bundled. To this end we developed a protocol for the functionalization of AuNWs with the ligand  $\text{HS}(\text{CH}_2)_{11}(\text{EG})_7\text{OCH}_2\text{COOH}$  and their subsequent phase transfer to water.

Briefly, following an AuNW synthesis protocol adapted from literature,<sup>13</sup> the AuNWs are washed of OLAM three times using ethanol to prepare them for functionalization. The washed AuNWs in hexane are then introduced to a 16 mM aqueous solution of  $\text{HS}(\text{CH}_2)_{11}(\text{EG})_6\text{OCH}_2\text{COOH}$  and vortexed resulting in the

formation of an emulsion which collapses over the course of the next 24 hours leaving the AuNWs in the aqueous phase (Fig. 2.1a and b).

Following centrifugation and washing at 2k rcf overnight to remove excess  $\text{HS}(\text{CH}_2)_{11}(\text{EG})_6\text{OCH}_2\text{COOH}$ , TEM images of the functionalized AuNWs show they survive the process intact with little alteration in their appearance (Fig. 2.1 c and d). However, image analysis of AuNW lengths before and after functionalization shows that there is a reduction in average length, possibly owing to the forces exerted on the AuNWs while being vortexed during phase transfer or during the centrifugation step.

$\text{HS}(\text{CH}_2)_{11}(\text{EG})_6\text{OCH}_2\text{COOH}$  binds to AuNWs via the thiol moiety, owing to sulfur's exceptional binding strength with gold in comparison to carboxylic acids.<sup>73</sup> The carboxylic acid presented to the solution makes the wires more soluble in the aqueous phase (which can be further aided if needed through raising the pH, deprotonating the carboxylic acid, and making the resultant AuNWs negatively charged), resulting in the observed phase transfer. Finally, the nanowires no longer bundle as the depletants (the free oleylamine molecules) have been removed from solution and no other molecule in solution behaves as such. Observation of the aqueous AuNW dispersion under a microscope shows few visible aggregates and no bundles, and a SAXS spectrum exhibits no structure factor, indicating that total individualization of the AuNWs has been achieved.

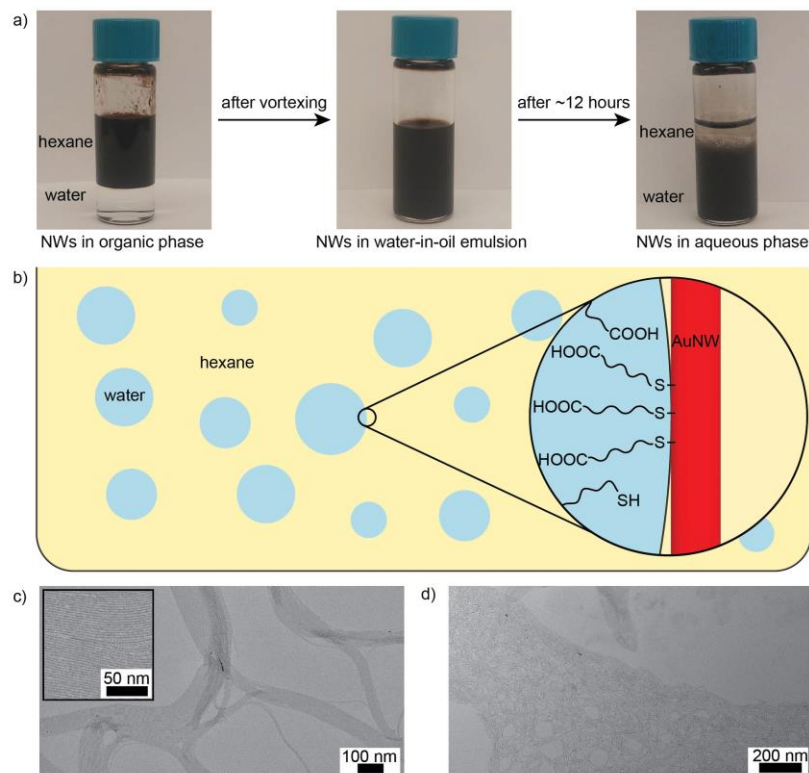


Figure 2.1 Nanowire Functionalization. a) Pictures of the functionalization mixture at different stages. The dark color is due to the presence of nanowires. b) An illustration of the oil-in-water emulsion formed upon mixing the nanowire-containing hexane phase with the ligand-containing aqueous phase. Presumably, a Pickering emulsion forms with the nanowires resting at the interface before thiol-Au bonds form, ultimately pulling the nanowire into the aqueous phase. c) TEM image of the nanowires as-synthesized. d) TEM image of the nanowires after functionalization.

### 2.2.2. AuNW Assembly Using $\text{Ca}^{2+}$

It is well known that divalent cations, and calcium(II) specifically, can cause the assembly and aggregation of species containing carboxylic acid groups, famously so in the case of alginate gels.<sup>74, 75</sup> In order to bind strongly to  $\text{Ca}^{2+}$ , the carboxylic acid group ( $\text{COOH}$ ) needs to be deprotonated to a carboxylate group ( $\text{COO}^-$ ), after which it

can bind to a  $\text{Ca}^{2+}$  ion in either a monodentate or bidentate fashion, although the bidentate mode is more thermodynamically stable.<sup>76</sup> A single  $\text{Ca}^{2+}$  ion is capable of accepting two  $\text{COO}^-$  groups, which allows it to act as a cross linker between species, as is the case with calcium alginate gel. Due to sterics, interparticle binding is preferred allowing a single  $\text{Ca}^{2+}$  to act as a cross linker between AuNWs functionalized with  $\text{HS}(\text{CH}_2)_{11}(\text{EG})_6\text{OCH}_2\text{COOH}$  by binding to  $\text{COO}^-$  groups on two different nanowires.

Briefly, the assembly of AuNWs by  $\text{Ca}^{2+}$  was induced as follows. To increase the number of binding sites on the AuNWs for  $\text{Ca}^{2+}$ , the solution is made basic using KOH. Following this,  $\text{Ca}^{2+}$  is added in the form of  $\text{CaCl}_2$  and the solution is vortexed. Depending on the pH of the solution and the concentration of calcium, assembly occurred within 24 hours yielding a dark flocculate.

Figure 2.2a shows X-ray diffraction spectra of AuNW aggregates assembled with different concentrations of  $\text{Ca}^{2+}$  and different pHs from an AuNW dispersion of 3.2 mg/mL. At pH 7 and with no  $\text{Ca}^{2+}$ , there are no Bragg diffraction peaks indicating no assembly has taken place. At pH 7 and 0.5 M  $\text{CaCl}_2$  there are distinct peaks indicating assembly. Under more basic conditions (pH 11) holding the same  $\text{CaCl}_2$  concentration, the peaks become more pronounced with a peak intensity ratio of 1.5 between them. The presence of sharp Bragg peaks indicates long range order within the AuNW assemblies. The increase in intensity between pH 7 and pH 11 without an obvious change in peak width implies an absolute increase in the quantity of

assembled AuNWs, thus indicating that at higher pH the number of AuNWs which will assemble from solution is higher due to having more  $\text{COO}^-$  moieties available for  $\text{Ca}^{2+}$  binding.

The peak position ratio of the SAXS spectrum (from lowest  $q$  to highest  $q$ ) is  $1:\sqrt{3}:\sqrt{4}:\sqrt{7}:3$ , which indicates the  $\text{Ca}^{2+}$ -assembled AuNWs pack in a 2D hexagonal close packed (HCP) configuration.<sup>77</sup> This packing configuration provides the largest possible surface area contact between AuNWs, allowing maximization of  $-\text{COO}^-$ - $\text{Ca}^{2+}$ - $-\text{OOC}-$  cross-linking interactions, suggesting the assembly is driven thermodynamically.

The centre-to-centre inter-nanowire distance ( $d$ ), calculated from the (10) peak using  $d = \frac{2\pi}{q}$ , is 7.39 nm. The calculated end to end length of  $\text{HS}(\text{CH}_2)_{11}(\text{EG})_6\text{OCH}_2\text{COOH}$  at full extension is 4.04 nm. Taking into account the the  $\sim 2$  nm diameter of AuNWs<sup>58</sup> and the 99 pm ionic radius of  $\text{Ca}^{2+}$ , we can estimate that  $d$  at full ligand extension would be 10.5 nm. As the actual value is 7.39 nm, we can infer that the  $\text{HS}(\text{CH}_2)_{11}(\text{EG})_6\text{OCH}_2\text{COOH}$  molecules bound to the AuNWs are in a partially coiled state.

Experiments were also conducted attempting to use divalent metal cations other than  $\text{Ca}^{2+}$  to induce assembly. It was found that  $\text{Mg}^{2+}$ ,  $\text{Ba}^{2+}$ ,  $\text{Pb}^{2+}$ , and  $\text{Zn}^{2+}$  also induce assembly in a similar manner to  $\text{Ca}^{2+}$ , with assemblies forming particularly rapidly in the case of  $\text{Pb}^{2+}$  and  $\text{Zn}^{2+}$ .

A potential alternate mechanism for assembly is that of electrostatic screening caused by the introduction of the calcium salt reducing the repulsive forces such that the AuNWs assemble through van der Waals interactions. To test which mechanism was primarily responsible, control experiments replacing the  $\text{CaCl}_2$  solution with solutions of excess KCl were carried out. In these controls, the AuNW solution was brought to pH 11 in the presence of 4.5 M KCl and no assembly occurred, as determined visibly by eye and through SAXS measurements. Considering the ionic strength of the solution in the control experiment was approximately 4.5 M and the ionic strength of the  $\text{Ca}^{2+}$ -containing solutions in Figure 2.2a was approximately 1.5 M, the fact that no assembly occurred with the higher ionic strength solution indicates that the  $\text{Ca}^{2+}$ -induced assembly of AuNWs is not driven by charge repulsion screening due to an increase in ionic strength of the solution (although this probably plays some effect to allow the nanowires to become close enough to crosslink) and the primary mechanism must be via cross-linking induced by  $\text{Ca}^{2+}$  chelation.



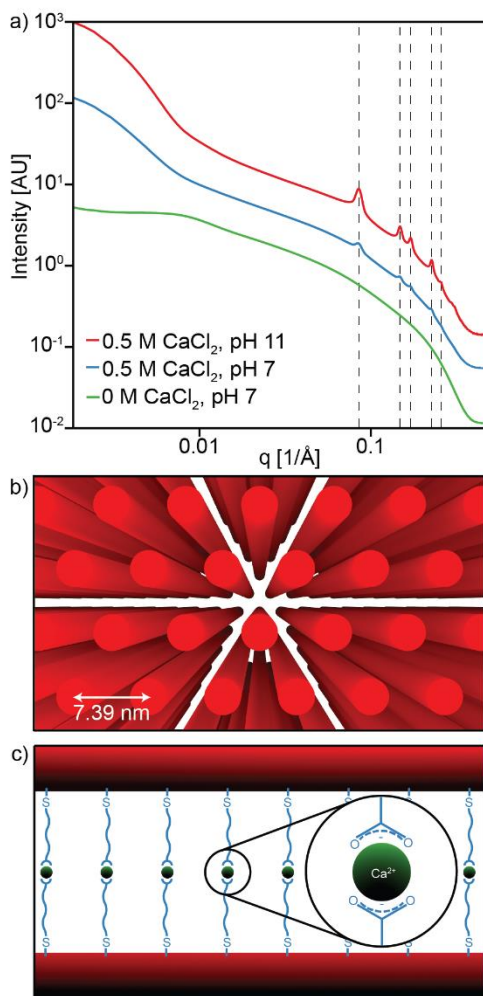


Figure 2.2 Nanowire Assembly Through  $\text{Ca}^{2+}$  Chelation. a) SAXS spectra of three samples of AuNWs varying  $\text{CaCl}_2$  and pH. Dotted vertical lines are added to guide the eye. b) An illustration of the HCP structure formed from bundled nanowires. The nanowires are viewed from the tips for ease of viewing. c) An illustration of the  $\text{Ca}^{2+}$  chelate linkages between nanowires.

### 2.2.3. AuNW Assembly in Acidic Conditions

While in a deprotonated state the carboxylate group of  $\text{HS}(\text{CH}_2)_{11}(\text{EG})_6\text{OCH}_2\text{COOH}$  is capable of causing AuNW assembly via  $\text{Ca}^{2+}$  cross-

linking, this mode only represents half of its supramolecular functionality. It is well known that molecular carboxylic acids, while protonated, can undergo hydrogen bonding (H-bonding) with each other<sup>78</sup> due to the fact that carboxylic acid moieties contain both an H-bond donor in the form of O-H and an H-bond acceptor in the form of the lone pairs on the C=O oxygen. This “double H-bond” is strong enough to cause acetic acid to dimerize even in the gas phase.<sup>79</sup> This hydrogen-bonding mechanism can also be leveraged to form hydrogen-bonded polymers in either liquids or crystalline solid phases.<sup>80</sup> This capability of carboxylic acid groups also allows us to assemble AuNWs through H-bonding in acidic conditions.

The assembly of AuNWs under acidic conditions can either be performed through addition of HCl to lower the pH or through use of buffers to hold the pH constant. Assembling AuNWs through use of HCl addition is simple: addition of HCl is followed by vortexing and within 24 hours the AuNWs assemble yielding a dark flocculate. However, due to the small volumes but high concentrations required for SAXS analysis, it is impossible to test the exact pH of samples formed in this way using the pH probe setup we have available. In addition to the simple HCl addition method, a series of buffers at varying pHs were used to help test how assembly state changes precisely with pH. Concentrated solutions of functionalized AuNWs were added to buffer solutions and then loaded into capillaries.

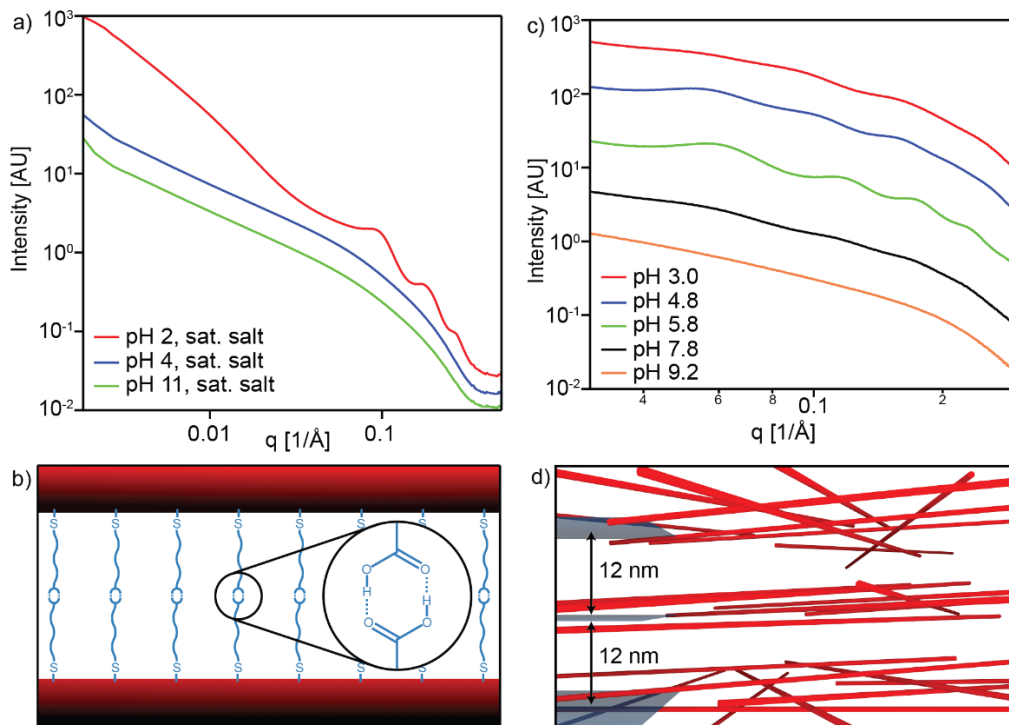


Figure 2.3 Nanoparticle Assembly Under Acidic Conditions. a) SAXS spectra of three samples of AuNWs varying pH through HCl or NaOH addition. b) An illustration of the hydrogen bond linkages between nanowires. c) SAXS spectra of five samples of varying pH through use of buffers. d) An illustration of the possible lamellar structure formed from AuNWs assembled under acidic conditions using buffers.

Figure 2.3a shows X-ray diffraction spectra of 6.4 mg/mL AuNW solutions brought to different pH values by the addition of HCl in the presence of 4.3 M KCl. The structure peaks exhibited by the AuNWs in acidic conditions indicate assembly is occurring. The peaks displayed in the pH 2 are broader than the peaks seen during  $\text{Ca}^{2+}$  induced assembly, indicating a lower degree of ordering or a smaller domain size. The peak position ratio of the pH 2 trace is 1 : 1.86 : 2.88. Given that 1.86 is the average of  $\sqrt{3}$  and  $\sqrt{4}$ , and 2.88 differs from the average of  $\sqrt{7}$  and 3 by only 2% (the

ideal peak position ratios of 2D HCP crystals) we can see that the second and third peaks in the pH 2 trace are actually convolutions of the peaks of an ideal 2D HCP lattice, indicating that the structure observed in the pH 2 trace does not exhibit a high degree of long range order but is approaching a 2D HCP structure. The centre-to-centre inter-nanowire distance ( $d$ ), calculated from the (10) peak using  $d = \frac{2\pi}{q}$ , is 6.71 nm, a 9.2 % smaller  $d$  spacing than for  $\text{Ca}^{2+}$  induced assembly, despite the AuNWs being capped with the same ligand. The 6.8 Å difference in  $d$  spacing can be fully accounted for by the lack of a  $\text{Ca}^{2+}$  ion in between ligands. The Ca-O bond length in carboxylate complexes is  $\sim 2.4$  Å, and the ionic radius of  $\text{Ca}^{2+}$  is 0.99 Å.<sup>76</sup> Considering the presence of Ca-O bonds on either side of the calcium ion, and its own diameter, we get a distance of 6.8 Å, accounting well for the difference in  $d$ -spacing. This suggests that the ligands adopt similar positions and orientations no matter the mechanism of assembly, but in one case must be spread further apart to accommodate the ion.

We additionally tested the affect of ionic strength on AuNW assemblies in acidic conditions. Figure 2.4a shows AuNW assemblies at pH 2 with 0, 0.3, and 4.3 M KCl. It can be seen that peak sharpness increases as [KCl] increases from 0 to 0.3 M, but there does not appear to be additional benefits to increasing [KCl] to 4.3 M. The increase in peak definition implies an increase in ordering as ionic strength increases. This is likely due to a decrease in the strength of inter-AuNW electrostatic interactions due to charge screening affects. At pH 2, all  $\text{COO}^-$  groups on the AuNWs

should be protonated and therefore not charged, so these groups are not likely to be contributing to this effect. It is possible that there may be oleylamine remaining in the ligand shell from before functionalization with  $\text{HS}(\text{CH}_2)_{11}(\text{EG})_6\text{OCH}_2\text{COOH}$ . These oleylamine ligands would be protonated into a positively charged oleylammonium state at pH 2, and neutralization of their repulsive electrostatic interactions at higher ionic strengths could contribute to the observed increased ordering.

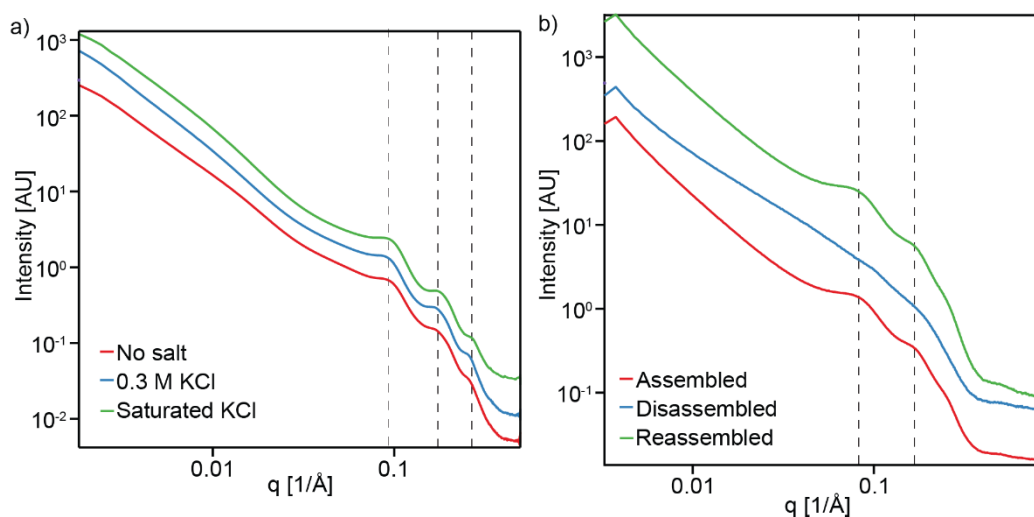


Figure 2.4 The Effect of Salt Concentration on Acidic Assembly, and Reversibility of the Acidic Assembly. a) SAXS spectra of three samples of AuNWs at pH 2 varying KCl. Dotted vertical lines are added to guide the eye. b) SAXS spectra of AuNWs demonstrating reversibility. AuNWs can be assembled through addition of acid and disassembled through addition of base. This process is reversible upon addition of more acid.

We also tested the reversibility of the assembly. In Figure 2.4b, it can be seen that wires, having been assembled at low pH, would disassemble once HCl was

neutralized with KOH. Assembly can be induced again with the addition of further HCl. This dynamic reversibility is promising for the potential development of stimuli-responsive “smart” materials.

It was expected that the samples where buffers were used to control pH would show a similar structure, however, that was not the case. Figure 2.3c shows X-ray diffraction spectra of 6.4 mg/mL AuNW solutions and any aggregates contained therein at different pH values. At higher pH values the COOH groups are deprotonated, causing the AuNWs to be individualized and thus no peaks are seen. As the pH is lowered, the AuNWs begin to assemble and diffuse scattering peaks can be seen at pH 5.8. These pseudo Bragg peaks have a positional ratio of 1:2:3:4 which, in combination with their diffuse nature, is indicative of the formation of some type of a layered or lamellar phase.<sup>81</sup> The diffuse nature of the peaks is explained by fluctuation in the size of the layers and imperfect ordering of the overall structure.<sup>82</sup> The interlayer spacing, calculated from the first peak on the pH = 5.8 trace using  $d = \frac{2\pi}{q}$ , is 11.8 nm, which is slightly too large to suggest H-bonding between ligands. The centre-to-centre distance between two AuNWs joined by H-bonds between COOH groups on the end of HS(CH<sub>2</sub>)<sub>11</sub>(EG)<sub>6</sub>OCH<sub>2</sub>COOH ligands at full extension is ~11 nm. This value represents a maximum inter-AuNW distance, and so we can assume that the d spacing derived from pH = 5.8 SAXS trace, as it is larger than 11 nm, is representative not of the spacing between AuNWs but of the spacing between these layered elements. It is difficult to discern how exactly these layers are structured as

the 2D diffraction data is isotropic indicating that many domains of differing alignment are present. Due to the flexibility of AuNWs, it is possible that in this instance they are crystallizing into lamellae with an amorphous internal structure but a periodicity between them. The pH 4.8 trace in Figure 2.3c contains more diffuse peaks than the pH 5.8 trace but still maintains the same peak position ratio. The pH 4.8 trace is also shifted down by  $0.003 \text{ \AA}^{-1}$  implying larger spacing between layers. At pH 3, the structural features of the SAXS trace are much diminished, implying minimal long-range ordering of any sort at this low pH.

The reason for the formation of a lamellar type order in the case of acid-driven assembly rather than a hexagonal packing is still an open question, as is exactly why this structure forms when buffer lowers the pH as opposed to HCl.

#### **2.2.4. AuNW Fiber Extrusion**

This work so far demonstrates the ability to functionalize AuNWs and, through management of their resulting surface chemistry, control their assembly states in solution. However, while control of assembly state in solution very likely will impact their formation into useful materials, more work needs to be done to directly investigate how functionalization with carboxylic acid-presenting thiols affects resulting materials.

To begin this endeavor, we spun fibers composed of AuNWs functionalized with 11-mercaptoundecanoic acid (MUA) utilizing a wet spinning method previously

used to spin fibers from carbon nanotubes (CNTs).<sup>83, 84</sup> MUA has similar chemical properties to and was used in lieu of  $\text{HS}(\text{CH}_2)_{11}(\text{EG})_6\text{OCH}_2\text{COOH}$  to reduce cost given the larger volumes of sample needed for this method. In this method, a concentrated solution of AuNWs is forced through a spinneret into a coagulant solution. In our experiment, we wanted to determine how fibers formed from AuNW-AuNW interactions caused by acidic conditions would differ from fibers formed from AuNWs binding through calcium chelation. To this end, the same batch of functionalized AuNWs were extruded into two different coagulant solutions. The first solution contained 100 mM HCl and 300 mM NaCl to induce assembly through acidic conditions. The second solution contained 100 mM KOH and 100 mM  $\text{CaCl}_2$  to induce assembly through  $\text{Ca}^{2+}$  chelation. These solutions were made to match ionic strength, so any differences observed should only be from the difference in the intermolecular forces at work assembling the AuNWs.

Extruding AuNWs under acidic conditions leads to stretchable fibers that can be lightly manipulated (Figure 2.5a). They are not very mechanically strong and so are prone to breaking before they could be spooled. However, small strands of fibers in the span of inches can be formed and even removed from solution (Figure 2.5b).

Despite the strength of  $\text{Ca}^{2+}$ -carboxylate chelates, extruding AuNWs into the calcium-containing solution produced poor fibers (Figure 2.5c). These structures were extremely prone to breaking and attempts to pull them out of the solution led to fragmentation (Figure 2.5d). One hypothesis as to this strange behavior is the



strength of the  $\text{Ca}^{2+}$ -carboxylate chelates actually leads to a stronger, but more brittle fiber. While the fibers formed under acidic conditions are somewhat elastic, the fibers formed from  $\text{Ca}^{2+}$  chelation are unable to deform as easily leading to breaks.

This work demonstrates a preliminary and qualitative study into the material properties of carboxylic acid-presenting AuNWs, but already we have demonstrated significant changes in a material composed of the same starting material. Further study will continue to show that our ability to control the surface chemistry of AuNWs on the molecular level will affect the macroscopic properties of the final material.

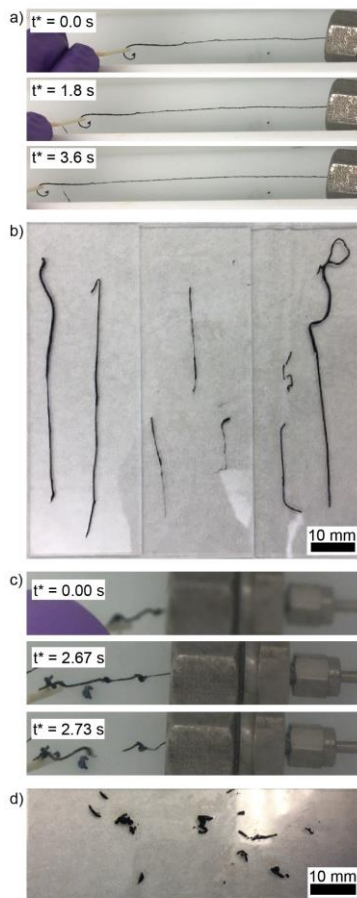


Figure 2.5 Macroscopic Fibers Formed From Nanowires. a) Frames of a video showing the extrusion of fibers into a coagulant bath containing 100 mM HCl and 300 mM NaCl. b) Images of fibers collected from the acidic coagulant bath. c) Frames of a video showing the extrusion of fibers into a coagulant bath containing 100 mM NaOH and 100 mM  $\text{CaCl}_2$ . d) Images of fragments of fibers collected from the  $\text{Ca}^{2+}$ -containing coagulant bath. Larger fibers could not successfully be removed from the bath due to their brittle nature.

### 2.3. Conclusion

The work shown here represents a significant development in our ability to manipulate AuNWs with a fine degree of control, first of all in developing a robust

ligand exchange and phase transfer procedure, as well as subsequently using a supramolecular system with two assembly functionalities yielding different structures and properties. We have demonstrated the successful phase transfer of AuNWs to water with a supramolecularly active ligand, a process which can be extended to other thiols. Additionally, we now have the ability to assemble AuNWs using either hydrogen bonding or metal chelation. The ability to trigger the assembly via the introduction of a chemical stimulus, and indeed to disassemble the AuNWs in the case of hydrogen bond driven assembly, exhibits a level of dynamicity in AuNW assembly not before seen. Beyond in solution assembly, this control has implications for materials fabrication from AuNW inks functionalized with  $\text{HS}(\text{CH}_2)_{11}(\text{EG})_6\text{OCH}_2\text{COOH}$ , allowing material properties of fibers or films to be altered depending on chemical environment.

## 2.4. Materials and Methods

### 2.4.1. Ultrathin Gold Nanowire Synthesis

Ultrathin gold nanowires were synthesized and washed adapted from a protocol by Yang *et al.*<sup>13</sup> Briefly, 20 mg  $\text{HAuCl}_4 \cdot 3\text{H}_2\text{O}$  were added to 1.35 mL n-hexane, followed by 330  $\mu\text{L}$  70% technical grade oleylamine. The resulting solution was vortexed and 500  $\mu\text{L}$  triisopropylsilane was added followed by a second round of vortexing. The reaction was left to occur for 12 hours. This basic synthesis can also be scaled up to at least 40 times without any apparent loss of AuNW quality or purity.

#### **2.4.2. Ultrathin Gold Nanowire Functionalization with**

##### **HS(CH<sub>2</sub>)<sub>11</sub>(EG)<sub>6</sub>OCH<sub>2</sub>COOH**

8 mL ethanol was added to the crude product causing the nanowires to aggregate. The product was centrifuged at 500 rcf for 5 mins, the supernatant was removed, and the nanowires were resuspended in 2.5 mL of hexane. The nanowires were washed twice more using the same conditions.

The washed nanowires were then added to a solution of 10 uL HS(CH<sub>2</sub>)<sub>11</sub>(EG)<sub>6</sub>OCH<sub>2</sub>COOH in 1 mL H<sub>2</sub>O and vortexed for 7 seconds followed by a 10 second pause and another 7 seconds of vortexing. The resulting emulsion was left for 12 hours for the functionalization to come to completion producing a hexane/H<sub>2</sub>O/nanowire gel. 20 uL aqueous 2 M KOH solution was added to the nanowires to break up the gel. The resulting solution was then diluted with 11 mL H<sub>2</sub>O and centrifuged at 2000 rcf for 12 hours. The supernatant was carefully removed and the sediment was resuspended in 50 uL H<sub>2</sub>O leaving a concentrated nanowire ink.

#### **2.4.3. Ultrathin Gold Nanowire Assembly**

Nanowire assembly solutions were fixed at a total of 40 uL in order to fit into the X-ray diffraction capillaries. Solutions were fully prepared externally before being added to the capillary. In the case of assembly driven by divalent cations nanowires were added to water followed by KOH then the divalent salt. In the case of assembly

under acidic conditions nanowires were added to water followed by NaCl followed by HCl.

#### **2.4.4. Ultrathin Gold Nanowire Fiber Extrusion**

AuNWs were synthesized in the same manner above except  $\text{HS}(\text{CH}_2)_{11}(\text{OCH}_2)_7\text{COOH}$  was replaced with 11-mercaptoundecanoic acid and the synthesis was scaled up forty times (using 800 mg  $\text{HAuCl}_4 \cdot 3\text{H}_2\text{O}$ ) before being concentrated to 2.8 percent AuNWs by volume. These AuNWs were loaded into a syringe and passed through a filter composed of two membranes (a 1.5 in., 40 mesh membrane and a 36 mm, 500 mesh) to remove any large aggregates before being extruded through a 150  $\mu\text{m}$  spinneret at a rate of 0.036 mL/min. As fibers began to be extruded, wires were pulled gently with a wooden spatula to aid in formation. A gently rotating spool would ideally have been used to keep the draw speed consistent but the wires were too fragile to be pulled that far without breakage, leading to inconsistent diameters.

#### **2.4.5. SAXS Measurements**

Small angle X-ray scattering (SAXS) measurements were carried out under ambient conditions at the 12-ID-B beamline of the Advanced Photon Source at Argonne National Laboratory. X-rays with an energy of 14 keV were used. Exposure times varied between 0.1 and 1 seconds. The samples were contained in

Charlesupper special glass capillary tubes with a 1.5 mm outer diameter, 80 mm length, and 0.01 mm wall thickness.

#### **2.4.6. Materials**

70% technical grade Oleylamine, 99.9%  $\text{HAuCl}_4 \cdot 3\text{H}_2\text{O}$ , triisopropylsilane, hexanes,  $\text{CaCl}_2$ ,  $\text{MgCl}_2$ ,  $\text{BaCl}_2$ ,  $\text{ZnCl}_2$ ,  $\text{PbCl}_2$ ,  $\text{KOH}$ ,  $\text{NaOH}$ , 37% hydrochloric acid, and mercaptoundecanoic acid were all purchased from Millipore-Sigma.  $\text{HS}(\text{CH}_2)_{11}(\text{OCH}_2)_7\text{COOH}$  was purchased from Prochimia.

# **Investigating Thresholding Behavior in Equilibrium and Nonequilibrium Nanoparticle Assemblies**

## **3.1. Abstract**

Biology utilizes cooperativity and multivalency to grant systems sharp transitions between states, also known as thresholding behavior. Developing artificial systems with a high degree of thresholding is advantageous for the development of dynamic and responsive materials. DNA-mediated nanoparticles have been shown for decades to be a well-controlled system that assembles through collective interactions of thousands of surface-bound DNA strands. By controlling whether or not the DNA strands are duplexed, we can control the flexibility of the DNA and as a result, the degree of thresholding.

### 3.2. Introduction

Synthetic structures assembled from colloidal nanoparticle building blocks have the opportunity to revolutionize materials discovery, as these architectures exhibit novel optoelectronic properties as a function of both the particle size/shape and their relative arrangement.<sup>85, 86</sup> However, the vast majority of lithographically-defined or self-assembled nanomaterials are static, incapable of changing their structure in response to external stimuli, and thus have a singular set of immutable properties.<sup>30</sup> Biological systems, on the other hand, have developed exquisite chemical strategies that allow them to adapt and reconfigure due to changes in their environment.<sup>87</sup> In many cases this behavior requires a non-linear response to stimuli, i.e. increasing the concentration of an analyte by a small amount elicits a large effect.<sup>88</sup> The ability to imbue synthetic nanoparticle-based systems with similar non-linear interactions would allow for a new class of materials capable of autonomous reconfigurability of structure and properties in response to external stimuli.

The two most ubiquitous processes that govern non-linear interactions in biological systems are cooperativity and multivalency. A cooperative interaction occurs in a system of identical subunits when the binding of one analyte results in electrostatic or conformation changes in neighboring subunits that makes subsequent binding of the same analyte more or less favorable (Figure 3.1a). In a system with positive cooperativity, one binding event makes the neighboring binding events more favorable, resulting in a thresholding behavior characterized by a sharp



transition between a fully bound state and a fully unbound state. A related phenomenon known as multivalency (Figure 3.1b) occurs when one binding event does not result in electro-static or conformational changes to neighboring subunits but nonetheless shows the same thresholding behavior.<sup>89</sup> Multivalent interactions begins with an initial intermolecular binding event. All subsequent binding events can be considered intramolecular interactions since the multivalent host and guest molecules are confined together, typically resulting in more favorable binding events after the first initial binding event. However, because thresholding behavior is observed in both cooperative and multivalent systems, it remains a significant challenge to differentiate the two effects. Moreover, many biological systems or model complexes are simultaneously multivalent and co-operative (Figure 3.1c), further complicating the ability to understand the chemical mechanisms that underlie their behavior. A deeper understanding of these phenomena are important for the development of synthetic systems that display a high degree of thresholding.

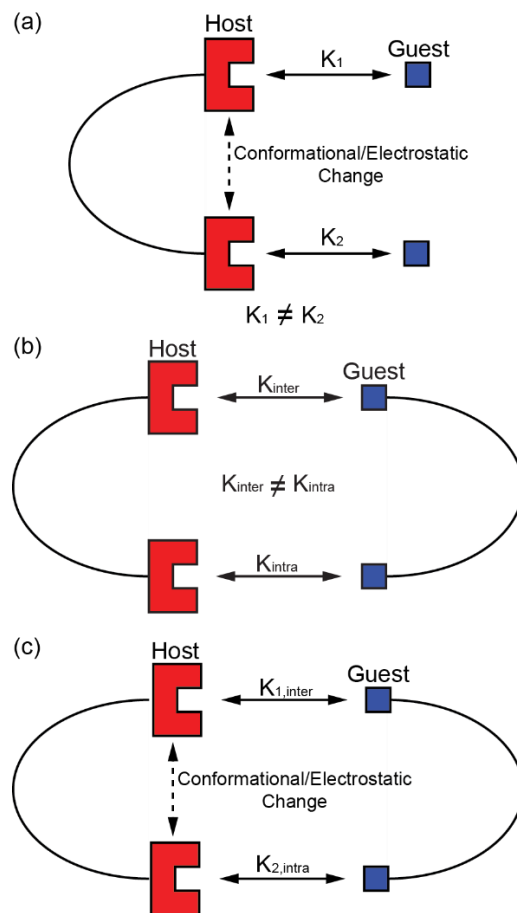


Figure 3.1 Cooperativity and Multivalency. a) A model of a cooperative system. b) A model of a multivalent system. c) A model of a cooperative and multivalent system.

### 3.3. Background

Cooperativity was first discovered by Christian Bohr in 1904 in his studies of the oxygen-hemoglobin disassociation curves, discovering that oxygen binds to hemoglobin in a highly nonlinear fashion.<sup>90</sup> The intricacies as to how this effect took place were discovered much later, but this idea that molecules can “sense” and

respond to binding events to make subsequent binding events more or less favorable revolutionized the understanding of how bio-materials bind to substrates.<sup>88</sup>

In 1910, Hill developed a theoretical model to quantify the cooperativity effect:

$$\log\left(\frac{\theta}{1-\theta}\right) = n \log[L] - \log K_d$$

Equation 3.1 Hill Equation.

By plotting  $\log(\theta/(1-\theta))$  vs  $\log[L]$ , a linear curve is observed with the slope of the curve (denoted as  $n$  in the Hill equation) determining whether the binding relationship under study displays cooperativity. A slope of 1 denotes the system was noncooperative, a slope greater than 1 denotes the system is positively cooperative, and a slope less than 1 denotes a system is negatively cooperative.<sup>91</sup> Hill plots see continued use to study cooperative binding today.<sup>88</sup>

Given the utility of cooperativity as demonstrated by biological systems, much work has been dedicated into replicating these behaviors artificially. However, it remains unclear how to purposefully and explicitly instill cooperativity in those systems. Early reports of artificial cooperativity were later proven to be incorrect. Jean-Marie Lehn<sup>92</sup> and Harry Anderson<sup>93</sup> independently reported systems that allegedly self-assembled through a cooperative mechanism. These systems demonstrated thresholding behavior between disassembled and assembled states, and their resultant Hill plots showed slopes greater than 1. As a result, these systems

were declared to be artificial systems that assembled cooperatively. However, Gianfranco Ercolani demonstrated mathematically that the detected thresholding was actually due to multivalency, not cooperativity. Ercolani further demonstrated that the Hill plot was not applicable to systems with multivalent interactions, i.e., a large portion of self-assembling systems.<sup>94</sup>

Over the next decade, the understanding of how cooperative systems and multivalent systems function has increased with new models to characterize these systems.<sup>88, 89</sup> These systems are characterized by determining the extent to which they cause thresholding behavior ("ΔΔG"). The equations change depending on the number of binders the system possesses, but useful information can be acquired through study of the simplest cooperative and multivalent systems displayed in Figure 3.1a and b respectively. The multivalent system can be characterized through the following equation:

$$\Delta\Delta G = -RT\ln(EM),$$

Equation 3.2 Thresholding Behavior Caused by Multivalency

where R is the gas constant, T is the temperature, and EM is the "effective molarity constant," which is a ratio of the intramolecular binding constant and the initial intermolecular binding constant  $\left(\frac{K_{\text{intra}}}{K_{\text{inter}}}\right)$ .

The cooperative system can be characterized through a similar equation:

$$\Delta\Delta G = -RT\ln(\alpha),$$

### Equation 3.3 Thresholding Behavior Caused by Cooperativity

where EM is replaced with the cooperativity coefficient ( $\alpha$ ), which is a ratio of the second binding event affected by cooperativity and the initial binding event before cooperativity  $\left(\frac{K_2}{K_1}\right)$ .

More complicated systems are studied through the same equations but involve additional terms to quantify each additional binder present. However, there is still significant difficulty understanding how to characterize systems that exhibit both cooperative and multivalent mechanisms. By observing the simplest example of a multivalent and cooperative system displayed in Figure 3.1c, one might predict that  $\Delta\Delta G$  can be calculated by summing the effects of multivalency and cooperativity through the following equation:

$$\Delta\Delta G = -RT\ln(EM) - RT\ln(\alpha)$$

### Equation 3.4 Thresholding Behavior Cause by Both Multivalency and Cooperativity

While this equation is not necessarily theoretically inaccurate, it is now impossible to separately calculate EM and  $\alpha$  since both depend on the change in binding constants *only* due to either multivalent or cooperative effects. A new

mathematical model is necessary to differentiate cooperative and multivalent effects to determine exactly how much each effect affects the resulting thresholding behavior.

Much of the difficulty around creating a new model centers around not having a model system to study to understand how to differentiate cooperative and multivalent effects. Many of the systems recognized as being multivalent and potentially cooperative are biological, which are difficult to modify, and it remains a challenge to design synthetic cooperative systems. Ideally, a system with specific, programmable interactions that can be changed in predictable and measurable methods can be found that enables systems to become multivalent or cooperative. Fortunately, such a system has been developed over the past two decades: DNA-mediated nanoparticle assembly.

DNA is the pinnacle of supramolecular chemistry, displaying specific, programmable interactions based on the sequence of nucleotide bases it displays.<sup>95</sup> Due to its major biological importance, DNA was heavily studied and through the decades of study, tools were designed to modify biological DNA and even completely synthesize artificial strands of DNA.<sup>95</sup> As a result, DNA became a tool that could be used to design programmable, specific interactions in artificial systems.<sup>28,96</sup>

One of the first instances where DNA was used to instill specific interactions between nanoparticles was in 1996 by Chad Mirkin.<sup>97</sup> Mirkin used DNA strands modified with a thiol group on the 3' end to anchor DNA strands to 13-nm gold

particles so that the DNA strands extended orthogonally from the surface of the gold.<sup>98</sup> The loading of the DNA to the surface of the gold was accomplished through the steady increase of the ionic strength of the solution during the reaction to screen the charges of the polyanionic DNA strands so that they could pack closer together on the surface of the particle. This resulted in densely functionalized gold nanoparticles that were stable in solution. The introduction of a linker strand to the solution that bound to the solution-presenting DNA strands on the surface of the particle allowed the particles to extend self-complementary “sticky end” sequences that allowed the particles to form aggregates of DNA-functionalized particles.<sup>97</sup> Later work further developed this technique allowing the formation of superlattices with long-range order from these DNA-functionalized gold nanospheres.<sup>99,100,101,102,103,104,105</sup> These superlattices exhibited sharper transitions from disassembled to assembled particles than expected and had higher melting temperatures than would be predicted from the observation of an isolated interaction between two sticky ends of the same size.<sup>39,106,107</sup> These observations are now understood to be due to the high density of DNA ligands on the surface of the particle assembling particles through multivalent interactions.

The structures formed by DNA-functionalized spheres are primarily cubic lattices with lower symmetry lattices more difficult to achieve. A method to achieve lower symmetry lattices that has been extremely successful has been to use lower symmetry nanoparticles. Lower symmetry nanoparticle cores provide directionality to the DNA bonds that form, resulting in superlattices with corresponding lower

symmetry.<sup>17</sup> The structure of these superlattices could be predicted by determining which structure could maximize the number of DNA hybridization events. Assuming the number of DNA sticky ends presented is directly related to the surface area of the underlying gold nanoparticle, whatever superlattices had the highest surface-area contact are the most favorable superlattices to form. This model (known as the complementary contact model [CCM]) has been largely confirmed through experimental evidence and can be used predictively as well.<sup>101,108,109,17</sup> The work with DNA-mediated nanoparticle superlattices has provided a system with highly programmable interactions that can be used to tailor systems in a reliable and predictable way in order to study the thermodynamics of assembly. The high degree of control enabled by DNA-mediated nanoparticles will allow for controlled modifications to the system to probe how cooperativity and multivalency affect the DNA assembly.

Over the decades since Mirkin first developed DNA-functionalized particle assembly, multiple groups have developed models to quantify and predict the exact  $T_m$  and sharpness of the melting curve (quantified as the full-width of the derivative of the melting curve at half the maximum value, otherwise known as full-width at half-maximum or FWHM). These models often can extremely accurately explain the data they were derived from, but often fail to explain the melting curves of other DNA-functionalized particles. Ultimately, more understanding is needed to understand these sharp transitions and what roles multivalency and/or cooperativity play.



### 3.4. Results and Discussion

In order to differentiate multivalent and cooperative effects, a well-controlled system must be used that displays multivalency and cooperativity but can be modified to suppress cooperativity without significantly affecting the overall thermodynamics of binding. The experimental system used to accomplish this task consists of plate-like gold nanoparticles<sup>14</sup> (Figure 3.2a inset) functionalized with DNA molecules.<sup>17</sup> Because double stranded DNA (dsDNA) is considerably more conformationally rigid than single stranded DNA (ssDNA) (persistence length of ~50 nm vs. ~1 nm, respectively)<sup>95</sup> the presence or absence of a “duplexer” strand allows for control over the conformational freedom of the ligands. If the particles present sticky ends associated with dsDNA (Figure 3.2b), the particle-particle binding will be purely multivalent, i.e. the ligands are rigid before and after the particle interaction. On the other hand, if the particle presents sticky ends associated with ssDNA (Figure 3.2c), the particle-particle binding will be multivalent and potentially cooperative, as initial sticky-end binding events could have the opportunity to electrostatically and/or conformationally influence neighboring binding events. By monitoring the assembly of these particles as a function of temperature with and without the DNA duplexer present, the thermodynamics of multivalent vs. cooperative binding could be deconvoluted. Since the ssDNA and dsDNA modified particles present the same number of sticky ends for hybridization, it can be hypothesized that they will maintain a similar particle-particle binding enthalpy between the two cases while

allowing for differences in particle-particle binding entropy to be interpreted as cooperative effects.<sup>39</sup>

The disassembly of DNA-modified particles as a function of temperature can be monitored optically as a result of the large light absorption and scattering properties of gold nanoparticles.<sup>85,86</sup> Both the ssDNA- and dsDNA-functionalized particles show a sharp increase in the singlet fraction (percentage of particles that are not assembled) with increasing temperature (Figure 3.2a), exhibiting the thresholding behavior diagnostic of strong collective binding interactions. Two additional features of these data are noteworthy and relevant to multivalent vs. cooperative interactions. First, the temperature at which the dsDNA particles disassociate is considerably higher than the temperature at which the ssDNA particles disassociate. This is due to the larger reduction in conformational entropy upon particle-particle binding for the more flexible ssDNA. In other words, because the dsDNA is rigid both before and after particle-particle binding, the entropy cost is approximately 0; this is not the case for the ssDNA system. The second interesting feature of these data is that the disassociation transition occurs over a narrower range of temperatures for the ssDNA case compared to the dsDNA case. This can be quantified by measuring the full-width half-maximum of each transition, which reveals a value of  $0.7 \pm 0.2$  °C (n=13) for the ssDNA and  $2.8 \pm 0.8$  °C (n=18) for the dsDNA (Fig. 3.3). Under the assumption that the dsDNA and ssDNA systems have the same particle-particle binding enthalpy, the sharper transition of the ssDNA case must be due to the emergence of cooperative binding. These data show the ability for

oligonucleotide ligands to imbue inorganic nanoparticles with highly non-linear interactions that will be important for introducing reconfigurable properties into self-assembled systems.

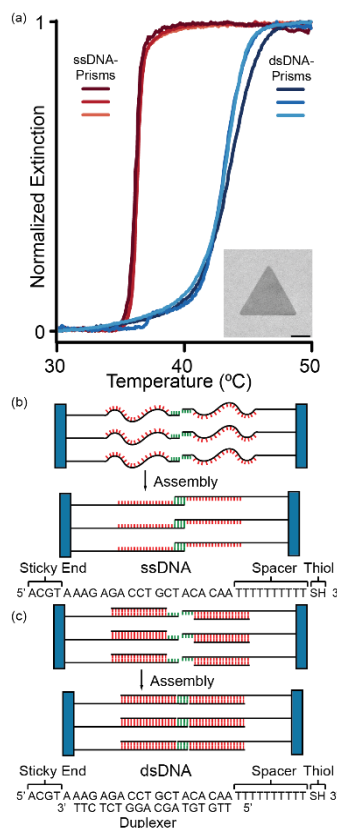


Figure 3.2 Self-Assembling Prisms through Single-Stranded and Double-Stranded DNA. a) UV-Vis extinction spectra showing differences in binding with ssDNA and dsDNA-functionalized prisms. Inset: TEM image of a Au nanoprism (scale bar: 50 nm). b) A model demonstrating the flexibility of ssDNA conformational change before and after binding along with the DNA design. c) A model demonstrating the rigidity of ssDNA on the surface of prisms before and after binding along with the DNA design.

One potential mechanism involving cooperativity to explain the higher degree of thresholding behavior observed with the ssDNA particles (Fig. 3.4a) involves

cations encouraging outstretched DNA conformations, thus preorganizing the system to assemble. It is known that the backbone of DNA consists of an array of negatively charged phosphate groups, most of which are accompanied by strongly-coordinated cations. The hypothesis for the onset of cooperativity is that when an initial ssDNA sticky end – sticky end binding event occurs, the linked strands will adopt a more outstretched, linear conformation than before they were bound. Because this more outstretched strand will bring with it an array of positively-charged coordinated cations, the neighboring strands will experience an attractive electrostatic interaction (or at least a reduced electrostatic repulsion from the neighboring DNA strand) encouraging them to also adopt more outstretched conformations.<sup>110</sup> This preorganization of adjacent, unbound strands into conformations more favorable for binding will increase their binding constant, thus giving rise to positive cooperativity.

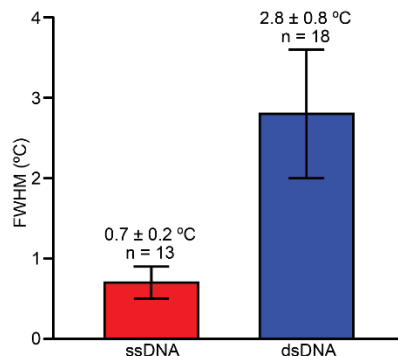


Figure 3.3 Assemblies with ssDNA Yield Sharper Transitions. A bar graph comparing the average FWHM of disassembly for both ssDNA-functionalized prisms and dsDNA-functionalized prisms.

There is another possible mechanism that can be used to explain the differences between these systems. While DNA is not the most flexible of polymers, it is still possible for the particle-bound DNA to adopt numerous configurations. These configurations will be explored stochastically but certain events might increase the lifetime with which the strands remain in specific configurations. With the current self-complementary DNA design, while interparticle interactions would be favorable due to sterics, intraparticle interactions are still likely possible. Such intraparticle interactions would encourage the DNA to remain relatively outstretched such that it might be preorganized to form more favorable interparticle hydrogen bonds once diffusion of the particles allows for it (Fig. 3.4b). This effect would be less of a cooperative mechanism and probably more likely observed as enhanced multivalency since while we are not increasing the number of binders, we are increasing the probability of having multiple binding events between two particles.

Both ssDNA- and dsDNA-functionalized particles would probably display this behavior in some way, but the effect would be much greater for ssDNA-functionalized particles due to the significantly higher flexibility of ssDNA and as a result, a significantly lower steric penalty to the initial intraparticle binding events.

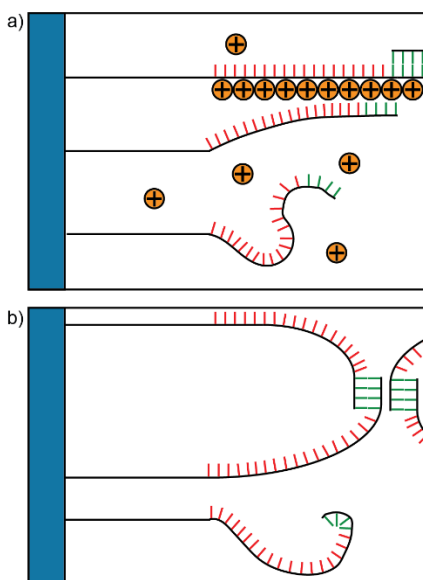


Figure 3.4 Potential Mechanisms Leading to Enhanced Thresholding Behavior of ssDNA-Functionalized Prisms. a) A model illustrating the hypothesis that an array of cations organized to the phosphate backbone of a hybridized sticky end encourages the hybridization of neighboring strands. b) A model illustrating the hypothesis that the formation of intraparticle loops preorganize the DNA such that the formation of sticky end interactions between particles is encouraged.

To test these proposed mechanisms, the systems under study must be modified such that one mechanism is primarily enhanced over the other. To test the first mechanism, assembly of ssDNA- and dsDNA-functionalized particles was

performed in the presence of LiCl as opposed to NaCl. Li<sup>+</sup> ions are smaller than Na<sup>+</sup> ions, and as such can pack more densely around the phosphate backbone.<sup>95</sup> This should enhance the observed cooperativity effect since there is a more dense collection of charge that can preorganize the neighboring strands. Upon performing this experiment, both ssDNA- and dsDNA-functionalized particles demonstrated an increased  $T_m$ . (Table 1) This is explained by the denser packing of Li<sup>+</sup> about the phosphate backbone reducing electrostatic repulsion and thus further stabilizing the assemblies (Fig. 3.5). However, while both ssDNA- and dsDNA-functionalized particles demonstrated a lower average FWHM, there was a larger spread, resulting in their data not being statistically significant than the average FWHM of the assemblies made in NaCl (Table 2).

Table 3.1 Average  $T_m$  of DNA-Functionalized Nanoprism Assemblies Under Various Conditions.

	140 nm prisms 500 mM NaCl	100 nm prisms 500 mM NaCl	100 nm prisms 500 mM LiCl
<b>ssDNA</b>	36.9 ± 0.1 °C	36.3 ± 0.1 °C	40.3 ± 0.8 °C
<b>dsDNA</b>	46.5 ± 0.4 °C	44 ± 1 °C	48 ± 2 °C

Table 3.2 Average FWHM of Melting of DNA-Functionalized Nanoprisms

	140 nm prisms	100 nm prisms	100 nm prisms
	500 mM NaCl	500 mM NaCl	500 mM LiCl
ssDNA	$0.8 \pm 0.1$ °C	$0.8 \pm 0.1$ °C	$0.6 \pm 0.3$ °C
dsDNA	$3.0 \pm 0.3$ °C	$3.4 \pm 0.6$ °C	$2 \pm 1$ °C

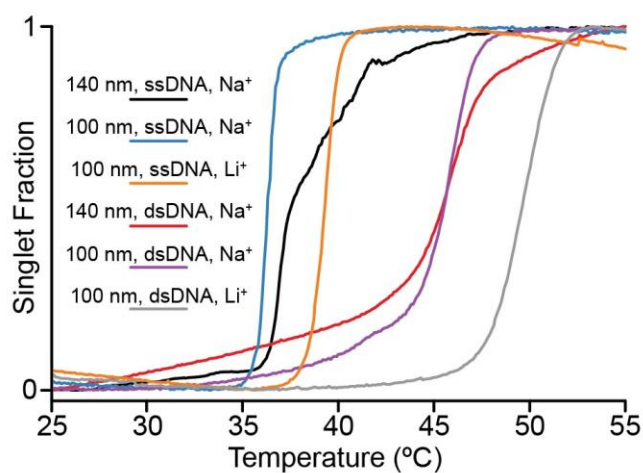


Figure 3.5 Cation Size Affects the Observed  $T_m$  in Assembled Nanoprisms. Melting curves of ssDNA-functionalized nanoprisms and dsDNA-functionalized prisms utilizing different-sized prisms and cations.

Since the previous experiment was inconclusive with regards to the cooperative mechanism, an additional experiment was proposed to test the mechanism of enhanced multivalency by intraparticle binding events leading to preorganization of DNA. The simplest experiment is to alter the system such that



intraparticle binding events cannot occur and only interparticle binding is allowed. To accomplish this, an alternate DNA system is used where the DNA is complementary, not self-complementary. As a result, no intraparticle binding events can occur so any enhanced thresholding behavior from ssDNA-functionalized particles compared to their dsDNA-functionalized counterparts must be due to the cooperative mechanism.

Unfortunately, despite numerous attempts to accomplish this experiment and to test more assemblies with LiCl to get stronger statistical data, further work assembling DNA-functionalized particles proved unreliable and unreproducible. The reason for this learned late into my tenure was evidently caused by a faulty purified water system leading to biological material contaminating the water that the particles were synthesized, functionalized, and assembled in. Due to the unpredictability of these experiments, no further direct data was able to be obtained. However, further data analysis still enabled certain insights.

One of the more recent and detailed models to explain the melting curves of DNA-functionalized particles was developed by Chaikin *et al* in 2010.<sup>111</sup> This model posits that rather than being two separate parameters,  $T_m$  and FWHM are related. The equation used to describe this relationship is as follows:

$$\partial T^1 = \left( \frac{\sqrt{2}-3}{7} \right) \left( \frac{z}{2} \right) N_p \left\{ \left[ 1 + \left( \frac{2 - \sqrt{2}}{A_w C} \right)^{\frac{2}{z}} \right]^{\frac{1}{N_p}} - 1 \right\} \left( \frac{A_w C}{2 - \sqrt{2}} \right)^{\frac{2}{z}} \left[ 1 + \left( \frac{2 - \sqrt{2}}{A_w C} \right)^{\frac{2}{z}} \right]^{\frac{1}{N_p}} \frac{\Delta H^0}{RT_m^2}$$

Equation 3.5 Chaikin Model for Determining FWHM from  $T_m$

In this equation,  $N_p$  is the number of potential bonds that can be formed,  $z$  is the coordination number of the assembly,  $\delta T$  is the FWHM,  $A_w$  is the “wiggling area” or the area that a particle in an aggregate or assembly can move while remaining bound,  $C$  is the total concentration of assembling particles, and  $\Delta H^0$  is the enthalpy of the free DNA in solution. While this equation works excellently with the data set from which the equation was developed, it cannot be applied to understand the difference between the ssDNA-functionalized prisms and dsDNA-functionalized prisms observed experimentally in this work. To explain the nearly 2 °C sharper FWHM observed in ssDNA-functionalized prisms compared to their duplexed counterparts, this equation predicts there must be a nearly 200 °C difference in  $T_m$ . While there is a noticeable difference in  $T_m$  (approximately 8 °C in both  $\text{Na}^+$ - and  $\text{Li}^+$ -induced assemblies), the increased thresholding behavior must have a different cause not factored into the development of this model.

While no models exist that can successfully model all aspects of these melting curves, it is possible more data can be gathered from the melting curves themselves to gain insight into what happens on the molecular level to cause this phenomenon.

The linear form of the van 't Hoff equation (shown below) can be used to determine thermodynamic quantities (specifically the enthalpy and entropy) of a chemical reaction.<sup>112</sup>

$$\ln(K_{eq}) = -\frac{\Delta H}{RT} + \frac{\Delta S}{R}$$

### Equation 3.6 Linear Form of the van 't Hoff Equation

In this equation,  $K_{eq}$  is the equilibrium constant of the reaction,  $R$  is the universal gas constant,  $T$  is temperature,  $\Delta H$  is the enthalpy change of the reaction, and  $\Delta S$  is the entropy change of the reaction. By plotting  $\ln(K_{eq})$  vs.  $1/T$ , a line is formed from the data where the slope is equivalent to  $-\Delta H/R$  and the intercept is equivalent to  $\Delta S/R$ . By normalizing the melting curves, the y-axis can instead be considered a singlet fraction ( $f$ ) rather than extinction. Similarly, a mathematical relationship can be determined equating the singlet fraction to  $K_d$ , the collective equilibrium constant for the release of a single nanoparticle from an aggregate. While the exact derivation of this equation is beyond the scope of this work, Macfarlane *et al* has demonstrated it in their recent work.<sup>113</sup> The equation is as follows:

$$f = \frac{1}{1 + \frac{1}{K_d}}$$

Equation 3.7 Correlation Between Singlet Fraction and Collective Equilibrium Constant

Thus, the data obtained from a melting curve can be plotted as a van 't Hoff plot (3.6a) such that the enthalpy and entropy of disassembly can be determined. When the melting curves collected are analyzed in this way, multiple patterns are observed. Compared to dsDNA-functionalized particles, there is approximately a three times increase in entropy on average upon dissolution for ssDNA-functionalized particles (Fig. 3.6c). This fits with literature precedent that ssDNA-functionalized particles have a much higher entropic cost to assembly due to the loss of configurational freedom of the flexible single-stranded DNA upon hybridization. Furthermore and perhaps more relevantly, there is an approximately three times greater loss of enthalpy on average upon of disassembly for ssDNA-functionalized particles as opposed to their dsDNA-functionalized counterparts (Fig. 3.6b). This renders our initial assumption that the enthalpy of binding between ssDNA- and dsDNA-functionalized particles would be similar completely incorrect. Since the only contribution to the enthalpy of dissolution should be the breaking of sticky end interactions, it can be inferred that ssDNA-functionalized particles have approximately four times the number of sticky end bonds compared to dsDNA-

functionalized particles. This is unexpected as the presence of the duplexer strand does change the number of sticky ends on the surface of the particles, and so one would not typically expect a large difference in the number of sticky ends available for hybridization.

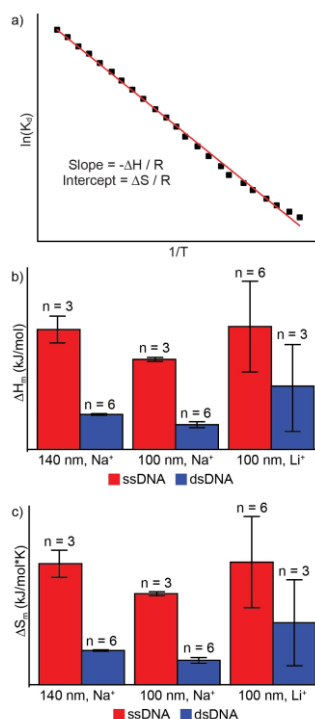


Figure 3.6 van 't Hoff Analyses of Prism Disassembly. . a) An illustration of a van 't Hoff plot. b) The enthalpy of disassembly of various systems of self-assembled DNA-functionalized prisms. determined through van 't Hoff plots. c) The entropy of disassembly of various systems of self-assembled DNA-functionalized prisms. determined through van 't Hoff plots.

The exact reason for this larger number of interactions is not entirely clear, but the simplest explanation could simply be that the greater flexibility of the ssDNA

allows for a greater ability to maximize the number of DNA hybridization events. Meanwhile, it is possible that the duplexed DNA is prevented from certain hybridization events due to the relative stiffness of the dsDNA. It should also be noted that this observation does not necessarily disprove the possibility of the other two potential mechanisms, although those other mechanisms would probably be observed as more of an entropic effect as they both rely on preorganization of the DNA strands. Ultimately, more experimental data must be gathered or molecular modeling performed to fully understand every aspect of the thermodynamics of this system, but we can certainly conclude that a significant portion of the increased sharpness observed in disassembly of ssDNA-functionalized prisms is due to the increased multivalency of the system despite not actually increasing the number of sticky ends in the system.

### **3.5. Methods**

#### **3.5.1. Nanoparticle Synthesis and Purification**

Gold triangular prisms were synthesized following the protocol established by Jones *et al.*<sup>114</sup> Briefly, gold seed particles are synthesized in water by first combining 250  $\mu\text{L}$  10 mM  $\text{HAuCl}_4$  and 500  $\mu\text{L}$  10 mM sodium citrate in 18.95 mL of water. Then, 1 mL of ice cold 0.01 M  $\text{NaBH}_4$  was added quickly to cause burst nucleation. The entire solution was then heated between 40-45  $^\circ\text{C}$  to decompose excess  $\text{NaBH}_4$ . The solution was then allowed to cool to room temperature and the seed concentration was

determined through UV-Vis spectroscopy. Seed particles were then added to a growth solution consisting of 50  $\mu\text{M}$  NaI, 0.05 M cetyltrimethylammonium bromide (CTAB), 0.267 mM  $\text{HAuCl}_4$ , 0.535 mM NaOH, and 0.535 mM ascorbic acid. The amount of seed particles added determines the size of the prisms, as determined by Jones *et al.*<sup>114</sup>

To purify spherical byproducts from the triangular prisms, NaCl was added to the solution to cause depletion assembly. The exact concentration of NaCl needed to ensure this depends on the size of the prisms, as determined by Jones *et al.*<sup>114</sup> After depletion assembly, the prism assemblies can be separated from the spherical particles by gentle centrifugation and removal of supernatant. This process can be repeated 2-3 times or more as needed to ensure a high level of purity, as determined by the difference in  $\lambda_{\text{max}}$  observed in the UV-Vis spectra of nanospheres and nanoprisms.

### 3.5.2. DNA Functionalization

Both oligonucleotide sequences (see Figure 3.2b) used in this work were purchased specially from Integrated DNA Technologies and used without further alterations. Particles were functionalized in accordance with a protocol as established by Jones *et al.*<sup>114</sup> In short, solutions of the thiolated oligonucleotide were treated with dithiothreitol (DTT) to ensure breakage of any disulfide bonds and purified via a desalting column. These solutions were then added to solutions of nanoprisms that had been spun twice in water from their native 0.05 M CTAB stock solution to ensure a minimal amount of CTAB that could prevent ligand replacement. After about 30

minutes, the solutions were brought to 0.1% SDS and 0.01 M phosphate buffer (pH = 7.4) and raised to 40 °C. These solutions were then slowly raised to 0.5 M NaCl with periodic sonication over the course of about 3 hours, and then left to finish functionalization overnight. The then-functionalized particles were spun down three times and redispersed in 0.01% SDS.

### 3.5.3. DNA Assembly

Assembly experiments were performed in a stirring cuvette in a Cary 5000 UV-Vis\_NIR Spectrophotometer with a temperature-controlled cell-changer attachment. Solutions were made at 1 mL volumes and contained approximately 0.1 OD DNA-functionalized nanoprisms, 500 mM NaCl or LiCl, 0.01% SDS, and 0.01 M phosphate buffer (pH = 7.4). Certain solutions had 0.1  $\mu$ L of 100  $\mu$ M duplexer DNA added to ensure the DNA became duplexed during the assembly process. The cuvettes were then monitored at the  $\lambda_{\text{max}}$  of the DNA-functionalized nanoprisms used as the solutions were carefully cooled from 50 °C to 15 °C and then heated again from 15 °C to 50 °C at a consistent rate of 0.1 °C/min. (The exact temperatures used varied depending on the experiment, but this was typical.) The extinction of each cuvette was recorded in increments of 0.1 °C.

### 3.5.4. $T_m$ and FWHM

Raw data was pasted into Origin, normalized, and differentiated. The resulting peak function was then trimmed to only display the peak (the area of the curve where



the transition occurred) and then fitted to a Gaussian in Origin's software. From this fitted curve, the peak could be determined (and was recorded as the  $T_m$ ) and the FWHM was calculated.

### 3.5.5. van 't Hoff Analysis

The transitional area of the melting curve was normalized before a plot was formed of  $\ln(K_d)$  vs.  $1/T$ , using the relationship determined by Macfarlane *et al*<sup>113</sup> to translate the extinction values to  $K_d$  and converting the temperature values from °C to K. From these plots, the slope was determined to be  $-\Delta H/R$  and the intercept was determined to be  $\Delta S/R$  (as explained in the Results and Discussion section). Multiplying by  $-R$  and  $R$  respectively gave values in kJ/mol and kJ/(mol\*K) respectively.

## 3.6. Conclusion

Cooperativity and multivalency are ubiquitous concepts in molecular biology and biochemistry.<sup>115,116,117</sup> Despite that, there is still a great deal of work left to adapt these mechanisms into synthetic systems. While assembled systems of DNA-functionalized particles have long been recognized to have sharp transitions, this work demonstrates that there is still much more work to be done. No current models can explain the extremely sharp melting response in these ssDNA-functionalized prisms, but we can demonstrate that this effect largely comes from enhanced multivalency compared to their duplexed counterparts. The melting response

observed is highly non-linear, as the assembled nanoparticles are able to dramatically alter their structure and subsequent optical properties over a temperature range of less than 1 °C. The mechanistic and practical understanding achieved from this project will enable the design of new reconfigurable nanomaterials, capable of enormous changes in structure and properties in response to external stimuli due to the nonlinearity of these interactions. The hope is that in the future other researchers will be able to take the findings from this study and leverage them to even greater functionality, such as the development of nonequilibrium systems. However, even through greater discoveries in synthetic and functionalization techniques, such nonequilibrium systems still represent other difficulties for researchers to overcome.

## Chapter 4

## Measuring Challenges in Dynamic and Nonequilibrium Nanoscale Systems<sup>2</sup>

### 4.1. Abstract

Biological systems exhibit strikingly sophisticated properties including adaptability, directed motion, regulation, and self-organization. Such systems are often described as being “non-equilibrium” or “out-of-equilibrium” and it can be instructive to think of them as adopting thermodynamic states that require a constant supply of energy to maintain. Despite their ubiquity, systems that demonstrate these

---

<sup>2</sup> This chapter was originally published as a perspective in *Analytical Chemistry* in 2019. It has been reproduced with permission from Marolf, D. M.; Jones, M. R. Measurement Challenges in Dynamic and Nonequilibrium Nanoscale Systems. *Anal Chem* **2019**, *91* (21), 13324-13336. DOI: 10.1021/acs.analchem.9b02702. Copyright 2019 American Chemical Society.

abilities require a remarkably stringent set of chemical requirements to exist. Broadly speaking, they must be (a) capable of consuming some external source of energy that (b) acts as a fuel to do some form of work, (c) all while maintaining highly organized structural features at the nanometer length scale that persist in space and over time. It remains a grand challenge in the field of chemistry to synthesize artificial systems capable of similarly complex non-equilibrium behavior both as a means for greater fundamental understanding and as a way to imbue non-natural structures with dynamic behavior for various applications. Yet an oft-overlooked challenge in this field involves not just the synthesis of non-equilibrium materials but also their characterization. The requirements for measuring nanometer-scale systems of non-equilibrium building blocks with the appropriate temporal and spatial resolution are demanding and have heretofore been largely unavailable to researchers. In this perspective we highlight challenges and recent advances in the measurement of dynamic nanoscale systems. We argue that progress in this area is crucial and must occur in parallel to synthetic goals if any meaningful understanding is to occur.

## **4.2. Introduction**

In the study of ordered non-equilibrium systems (Fig. 4.1a) and their behavior over time, there is often the goal of discovering and understanding so-called “emergent properties”, often defined aphoristically as occurring when “the whole is greater than the sum of its parts”.<sup>118</sup> When an object (molecule, particle, protein) behaves one way in isolation but exhibits some new behavior when present as a

member of a collection of objects, that new behavior is said to “emerge” from the system (Fig. 4.1b).<sup>119</sup> Since these properties only arise when a multitude of members are acting in concert, it is often difficult to predict their appearance even with a detailed understanding of the structure and function of the individual monomers.<sup>120</sup> The emergent property is thus the product of a non-obvious or non-linear accounting of the properties of the isolated building blocks. One excellent example of such a property is flocking or swarming behavior<sup>121</sup> – the individual members when isolated may move according to one set of rules, but when present as a collective, exhibit some new (emergent) group-wide behavior.<sup>122</sup> Although not a requirement, a great number of fascinating emergent properties have been observed in systems that are operating out-of-equilibrium,<sup>123 124</sup> including homeostatic self-regulation, adaptability, spontaneous symmetry breaking, and various forms of self-organization.<sup>120 125</sup>

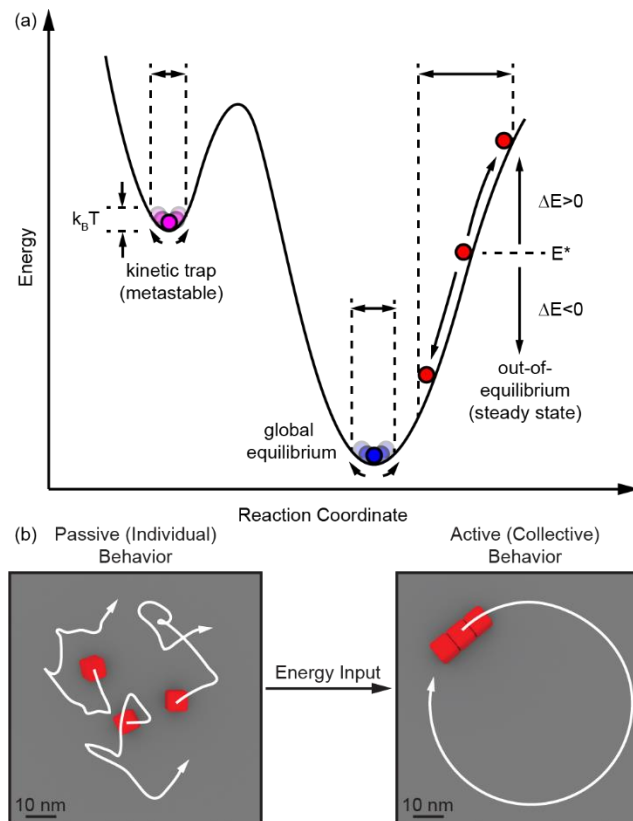


Figure 4.1 The Advantage of Dissipative Processes. a) A simplified, hypothetical energy diagram indicating the difference between global equilibrium, metastable kinetically trapped, and energy-dependent out-of-equilibrium states. In this framework, the out-of-equilibrium state has the unique property of being able to explore a wide range of reaction coordinate space with a relatively small input of energy. (b) Illustration of the difference between passive diffusive behavior of individual nanoparticles and the collective emergent behavior of a hypothetical nanoparticle assembly driven by the input of energy.

The drive to understand emergent properties highlights one of the principle difficulties in measuring non-equilibrium systems. First, by definition, an emergent property arises both from the function of the individual building blocks and from their complex interactions as a collective. Therefore, ensemble characterization

methods, while useful in measuring the behavior of the collective, often do not shed light on how the individual monomers contribute to that collective behavior. Second, these systems must be observed while they are out-of-equilibrium since the property arises only through the consumption and conversion of an energy source. Thus, any characterization tool must be amenable to having some form of energy imparted to the sample while the measurement is taking place. These two requirements place enormous restrictions on the methods that can be used to thoroughly understand systems that exhibit emergent, non-equilibrium, and self-organizing properties.

### **4.3. Why Nano?**

In order to understand the unique role that nanoscience plays in the measurement of dynamic non-equilibrium systems, it is relevant to understand the development of the field and its interdisciplinary nature. In general, two separate fields of research have heretofore simultaneously pursued the goals of non-equilibrium materials largely independent of one another: supramolecular chemistry and colloidal physics.

The supramolecular chemistry approach wields incredible synthetic acumen to design and make molecular constructs that assemble under so-called ‘dissipative’ conditions – those in which ordering is driven by an external fuel source, the energy of which must be released (dissipated) back to the environment, usually in the form of heat.<sup>126 49</sup> Numerous examples of supramolecular building blocks assembling

through the consumption of chemical or photonic energy have shown the formation of dissipative hydrogels,<sup>127</sup> fibers,<sup>128</sup> helices,<sup>129</sup> and more.<sup>130 131 120 48</sup> For example, Van esch and coworkers have shown that molecules with terminal carboxylate groups react with a chemical fuel (MeI) to form esters, resulting in their self-assembly into fibers; the resulting hydrogel slowly undergoes hydrolysis, dissipating the energy back to the environment and disassembling.<sup>128</sup> Sleiman and coworkers also demonstrated the use of light as an energetic stimulus to induce an azobenzene isomerization-based assembly of monomers into rod-like aggregates, which disassembled over time as the azobenzene units reverted to the more stable isomer.<sup>130</sup> These examples leverage the ability for chemists to make systematic structural changes to the molecular building blocks, allowing researchers to test various hypotheses regarding the mechanism of dissipation and the appearance of order under non-equilibrium conditions. However, because time-resolved imaging at the single-molecule level is only possible under highly-specialized circumstances, the characterization of these structures has largely been driven by ensemble-averaged techniques.<sup>48</sup> Consequently, the mechanistic role each individual monomer is playing in the observed non-equilibrium ordering can only be inferred from the average behavior of the monomers as a whole. At times, such an averaging may be appropriate, but in many systems that exhibit emergent properties it does not reveal the entire picture.

The colloidal physics approach, on the other hand, has investigated questions of non-equilibrium ordering and emergent properties at a much larger length scale



than the chemistry community. In general, colloidal particles of 1  $\mu\text{m}$  or larger are modified to generate some form of self-propulsion, typically driven by spontaneous or photocatalyzed chemical reactions that fuel hydrodynamic forces.<sup>132 133</sup> These dynamic particles constitute the building blocks of what is sometimes referred to as “active matter”, and exhibit many fascinating non-equilibrium properties such as swarming,<sup>134 135</sup> self-organization,<sup>136</sup> and emergent chirality.<sup>137 138</sup> For example, Chaikin and coworkers demonstrated photochemically self-propelled colloids that assemble into 2D hexagonally-packed crystals that move collectively, grow, and break into smaller pieces while illuminated.<sup>139</sup> In addition, Granick and coworkers have mapped a rich phase space of magnetic Janus particles that dynamically assemble into microtubes, zigzag chains, and planar sheet morphologies in a precessing magnetic field.<sup>140</sup> Using these systems, analytical models have been developed that help explain the properties of ordered non-equilibrium systems and what emergent properties they exhibit.<sup>141</sup> The productivity of the physics approach is due, at least in part, to the ability for these systems to be monitored at the single-particle level using optical microscopy.<sup>132</sup> Being of a sufficiently large size to be resolved by optical photons means that the behavior of particles individually and as a collective can both be quantified and analyzed with a high degree of accuracy. However, whereas the physics approach is superior in its characterization and analysis, it suffers in synthetic optionality and the complexity of the assembling building blocks. With a few notable exceptions,<sup>142 143 144 145 146 147 148 149</sup> the particles being investigated are primarily spherical, often bearing some partial coating or heterogeneous domain responsible

for the chemical reaction driving self-propulsion. The resulting interactions are therefore largely isotropic, dramatically limiting the complexity of the particle-particle forces necessary to give rise to emergent properties in a collective.

#### **4.4. Perspective**

While investigations into non-equilibrium self-organization from the chemistry and physics communities have been immensely productive, both suffer from drawbacks. Chemists working at the atomic length scale can synthesize virtually any molecule with a rationally designed set of complex interactions, but lack the ability to observe the assembly process at the single-building-block level. Physicists working at the micron length scale have the ability to track single-particle trajectories, resulting in sophisticated models for non-equilibrium behavior, but lack the synthetic versatility to program more complex, anisotropic interactions that are necessary for emergent properties to arise. In this perspective, we propose that studying dynamics at the nanometer length scale offers an attractive compromise. Being intermediate between the two extremes (molecular and micron), nanoparticle building blocks offer a rich synthetic diversity in composition, size, shape,<sup>6</sup> and surface ligand chemistry<sup>150</sup> while at the same time being amenable to real-time single-particle observation given recent advances in a number of imaging methodologies. Furthermore, inorganic nanoparticles often exhibit unusually high optical extinction cross-sections,<sup>85</sup> tunable photoexcited charge carriers,<sup>151</sup> and size-dependent catalytic reactivity,<sup>152</sup> making them ideal structures for absorbing external

sources of energy that is used to drive self-organization processes, a key requirement for non-equilibrium or emergent behavior. Thus, nanoscience rests at an interface that positions it to make significant contributions to this field.

Here, we will discuss the spatial and temporal demands on characterization tools capable of measuring nanoscale dynamic and non-equilibrium assembly processes. We will cover these techniques at or near the resolution boundaries and attempt to highlight what advances might push them to be more useful to the community. This includes what kinds of nanoscale systems they are most useful for, how perturbative they are to the sample, and by what means they allow for the input of chemical fuel or external energy. We then discuss post-processing analysis and image processing tools, many of which are borrowed from the physics community, that can be leveraged to understand these systems. Finally, future directions, particularly those that address inevitable problems of big data, will be considered.

## 4.5. Techniques

In this perspective, we are limiting the discussion to methods capable of in-situ single particle monitoring, as these techniques are best suited to elucidate emergent properties in self-assembling systems. Consequently, there are numerous characterization tools we will not cover in depth that are limited to measuring ensemble averages. These include various forms of optical spectroscopy,<sup>153–35</sup> small- and wide-angle x-ray scattering (SAXS/WAXS),<sup>154–155</sup> NMR,<sup>127</sup> and mass

spectrometry.<sup>128</sup> Such techniques will undoubtedly play an important role in corroborating results from single-particle measurements and have been discussed in excellent review articles elsewhere.<sup>156 157 158</sup>

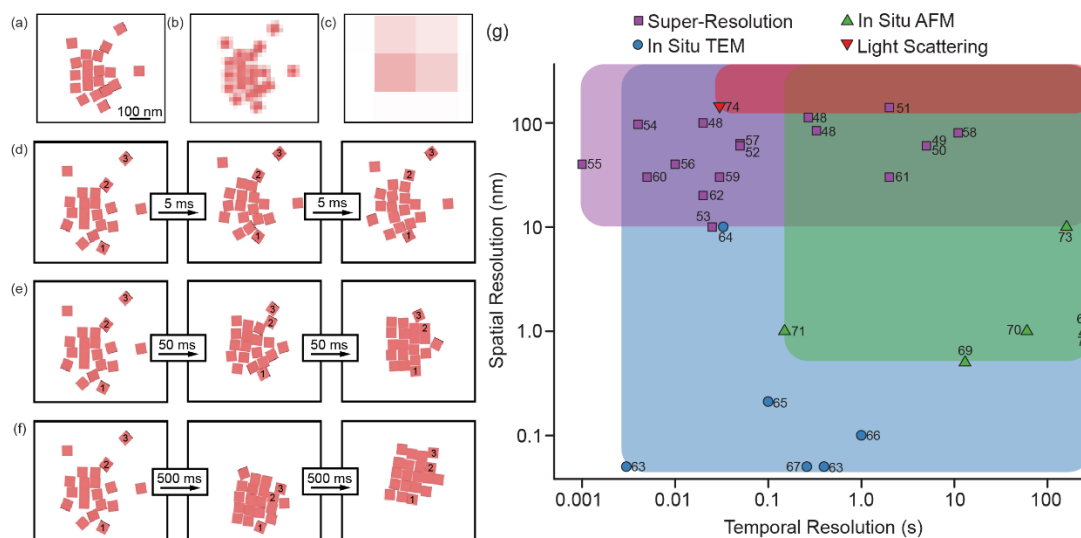


Figure 4.2 Understanding How Spatial and Temporal Resolutions of Instrumentation Limit Systems Able to Be Effectively Studied. (a-c) Simulated image of an assembly of 50 nm cubes imaged at (a) 2.5 nm, (b) 20 nm, and (c) 200 nm spatial resolution. (d-f) A simulation of 50 nm cubes assembling at (d) 5 ms, (e) 50 ms, and (f) 500 ms temporal resolution. Three particles of interest have been labeled (1, 2, and 3) to help track the assembly process. (g) A spatiotemporal map of the single-particle imaging techniques covered in this perspective; data collected from references 161 162 163 164 165 166 167 168 169 170 171 172 173 174 175 176 177 178 179 180 181 182 183 184 185 186 187.

For the purposes of determining whether a characterization tool has the appropriate spatial and temporal resolution to investigate dynamic nanoscale systems, consider the diffusion and assembly of a collection cube-shaped

nanoparticles with an edge length of  $\sim 50$  nm (Fig. 4.2). Although such a particle has a nominal size of 50 nm, the fact that it is non-spherical means that in order to resolve certain single-particle features such as tips and edges, a spatial resolution significantly below 50 nm is necessary. This would be important, for example, in being able to monitor not just the translational motion of the particles, but also their rotation and subsequent orientational ordering. Thus, although certain techniques, such as those that rely on light scattering, are capable of tracking single-particle trajectories, the fact that they are diffraction-limited and have a minimum resolution of  $\sim 200$  nm indicates that they will not be sensitive to the orientational ordering of anisotropic particles in this size range (Fig. 4.2c).<sup>159</sup> We will include discussions of diffraction-limited light scattering tools below, as they can be useful in providing single-particle data, but with an understanding that certain kinds of information, such as orientational ordering, will be impossible to obtain. More powerful are the techniques that can spatially resolve the considered cube-shaped particle below  $\sim 50$  nm such that its geometric features and rotational dynamics can be understood. Super-resolution microscopy makes clever use of the emission of fluorophore labels on nanoscale objects to obtain sub-diffraction-limited images, despite the use of optical photons. Although the spatial resolution of this technique continues to improve, a typical minimum feature size detectable using super-resolution microscopy is  $\sim 20$  nm (Fig. 4.2b). For many systems, this will serve as a powerful tool for understanding single-particle assembly dynamics but nonetheless remains somewhat limiting in that single-particle geometric features are difficult to resolve.

Methods that have adapted transmission electron microscopy (TEM) and atomic force microscopy (AFM) to be compatible with liquid-phase systems provide the greatest spatial resolution of  $\sim 1$  nm or lower, capable of monitoring single-particle translational and orientational assembly processes (Fig. 4.2a).

Equally important to spatial resolution is the necessity for characterization methods to temporally resolve the motion and assembly of nanoscale systems. Considering the same  $\sim 50$  nm cubic nanoparticle, free-space single-particle diffusion is rather fast, with room-temperature motion being on the order of one particle length per 0.1 ms or 500 nm/ms. Temporal resolution of this degree can be considered an upper-bound and in general has yet to be demonstrated with many single-particle techniques. Fortunately, a collection of particles assembling in some way will have considerably slower temporal dynamics, such that several of the techniques mentioned above can provide useful information. Typical in-situ AFM methods suffer in temporal resolution due to the rastering of the cantilever-based tip that constructs images on the order of minutes (Fig. 4.2f).<sup>160</sup> Organizational processes such as crystallization that occur via many repetitive molecular steps may be amenable to in-situ AFM but single-particle dynamics are challenging to observe with this technique. Recent advances in direct electron detectors have pushed liquid-phase TEM into the milliseconds regime, which is sufficient to resolve a number of nanoparticle assembly processes (Fig. 4.2e). However, by far the greatest temporal resolution lies with optical methods, such as super-resolution microscopy, which benefit from decades of time-resolved optical spectroscopic measurements that have driven the development

of detectors and equipment capable of monitoring fast molecular and nanoscale processes (Fig. 4.2d). With these resolution boundaries in mind, we discuss each of the above techniques in more detail, highlighting improvements, specific systems on which they may be most informative, and methods by which external energy may be applied to drive out-of-equilibrium behavior.

#### 4.5.1. In Situ Atomic Force Microscopy

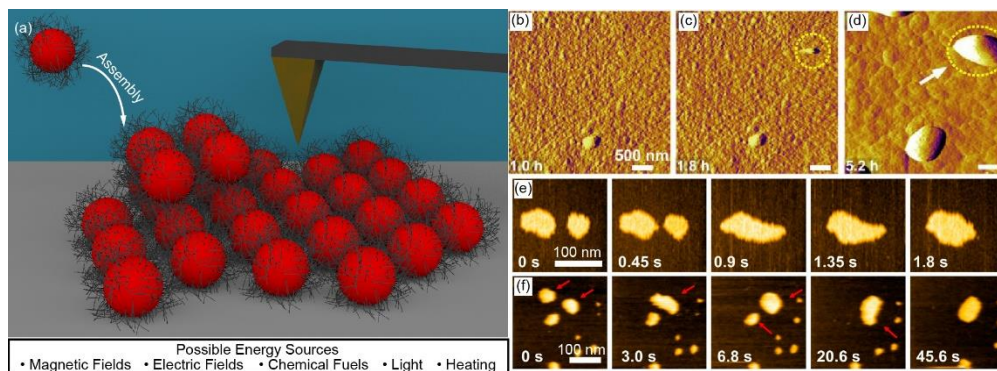


Figure 4.3 Capacity for In Situ AFM to Probe Dissipative Nanoparticle Assembly. a) Illustration of nanoparticle assembly measured through in-situ AFM. The physical interaction between the cantilever and the particles generates image contrast. (b-d) In-situ AFM images demonstrating the growth of zeolite crystals over time. Adapted with permission from ref. <sup>185</sup>. Copyright 2018 Nature Publishing Group. (e-f) In-situ AFM images demonstrating the fusion of lipid-nanodiscs in solution. Adapted with permission from ref. <sup>184</sup>. Copyright 2018 American Chemical Society.

Atomic force microscopy (AFM) has been a stalwart characterization tool for materials and surface scientists for decades. In its conventional implementation, AFM functions through the rastering of a sharp cantilever-based tip across a surface, the motion of which is detected by the reflection of a laser onto a position-sensitive

photodetector.<sup>188</sup> This approach allows for incredibly sensitive measurements of surface topography with recent examples on nanoparticle samples showing a spatial resolution of  $\sim 2$  nm laterally (parallel to the surface) and  $\sim 0.15$  nm axially (perpendicular to the surface).<sup>189</sup>

While traditionally used to study samples *ex situ*, there has been an active effort to extend AFM to study samples *in situ* to observe the structure of biological materials and other sensitive samples in their native, solvated, environment.<sup>182 183 184 186 190 191</sup> This is typically accomplished through use of a fluid cell, which creates an isolated environment for the sample and prevents degradation of sensitive portions of the piezoelectric scanner.<sup>192</sup> *In-situ* AFM experiments can be slightly perturbative when run in contact mode, where the probe makes physical contact with the sample. However, these measurements can be made less perturbative when conducted in amplitude modulation mode, where the cantilever is oscillated at or near its resonant frequency and the amplitude of the oscillation is measured to detect tip-sample interactions. Using this mode, perturbations can be minimized, enabling the study of sensitive systems, such as those composed of soft or biological components. For example, this imaging mode enabled the detection of conformational changes in a single ATPase protein without altering the rate of conformational transition over millions of points of contact with the AFM tip.<sup>190</sup> Thus, when performed correctly, the lack of sample perturbation is an advantage of *in situ* AFM, ensuring that whatever assembly dynamics are observed, they can be generalized to *ex-situ* circumstances.



Due to the extremely high axial resolution of AFM, this technique is best suited to study 2D assembly processes such as the diffusion and attachment of particles to a growing superlattice as adatoms or at step edges (Fig. 4.3a). To date, measurements of this exact circumstance are rare but similar examples and other instructive cases are relatively common. For example, the use of in situ AFM to track the formation of nuclei and observe the layer-by-layer growth of zeolite crystals on a surface shows the ability for this technique to monitor slow but important organization processes such as crystallization (Fig. 4.3b-d).<sup>185</sup> In-situ AFM also benefits from being relatively robust to the introduction of new stimuli to drive the system out of equilibrium during imaging. Since the methodology uses the mechanical actuation of a tip to construct an image, convenient stimuli such as light or time-varying electric/magnetic fields will introduce minimal perturbation to the measurement while simultaneously being able to energetically excite the sample. This approach is exemplified in the work of Masayuki and coworkers who observed the motion of nanomachines on DNA scaffolding under UV irradiation through in-situ AFM.<sup>193</sup> Liquid phase AFM can also monitor changes to a system after introduction of chemical fuels or during the maintenance of a temperature gradient, both of which are frequently used to drive non-equilibrium behavior. For example, Scheuring and coworkers observed how cytoplasmic proteins known as annexins stabilize membranes as buffered  $\text{Ca}^{2+}$  solutions were pumped into the sample chamber.<sup>194</sup> Perhaps more so than any other methodology covered in this perspective, in-situ AFM is amenable to monitoring how systems respond to external stimuli in a manner that

does not negatively influence image acquisition, making it appealing for understanding non-equilibrium responses of nanoparticle systems.

Despite the many advantages of AFM, one major challenge with this technique is that typical temporal resolution is rather poor due to the need to continuously raster the tip to form an image; a high-resolution image will typically take minutes to obtain. Thus far, most examples of in-situ AFM being used to investigate dynamic processes have interrogated systems with relatively slow assembly kinetics. For example, Rimer and coworkers have observed that the growth of the zeolite silicalite-1 occurs over the course of several hours via silica nanoparticle aggregation, structural rearrangement, and finally monomer addition.<sup>195</sup> Recently, improvements to the piezoelectric and photodetector hardware have increased temporal resolution such that full scans can be made in under a second (Fig. 4.3e-f). Using this high-speed hardware, Fukumori and coworkers were able to image the surface of living bacterial cells and track the dynamics of single proteins on the cell surface.<sup>196</sup> Unfortunately, these techniques are not yet widely-implemented.<sup>189</sup> Therefore, future improvements to the temporal resolution of in-situ AFM are needed before it will become a widely used tool in studying far-from-equilibrium assemblies. However, current systems with slow kinetics, such as hours- or days-long nanoparticle crystallization experiments, may benefit greatly from dynamic AFM characterization.

#### 4.5.2. Light Scattering

Although relatively straightforward and common, light scattering is nonetheless a useful tool for studying nanoparticle solutions and may be easily adapted to non-equilibrium experiments. In a typical light scattering experiment, a laser source is passed through a suspension of particles, and the intensity and/or angle of scattered light is detected (Fig. 4.4a). Most often it is assumed that the relevant physical process is Raleigh scattering (where the particle size,  $d$ , is much smaller than the excitation wavelength of light) which exhibits a  $d^6$  dependence on the intensity of scattered light.<sup>197</sup> This powerful dependence on particle size means that techniques based on light scattering can be extremely sensitive, even with small particles or those composed primarily of organic components. When coupled to a microscope where the scattered light is detected with a CCD camera, it is possible to track the motion of individual objects through a technique known as Nanoparticle Tracking Analysis (NTA, Fig. 4.4b).<sup>198 199</sup> Collecting videos of nanoparticle movement in solution allows for calculation of particle concentration and particle size using the Einstein-Stokes equation, assuming motion is Brownian and the viscosity of the medium is known (Fig. 4.4c). Single particle tracking has been shown in structures as small as 30 nm in size,<sup>198</sup> making it potentially useful in monitoring the dynamics of many nanoscale systems. In addition, although there are few examples of stimulus-driven assembly processes observed with light scattering techniques, it is in principle amenable to multiple forms of energy input to support non-equilibrium behavior with minimal perturbation.

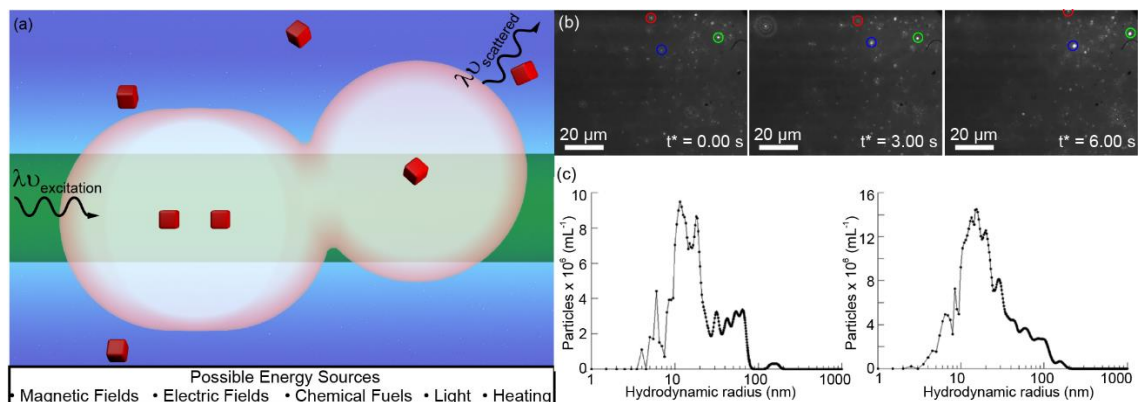


Figure 4.4 Capacity for Light Scattering to Probe Dissipative Nanoparticle Assembly. a) Illustration of the imaging of diffusing nanocubes in solution through light scattering. Particles that approach within a diffraction limit of one another ( $\sim 100 \text{ nm}$ ) cannot be differentiated. b) Frames from a video utilizing nanoparticle tracking analysis to observe the movement and growth of transition metal oxide nanoparticles. Adapted with permission from ref. <sup>203</sup>. Copyright 2011 American Chemical Society. c) Size distributions of two batches of maltoheptaose-*block*-polystyrene nanoparticles formed under different synthetic conditions. Adapted with permission from ref. <sup>204</sup>. Copyright 2013 American Chemical Society.

Despite the simplicity of the technique, several drawbacks prevent light scattering methods from being easily adapted to nanoscale dynamic systems. The primary difficulty lies in the diffraction-limited nature of traditional light scattering techniques that make single-particle tracking and characterization of assembly mechanisms possible only in highly-specialized circumstances. Since single particles can be resolved only if they are further than one diffraction-limit apart ( $\sim 200 \text{ nm}$ ), nanoparticle orientation is difficult, and in most cases, impossible, to detect except through more advanced methods that excite and detect with linearly polarized light.<sup>200 201</sup> More importantly, NTA cannot differentiate an assembly of small

nanoparticles from a single larger particle, assuming both are much smaller than the wavelength of light. Such data can be useful for understanding the kinetics of the organization process but there would be limited direct mechanistic information. Thus, for most nanoparticle-based dynamic systems, light scattering and NTA are most appropriate when used in conjunction with other characterization methods.

Despite the diffraction-limited nature of light scattering, there are several systems where the technique could prove valuable. As mentioned above, light scattering can be used to study the kinetics of assembly of molecular species into nanoscopic objects, such as the formation of inorganic or organic nanoparticles. Edwards and coworkers took this approach to monitor the precipitation of tolinaftate (a poorly water soluble drug) over time as the average particle size, concentration, and overall polydispersity changed, demonstrating the ability for this technique to be used in pharmaceutical research where it is crucial to know the phase of various drugs for accurate testing.<sup>198</sup> In addition, light scattering is potentially useful in certain non-equilibrium systems of swarming or flocking nanoparticles. If active particles could be prepared with extremely long-range interparticle interactions that exceeded the diffraction limit, single-particle behavior could be observed both individually and in the collective.<sup>132 202</sup> The relative insensitivity of light scattering to various stimuli and the potential for high temporal resolution using more sophisticated optics makes this a potentially powerful technique given the above caveats.

### 4.5.3. Super-Resolution Microscopy

The difficulties surrounding the use of light-based imaging methods to resolve objects smaller than the diffraction limit are well-known. Indeed, decades of research have resulted in the development of super-resolution (SR) microscopy methods that aim to “beat” the diffraction limit while still using visible light as the imaging medium.<sup>205</sup> These techniques all rely on the recognition that the diffraction limit is only problematic in standard fluorescence microscopy if multiple fluorophores within a diffraction limit of each other all emit photons over the course of the measurement. If one can ensure that only one fluorescence emission event is taking place within the space of one diffraction limit, then the intensity of the emitted light can be modeled using a point-spread function (PSF) – a mathematical description of the blurred image of a poorly-resolved object.<sup>205</sup> Since the emission event can be assumed with high probability to have occurred at the center of the PSF, the fluorophore can be localized with a resolution below the diffraction limit (Fig. 4.5a). SR techniques that accomplish this can typically be divided into two categories: deterministic and stochastic methods. Deterministic techniques, such as stimulated emission depletion (STED) microscopy and ground state depletion (GSD) microscopy, leverage photochemistry to force emission to occur in a spot size less than the diffraction limit of light.<sup>205</sup> Stochastic techniques, such as stochastic optical reconstruction microscopy (STORM) and photoactivated localization microscopy (PALM), exploit the chemistry of fluorophores to ensure that only a small fraction will

emit over a given period time, thus enabling a super-resolved image to be constructed by overlaying the PSF localizations from multiple time points.<sup>205</sup>

To date, SR microscopy techniques have primarily been leveraged by scientists to probe the dynamic behavior of biological systems. For example, Eggeling *et al* used STED microscopy to observe with 40 nm resolution that the cytoskeleton directly influences phospholipid diffusion in the plasma membrane of cells.<sup>168</sup> More recently, however, there have been notable experiments that probe synthetic, particle-based systems. For example, Hell and coworkers used STED microscopy to observe the assembly of 200 nm polystyrene beads into a crystalline monolayer (Fig. 4.5b).<sup>173</sup> Although the voids between beads were as small as 30 nm, they were nonetheless able to be resolved using this technique. Most SR experiments achieve spatial resolutions between 20-40 nm and have a high temporal resolution around 10-100 ms, depending on the camera used.<sup>205</sup> More cutting edge techniques have improved the spatial resolution to as low as ~10 nm and Eggeling *et al* have shown the ability to track the dynamics of biomolecules in plasma membranes with less than 1 ms temporal resolution.<sup>206</sup> It is important to note that SR methods are capable of providing spatial information both along the optical axis and in the 2D lateral imaging plane, thus making the technique capable of providing three-dimensional information. Hell *et al* has demonstrated this capacity by observing the self-assembly of 20 nm polystyrene beads and monitoring the specific layer in which each bead resides.<sup>207</sup>

Given the high spatiotemporal resolution of this technique and its ability to track three-dimensional motion, super-resolution microscopy could prove to be invaluable in the study of numerous far-from-equilibrium nanoparticle systems. A spatial resolution between 10-40 nm is appropriately high to observe most nanoparticles, although if interparticle spacings are small ( $<10$  nm), differentiating individual particles in an assembly may still be challenging.<sup>208</sup> Particles that are geometrically anisotropic are also unlikely to be resolvable with SR, as features such as tips and edges that circumscribe a particle are often less than  $\sim 10$  nm in size. This will limit the ability to observe orientational motion and ordering during organization processes (Fig. 4.2b), thus making SR more amenable to measurements of translational dynamics and/or the investigation of predominantly spherical particles. With respect to temporal resolution, SR is perhaps the most well-developed of all the methods covered in this article. In addition to being able to monitor most diffusion and particle assembly processes, the dynamics of many systems rely not only on the particles themselves but also on changes to the orientation or motion of surface-bound ligands, e.g. in DNA-mediated hybridization.<sup>28 209</sup> These molecular-scale transitions occur on considerably faster timescales than many dynamic nanoparticle processes, but certain SR techniques may nonetheless be able to observe and understand these transitions in the context of the overall assembly mechanism.<sup>205</sup> Being able to probe the molecular-scale ligand dynamics in tandem with the single-particle and particle assembly dynamics would represent an unprecedented advance in revealing mechanisms of self-organization and emergent behavior. Furthermore,



there is nothing inherent to the operation of SR microscopy to prevent the use of magnetic or electric fields, chemical fuels, heating gradients, or light as energetic stimuli to induce non-equilibrium processes.

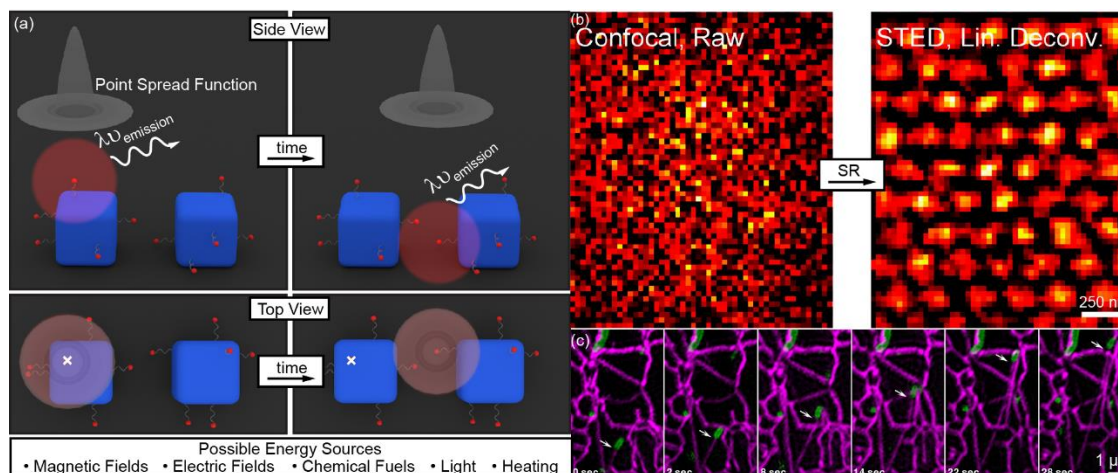


Figure 4.5 Capacity for SR Microscopy to Probe Dissipative Nanoparticle Assembly. a) Illustration of the imaging of nanocubes using super-resolution microscopy. Particles must be labeled with fluorophores that emit individually and thus can be mapped to a single point spread function and localized below the diffraction limit. b) Comparison of a diffraction-limited confocal image of assembled polystyrene beads and the same assembly imaged using a super-resolution microscopy technique (stimulated emission depletion, STED).<sup>173</sup> Reproduced with permission from ref. <sup>173</sup>. Copyright 2010 American Chemical Society. c) Super-resolved images of the formation of a microtubule (purple) forming from a mitochondrion (green) over time.<sup>161</sup> Reproduced with permission from ref. <sup>216</sup>. Copyright 2018 Cell Press.

Despite its high spatiotemporal resolution and potential utility in understanding nanoscale dynamics, SR microscopy does possess certain inherent challenges that must be addressed. The foundational reliance on fluorescence means that in order for SR techniques to image a given system, the particles under

examination must either be inherently fluorescent or labeled with luminescent molecules. Several common semiconducting nanoparticles are indeed fluorescent and have a wide range of reported sizes, shapes, and surface chemistries (e.g. CdSe, InP, ZnS).<sup>210</sup> However in order to have photoemission at visible wavelengths, these building blocks are typically smaller than  $\sim 10$  nm and thus will be difficult to spatially resolve.. However, anisotropic semiconductor nanostructures often have one or two dimensions on the order of 50 – 100 nm and may therefore be appealing starting points for SR nanoparticle investigations.<sup>211 212</sup> For systems in which intrinsic photoluminescence is limited, surface chemistry must be exploited to label the particle with an emissive dye. In some cases, attachment of a fluorophore is straightforward, e.g. using gold-thiol chemistry to anchor Cy5 to gold spheres.<sup>213</sup> However, for other systems with more poorly understood surface chemistry, new protocols may need to be developed to reliably attach fluorophores without hampering colloidal stability. Furthermore, the fluorophore tags must be compatible with the assembly mechanism, particularly if interactions are governed by ligand-mediated binding. Care must also be taken in selecting the appropriate fluorophore for a particular nanoparticle material system. For example, metal nanostructures such as gold and silver can quench fluorescence,<sup>213</sup> particularly if the dye is close to the particle surface or if there is spectral overlap between the emission of the dye and the plasmon absorption of the particle.<sup>214</sup> Therefore, the design of a nanoparticle system that can be monitored via SR involves a non-trivial set of chemical challenges that are nonetheless surmountable given the above design rules.

While super-resolution microscopy is often used to study sensitive biological materials and living cells (Fig. 4.5c), a common misconception is that the technique is non-perturbative. Photo-induced cell death is a well-known phenomenon,<sup>215</sup> indicating that the flux of photons necessary to create high-resolution videos of nanoscale phenomena will potentially impact the system through photothermal heating or photoinduced degradation of crucial chemical species. For this reason, systems that require light-based stimuli may be difficult to study using SR techniques. Moreover, carefully controlled experiments will be necessary to ensure that the behavior being observed is consistent with ex-situ experiments that are not under intense light illumination.

#### **4.5.4. Liquid-Phase Transmission Electron Microscopy**

Rather than improving spatial resolution by circumventing the diffraction limit imposed by optical photons, Materials Scientists have typically used high-energy electrons for imaging purposes, as they have wavelengths on the order of picometers and thus can resolve atomic-level structure. Transmission electron microscopes (TEM) have the highest spatial resolution of this class of techniques and function analogously to optical microscopes by generating and focusing electrons that are transmitted through a thin sample.<sup>217</sup> Although most electrons pass through the sample unimpeded, those that are absorbed, scattered, or diffracted contribute to contrast and allow for images to be obtained. Advances over the past decade have allowed aberrations in the electromagnetic lenses to be corrected for, enabling

atomic-resolution images, in some cases with added compositional and/or electronic structure information.<sup>218</sup> However, because the electron source and optics must be under high vacuum, the vast majority of transmission electron microscopes operate only under dry, ex-situ imaging conditions.

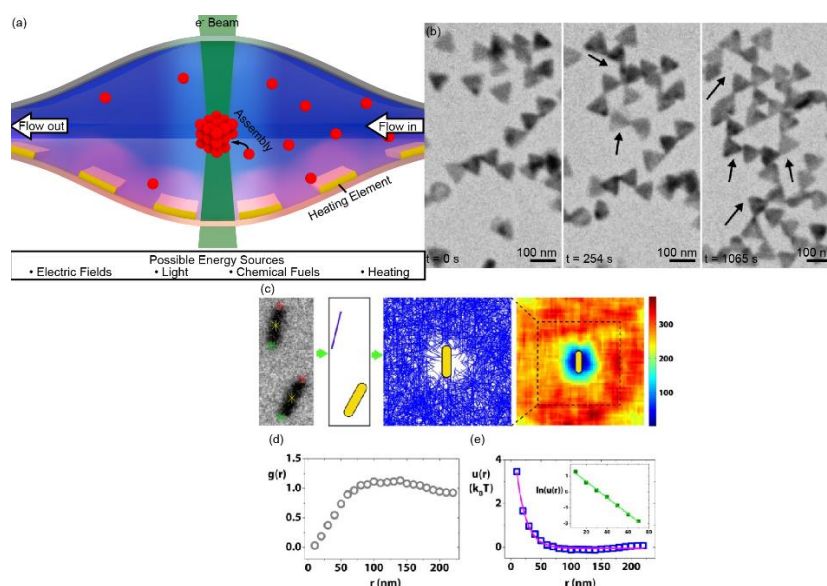


Figure 4.6 Capacity for Liquid Phase TEM to Probe Dissipative Nanoparticle Assembly. a) Illustration of sealed TEM liquid cell, allowing imaging of spherical nanoparticle assembly. Heating elements and inflow of new reagents to the cell are indicated as methods to initiate reaction. b) Liquid-phase TEM images showing assembly of gold nanoprisms over time.<sup>221</sup> Reproduced with permission from ref. 221. Copyright 2017 Nature Publishing Group. c) Spatially-mapping dynamic motion of nanorods leads to color-coded count of the total number of nanorods in each 5 nm by 5 nm pixel. d) Plots of the radial distribution function and the pairwise interaction potential of nanorods, extracted from the trajectories in part c).<sup>227</sup> Reproduced with permission from ref. 227. Copyright 2015 American Chemical Society.

Recent advances in microfabrication technologies have allowed for the design of special TEM sample holders that are able to form hermetically-sealed chambers

that isolate liquid samples from the high-vacuum environment of the instrument.<sup>219</sup> These liquid cells are fabricated with small windows consisting of thin, electron transparent materials (such as graphene or silicon nitride) that allow for transmission of the electron beam through the sample (Fig. 4.6a). Thus, without modifying the microscope itself, liquid-phase dynamics can be imaged.<sup>220</sup> Although resolution is reduced by imaging through liquid layers that are typically ~100 nm in thickness, liquid-phase methodologies nonetheless can achieve single nanometer spatial resolution,<sup>176 221 222</sup> with some examples approaching atomic resolution.<sup>223 178</sup> Most investigations to date have used the electron beam to reduce metal precursors in order to monitor the dynamics of nucleation and growth.<sup>224 225</sup> For example, Alivisatos and coworkers differentiated two simultaneous pathways in Pt nanocrystal growth - Pt<sup>0</sup> monomer addition and coalescence of small Pt particles into larger objects.<sup>226</sup> More recent work has shown the use of liquid phase TEM to follow the assembly of metal nanoparticles into well-ordered superlattices and even map the interaction potential between anisotropic particles (Fig. 4.6b-e).<sup>221 222 227 228 229</sup> Although investigations of inorganic materials are more common, improvements to the technique have allowed for the direct imaging of soft matter systems without the requirement of labeling or staining with an electron-dense reagent.<sup>230</sup> For example, Gianneschi and coworkers observed the fusion and growth of amphiphilic block copolymer micelles and Granick and coworkers were able to resolve the conformational fluctuations of individual polymer chains.<sup>231</sup> Single-particle and

single-molecule dynamic studies of this sort are rare and highlight the resolution advantages of liquid-phase TEM techniques.

Although liquid phase TEM is superior in spatial resolution (Fig. 4.2g), it also has advantages in the time domain that make it appealing for use in studying nanoscale dynamics. Although most CCD or CMOS detectors developed for traditional TEM were not designed with temporal resolution in mind, they nonetheless typically possess a frame rate on the order of 100 ms per image, which can be sufficient for observing some dynamic systems. Fortunately, this field has benefitted tremendously from advances driven by the cryogenic electron microscopy (cryo-EM) community, where high-resolution structural information can be obtained on frozen protein samples.<sup>232</sup> In order to minimize the beam dose and subsequent sample damage, so-called direct-electron detectors have been developed that are considerably more sensitive and have higher camera frame rates than traditional CCD or CMOS detectors. Therefore, the liquid-phase TEM community has recently been able to leverage the improved temporal resolution of new direct-electron detectors to obtain movies near 1 ms per image;<sup>233</sup> next-generation models are predicted to improve this figure to the 100  $\mu$ s regime. Thus, with the advent of the most recent detector technologies, liquid-phase TEM can resolve many of the dynamic processes that are expected to occur in non-equilibrium nanoparticle systems. In addition, many commercially available liquid-cell holders are fabricated with microfluidic channels that allow for the inflow of new chemical or solvent components during imaging,<sup>234</sup> thus allowing researchers to trigger and observe a dynamic process or introduce chemical fuels to drive a

system out of equilibrium. Electrochemical and heating elements can also be incorporated into commercial liquid cells and thus offer several methods for introducing stimuli to the system.

Despite the many benefits of liquid-phase TEM, several challenges limit the ease with which this technique may be applied to nanoscale systems. The primary difficulty lies in understanding and mitigating the role that the high-energy electron beam plays in perturbing the sample of interest. As the beam passes through the solvent, numerous radiolytic species are generated that range from highly-reducing solvated electrons ( $E^\circ = -2.90$  V in water) to highly-oxidizing hydroxyl radicals ( $E^\circ = +2.80$  V in water).<sup>235 236 219</sup> There is therefore a constant flux of chemically-reactive species being generated in any liquid-phase TEM experiment, the influence of which can be difficult to determine or decouple from the dynamics being observed. There are, however, a number of strategies that have shown some success in minimizing electron beam effects.<sup>237</sup> For instance, lowering the beam dose rate and minimizing the cumulative electron dose to the sample can minimize the damage done by radiolytic species;<sup>238 231</sup> this is particularly effective with new detector technologies that can produce an image with fewer electrons.<sup>237 239</sup> Radical scavengers can also be added to the solution that sacrificially react with and lower the concentration of radiolytic species, protecting the sample under study.<sup>239</sup> Indeed, if the system is prepared correctly, the dynamics observed in the liquid-phase TEM experiment can be replicated in ensemble measurements, demonstrating that the electron beam is playing a minimal role under the conditions studied.<sup>231</sup>

Through the design of careful control experiments, the impact of the beam on the behavior of the particles in solution can be observed and accounted for in understanding the system under investigation. Alternatively, as the radiolytic chemistry generated in liquid-phase TEM experiments becomes more well-understood, the electron beam can be thought of as powerful stimulus for intentionally driving a system out of equilibrium, rather than as a perturbation to be mitigated.<sup>239</sup> Indeed, the beam is often used to create steady-state reducing or oxidizing conditions to study the kinetics of nanoparticle growth or etching.<sup>176</sup> Furthermore, when operated in scanning transmission electron microscopy (STEM) mode, the beam is focused to a sub-nanometer-sized spot, and thus allows for the highly-localized deposition of energy to the system.<sup>239</sup> This may prove extremely powerful in setting up an in-situ experiment that monitors the spatial dynamics of a system after a chemical reaction is initiated at a specific location by the beam.

Although current liquid-cell designs allow for the straightforward introduction of chemical, thermal, and electrochemical stimuli, additional energy sources to drive systems out of equilibrium will likely be more challenging to implement. Depending on the specific microscope, there are usually stringent space requirements on the dimensions of the sample holder in order for it to fit correctly inside the TEM column. Indeed, current commercially available liquid cell designs accommodate an impressive arsenal of tools (liquid flow, heating, electrochemistry) into a small volume by means of advanced microfabrication techniques. Consequently, coupling additional functionality to the existing liquid cell platforms,



e.g. optical fiber for wavelength-specific optical excitation of a liquid sample, is a non-trivial enterprise and must be done in a way that maintains proper vacuum seals between the sample holder and the column. Thus, although future advances will likely address these difficulties, liquid-phase TEM is more limited in the types and magnitudes of stimuli for driving a dynamic system than some of the other techniques covered in this perspective.

#### **4.6. Data Analysis, Deep Learning, and Multiscale Modeling**

As the methods outlined above continue to produce images and movies with improving spatial and temporal resolution, the size of a single dataset will quickly become intractably large. For example, using present-day instrumentation, a liquid-phase TEM movie collected for 1 minute at a frame rate of 1 ms represents an uncompressed file size of 1.3 terabytes. This presents a problem that heretofore has not required addressing by the nanoscience community- how to process, analyze, and store large quantities of data that will be impossible for human researchers to analyze frame-by-frame on an acceptable timescale.<sup>240</sup> Fortunately, other scientific disciplines have already confronted this challenge and have developed methods to address it. The particle and astrophysics communities regularly gather massive quantities of data that need sophisticated computational methods to identify and promote meaningful data for human analysis while discarding the rest; it is not uncommon for some measurements to produce raw datasets on the order of petabytes – approximately one million gigabytes.<sup>241</sup> Rather than develop new digital

processing tools from scratch, adapting some of these existing methods for analyzing time-resolved data on dynamic nanoscale systems is an appealing strategy for addressing problems of big data.

Some of the first image processing tools developed for videographic data originate from the colloid physics community and have been used extensively to extract quantitative data from optical microscopy-based measurements.<sup>242</sup> In general, these techniques function by locating particles in each frame through an edge- or contrast-detection algorithm that differentiates a particle from the background. This allows the software to link the changing locations of particles in each frame in order to map single-particle trajectories, from which various properties can be calculated such as the velocity, diffusivity, or interaction potential. These techniques have become commonplace<sup>134 243</sup> and there are now many freely available codes that make this sort of analysis relatively straightforward.<sup>244</sup> More recently, researchers have leveraged these image processing tools to extract the same kinds of quantitative measurements but from videographic data on nanoscale dynamic systems. For instance, Mirsaidov and coworkers used rotational and translational particle tracking to understand the anomalous diffusion of nanoparticles adsorbed to a surface.<sup>245</sup> In addition, Alivisatos and coworkers showed that by mapping the numerous orientations that two gold nanorods sample as they approach one another, the pairwise interaction potential could be calculated from liquid-phase TEM movies (Fig. 6c-e).<sup>227</sup> Image processing methods continue to advance, particularly in ways that help to overcome some of the limitations of the measurement techniques

discussed above. For instance, Browning and coworkers have used an image reconstruction algorithm to generate high-fidelity liquid-phase STEM images using a fraction of the electrons normally required in conventional imaging; this minimizes the cumulative electron dose to the sample and thus mitigates radiolytic products and beam damage.<sup>246</sup> In addition, Helgeson and coworkers have developed a technique that can extract the diffusivity of sub-diffraction sized nanoparticles by analyzing intensity fluctuations between frames in a diffraction-limited optical microscopy video.<sup>247</sup> Integration of these methods with instrumentation software will help to minimize perturbation of sensitive samples and will allow for data analysis in real time.

Although image processing methods will allow for explicit quantitative results to be extracted from datasets, more advanced deep learning and machine learning algorithms will allow for the automatic identification of relevant results and thus may be helpful in sifting through large quantities of data.<sup>240</sup> Just as experimentalists develop intuition over years of work that allows them to quickly identify areas of interest in an experiment, neural networks can be trained with simulated or experimental data to identify those components of a dataset that are most important to the researcher.<sup>248 249</sup> After this training, the neural network can process large datasets more quickly, and in some cases more accurately,<sup>249</sup> than humans and promote relevant results for further analysis.<sup>250 251 252</sup> Within the last decade, significant progress has been made in implementing deep learning to enhance the efficiency of processing data from AFM,<sup>252</sup> SR microscopy,<sup>251</sup> and electron

microscopy.<sup>253</sup> For instance, a neural network has been trained to analyze electron microscopy images in order to identify defects in graphene sheets and count the number of atoms in a metal nanoparticle.<sup>253</sup> For stochastic SR techniques such as PALM or STORM that require thousands of diffraction-limited frames in order to construct a single super-resolved image, Zimmer and coworkers have demonstrated that a trained neural network can construct a super-resolved image using two orders of magnitude fewer diffraction-limited frames, thus drastically increasing overall throughput.<sup>254</sup> Interestingly, these deep learning approaches need not be applied only to the post-processing of data but can also be used in real-time to enhance the rate of data collection by incorporating feedback loops between the neural network and the instrument during data collection.<sup>254</sup> <sup>250</sup> This has been demonstrated recently by Li *et al* in the development of an atomic force microscope that can gather data on a sample, identify regions of interest during the imaging process, and then carry out more detailed experimentation and imaging at those regions of interest, all without human intervention.<sup>255</sup> More detailed discussions of progress in this area are available elsewhere,<sup>250</sup> <sup>251</sup> <sup>252</sup> <sup>255</sup> <sup>253</sup> <sup>254</sup> but the general trend towards large volumes of data and the need for automated analysis tools appears inevitable. This is especially true for the single-particle techniques covered in this perspective and thus highlights the need for collaborative work between computer science and chemistry researchers to address these challenges.

The tendency for emergent systems to depend on the properties of both single particles and their collective (multibody) interactions leads to a unique set of

challenges in developing models that can accurately capture non-equilibrium behavior. Typically, phenomena at each length scale are considered independently and then must be integrated to generate a model that predicts the properties of the hierarchical system as a whole; such a process is known as multiscale modeling.<sup>256</sup> This approach often simplifies various features of a system but in return can reduce the computational burden to make tractable problems that would otherwise require extraordinary resources to model atomistically. One approach identifies and models the most important components of the system that are necessary for accurately portraying a given property while averaging the remaining components as a single-parameter effective medium. For instance, it has been shown that solvent-free modeling can simplify computations while still accurately displaying the behavior of membrane proteins.<sup>257</sup> Another approach seeks to mathematically couple equations that are typically used on separate length scales, resulting in hybrid hierarchical models that function on multiple length scales.<sup>258</sup> Fortunately, there has already been measurable advances in developing multiscale modeling techniques that capture emergent behaviors. For instance, Chen and coworkers have developed a computational platform that can predict the emergent properties of bimetallic catalysts and identify which structures are ideal for a given reaction.<sup>259</sup> Multiscale modeling can also be beneficial in cases where the observed properties are sensitive to a large number of physical variables, thus making causation difficult to establish. For instance, Chatterjee and Vlachos developed a hierarchy of coarse-grained models that enabled the derivation of a phase diagram of assembled nanoclusters without

testing the multitude of individual variables present in the system.<sup>260</sup> Developing multiscale models to analyze nonequilibrium nanoparticle assemblies will help researchers predict systems that might display a given emergent property and will aid in the analysis of emergent systems to better understand the variables to which they are most reliant. Although the nuances of multiscale modeling are beyond the scope of this perspective, numerous resources are available that may facilitate theoretical investigations into nonequilibrium nanoparticle systems.<sup>256 257 258 261 262</sup>

263

#### **4.7. Conclusion**

Although the majority of nanomaterial systems are structurally static, generating and understanding systems that are dynamic represents a burgeoning field. Fundamental principles surrounding the concepts of emergent properties, non-equilibrium self-organization, and stimulus-based adaptation all represent important and fascinating avenues of scientific inquiry that can be investigated in these systems. However, the development of new research directions requires the appropriate tools to interrogate their questions. To date, there is no singular measurement technique that can satisfy all the requirements of tracking single-particle trajectories driven by external energy sources in a manner that is minimally perturbative. The vast opportunities for new scientific understanding and the development of advanced materials will be intrinsically linked to the characterization of dynamic nanoscale systems. By highlighting those approaches which are most amenable to addressing

the measurement challenges posed, and indicating needed areas of improvement, we hope to spur the community to contribute to the development of this new class of powerful methods and instrumentation.

## Chapter 5

# Conclusion, or There and Back Again

This thesis explored the development of higher level control of nanoparticle assembly through careful modulation of ligand chemistry. It will take many generations of researchers before synthetic systems begin to approach the complexity inherent in natural systems. However, this work represents a step forward in the development of self-assembling nanoparticles towards sophisticated synthetic systems with a high degree of function.

In Chapter 2, I presented my work applying traditional functionalization techniques to highly nontraditional particles, ultrathin Au nanowires. In this work, AuNWs were successfully functionalized and phase transferred into water, enabling their assembly states to be controlled using two different methods. Through introduction of  $\text{Ca}^{2+}$  ions, nanowires could be assembled into bundles with HCP order. Through adjustment of the pH to acidic conditions, nanowires could be assembled



into similar bundles (albeit with different spacings) through hydrogen bonding in addition to forming other assemblies with a lamellar structure. Furthermore, these assembly methods could be leveraged to form macroscopic fibers with vastly different properties based on their differences at the molecular level. Further research will continue this trend, exploring the complete phase space of assembled nanowires in addition to characterizing how the AuNWs assembled at the nanoscopic level translate their properties to materials at the macroscopic level.

In Chapter 3, I showed how DNA-functionalized nanoprisms could have extremely sharp transitions between the assembled and disassembled state based on the flexibility of the DNA linking monomer particles together. The breadth of these transitions could not be explained by current models that seek to explain the melting properties of assemblies of DNA-functionalized nanomaterials. Through careful data analysis using van 't Hoff plots, I demonstrated that flexible linkers had a higher entropic cost to hybridization during assembly, but were also able to make many more connections than their more rigid counterparts, explaining the primary driving force for this phenomenon. Future scientists will be able to take these findings and better adapt synthetic systems to have higher transitions between states through enhanced multivalency.

In Chapter 4, I explored one of the major challenges of developing dissipative self-assembling systems: finding the proper analytical technique to characterize such systems. I discussed the advantages and disadvantages inherent in in situ AFM, light

scattering, super-resolution microscopy, and liquid-phase TEM, as well as hypothesizing what kinds of systems each technique is best equipped to analyze. I finished with a discussion of the growing problem of big data, where the improvement on spatial and temporal resolutions in these forms of microscopy lead to massive amounts of raw data that will prove difficult for human researchers to study in a set timeframe, leading to the need for better data analysis techniques such as deep learning and multiscale modeling. The discussions in this chapter will prepare various research groups interested in dissipative self-assembly to have ready access to the necessary tools needed to develop nonequilibrium synthetic systems with high degrees of complexity.

Collectively, the goal of this thesis is to move the field closer to developing true biomimetic systems. Biological materials are profound in their depth and complexity, being able to rapidly respond to stimuli and grow due to their nature as far-from-equilibrium structures. We are admittedly, nowhere close to being able to instill the same level of function in synthetic systems. However, the fact that many of these biomaterials are natural nanomaterials means that such a goal is possible even if it will take practically countless scientists' lifetimes of work to accomplish. This thesis represents my contribution to that team effort in the hope that it will help and inspire others to do the same.

## References

- (1) Talapin, D. V.; Shevchenko, E. V. Introduction: Nanoparticle Chemistry. *Chem Rev* **2016**, *116* (18), 10343-10345. DOI: 10.1021/acs.chemrev.6b00566 From NLM PubMed-not-MEDLINE.
- (2) Clark, B. D.; Jacobson, C. R.; Lou, M.; Renard, D.; Wu, G.; Bursi, L.; Ali, A. S.; Swearer, D. F.; Tsai, A. L.; Nordlander, P.; et al. Aluminum Nanocubes Have Sharp Corners. *ACS nano* **2019**, *13* (8), 9682-9691. DOI: 10.1021/acsnano.9b05277 From NLM PubMed-not-MEDLINE.
- (3) Takahata, R.; Yamazoe, S.; Koyasu, K.; Imura, K.; Tsukuda, T. Gold Ultrathin Nanorods with Controlled Aspect Ratios and Surface Modifications: Formation Mechanism and Localized Surface Plasmon Resonance. *Journal of the American Chemical Society* **2018**, *140* (21), 6640-6647. DOI: 10.1021/jacs.8b02884 From NLM PubMed-not-MEDLINE.
- (4) Rehn, S. M.; Gerrard-Anderson, T. M.; Qiao, L.; Zhu, Q.; Wehmeyer, G.; Jones, M. R. Mechanical Reshaping of Inorganic Nanostructures with Weak Nanoscale Forces. *Nano letters* **2021**, *21* (1), 130-135. DOI: 10.1021/acs.nanolett.0c03383 From NLM PubMed-not-MEDLINE.
- (5) Ling, D.; Hackett, M. J.; Hyeon, T. Surface ligands in synthesis, modification, assembly and biomedical applications of nanoparticles. *Nano Today* **2014**, *9* (4), 457-477. DOI: 10.1016/j.nantod.2014.06.005.
- (6) Xia, Y.; Xiong, Y.; Lim, B.; Skrabalak, S. E. Shape-controlled synthesis of metal nanocrystals: simple chemistry meets complex physics? *Angewandte Chemie* **2009**, *48* (1), 60-103. DOI: 10.1002/anie.200802248 From NLM Medline.
- (7) Thompson, D. Michael Faraday's recognition of ruby gold: the birth of modern nanotechnology. *Gold Bulletin* **2007**, *40* (4), 267-269. DOI: 10.1007/bf03215598.
- (8) O'Brien, M. N.; Jones, M. R.; Brown, K. A.; Mirkin, C. A. Universal Noble Metal Nanoparticle Seeds Realized Through Iterative Reductive Growth and Oxidative Dissolution Reactions. *Journal of the American Chemical Society* **2014**, *136* (21), 7603-7606.
- (9) Qiao, L.; Pollard, N.; Senanayake, R. D.; Yang, Z.; Kim, M.; Ali, A. S.; Hoang, M. T.; Yao, N.; Han, Y.; Hernandez, R.; et al. Atomically precise nanoclusters predominantly seed gold nanoparticle syntheses. *Nat Commun* **2023**, *14* (1), 4408. DOI: 10.1038/s41467-023-40016-3 From NLM PubMed-not-MEDLINE.
- (10) Nikoobakht, B.; El-Sayed, M. A. Preparation and growth mechanism of gold nanorods (NRs) using seed-mediated growth method. *Chem Mater* **2003**, *15* (10), 1957-1962.
- (11) Hunter, R. J. *Foundations of colloid science / Robert J. Hunter*; Oxford University Press, 2001.
- (12) Klunker, M.; Connolly, B. M.; Marolf, D. M.; Nawaz Tahir, M.; Korschelt, K.; Simon, P.; Kohler, U.; Plana-Ruiz, S.; Barton, B.; Panthofer, M.; et al. Controlling the Morphology of Au-Pd Heterodimer Nanoparticles by Surface Ligands. *Inorg Chem*

**2018**, 57 (21), 13640-13652. DOI: 10.1021/acs.inorgchem.8b02236 From NLM PubMed-not-MEDLINE.

(13) Huo, Z.; Tsung, C. K.; Huang, W.; Zhang, X.; Yang, P. Sub-two nanometer single crystal Au nanowires. *Nano letters* **2008**, 8 (7), 2041-2044. DOI: 10.1021/nl8013549 From NLM PubMed-not-MEDLINE.

(14) Millstone, J. E.; Wei, W.; Jones, M. R.; Yoo, H.; Mirkin, C. A. Iodide ions control seed-mediated growth of anisotropic gold nanoparticles. *Nano letters* **2008**, 8 (8), 2526-2529. DOI: 10.1021/nl8016253 From NLM Medline.

(15) Xia, Y.; Xia, X.; Peng, H. C. Shape-Controlled Synthesis of Colloidal Metal Nanocrystals: Thermodynamic versus Kinetic Products. *Journal of the American Chemical Society* **2015**, 137 (25), 7947-7966. DOI: 10.1021/jacs.5b04641 From NLM Medline.

(16) Glotzer, S. C.; Solomon, M. J. Anisotropy of building blocks and their assembly into complex structures. *Nature materials* **2007**, 6 (8), 557-562.

(17) Jones, M. R.; Macfarlane, R. J.; Prigodich, A. E.; Patel, P. C.; Mirkin, C. A. Nanoparticle shape anisotropy dictates the collective behavior of surface-bound ligands. *Journal of the American Chemical Society* **2011**, 133 (46), 18865-18869. DOI: 10.1021/ja206777k From NLM PubMed-not-MEDLINE.

(18) Cai, Y. Y.; Choi, Y. C.; Kagan, C. R. Chemical and Physical Properties of Photonic Noble-Metal Nanomaterials. *Adv Mater* **2021**, n/a (n/a), e2108104. DOI: 10.1002/adma.202108104 From NLM Publisher.

(19) Ju, Y.; Kim, C. J.; Caruso, F. Functional Ligand-Enabled Particle Assembly for Bio-Nano Interactions. *Acc Chem Res* **2023**, 56 (13), 1826-1837. DOI: 10.1021/acs.accounts.3c00172 From NLM Medline.

(20) Lin, G.; Zhang, M. Ligand Chemistry in Antitumor Theranostic Nanoparticles. *Acc Chem Res* **2023**, 56 (12), 1578-1590. DOI: 10.1021/acs.accounts.3c00151 From NLM Medline.

(21) Neal, R. D.; Hughes, R. A.; Sapkota, P.; Ptasinska, S.; Neretina, S. Effect of Nanoparticle Ligands on 4-Nitrophenol Reduction: Reaction Rate, Induction Time, and Ligand Desorption. *ACS Catalysis* **2020**, 10 (17), 10040-10050. DOI: 10.1021/acscatal.0c02759.

(22) Kanelidis, I.; Kraus, T. The role of ligands in coinage-metal nanoparticles for electronics. *Beilstein J Nanotechnol* **2017**, 8, 2625-2639. DOI: 10.3762/bjnano.8.263 From NLM PubMed-not-MEDLINE.

(23) Lal, S.; Clare, S. E.; Halas, N. J. Nanoshell-enabled photothermal cancer therapy: impending clinical impact. *Acc Chem Res* **2008**, 41 (12), 1842-1851. DOI: 10.1021/ar800150g From NLM Medline.

(24) Yang, W.; Liu, S.; Bai, T.; Keefe, A. J.; Zhang, L.; Ella-Menye, J.-R.; Li, Y.; Jiang, S. Poly(carboxybetaine) nanomaterials enable long circulation and prevent polymer-specific antibody production. *Nano Today* **2014**, 9 (1), 10-16. DOI: 10.1016/j.nantod.2014.02.004.

- (25) Wu, Z.; Jin, R. On the ligand's role in the fluorescence of gold nanoclusters. *Nano letters* **2010**, *10* (7), 2568-2573. DOI: 10.1021/nl101225f From NLM PubMed-not-MEDLINE.
- (26) Kwon, S. G.; Krylova, G.; Sumer, A.; Schwartz, M. M.; Bunel, E. E.; Marshall, C. L.; Chattopadhyay, S.; Lee, B.; Jellinek, J.; Shevchenko, E. V. Capping ligands as selectivity switchers in hydrogenation reactions. *Nano letters* **2012**, *12* (10), 5382-5388. DOI: 10.1021/nl3027636 From NLM PubMed-not-MEDLINE.
- (27) Manoharan, V. N. COLLOIDS. Colloidal matter: Packing, geometry, and entropy. *Science* **2015**, *349* (6251), 1253751. DOI: 10.1126/science.1253751 From NLM PubMed-not-MEDLINE.
- (28) Jones, M. R.; Seeman, N. C.; Mirkin, C. A. Nanomaterials. Programmable materials and the nature of the DNA bond. *Science* **2015**, *347* (6224), 1260901. DOI: 10.1126/science.1260901 From NLM Medline.
- (29) Bishop, K. J.; Wilmer, C. E.; Soh, S.; Grzybowski, B. A. Nanoscale forces and their uses in self-assembly. *Small* **2009**, *5* (14), 1600-1630. DOI: 10.1002/smll.200900358 From NLM Medline.
- (30) Whitesides, G. M.; Grzybowski, B. Self-assembly at all scales. *Science* **2002**, *295* (5564), 2418-2421. DOI: 10.1126/science.1070821 From NLM Medline.
- (31) Rosenfeldt, S.; Förster, S.; Friedrich, T.; Rehberg, I.; Weber, B. Self-Assembly of Magnetic Iron Oxide Nanoparticles Into Cuboidal Superstructures. In *Novel Magnetic Nanostructures*, Domracheva, N., Caporali, M., Rentschler, E. Eds.; Elsevier, 2018; pp 165-189.
- (32) Rabani, E.; Reichman, D. R.; Geissler, P. L.; Brus, L. E. Drying-mediated self-assembly of nanoparticles. *Nature* **2003**, *426* (6964), 271-274. DOI: 10.1038/nature02087 From NLM PubMed-not-MEDLINE.
- (33) Kalsin, A. M.; Fialkowski, M.; Paszewski, M.; Smoukov, S. K.; Bishop, K. J.; Grzybowski, B. A. Electrostatic self-assembly of binary nanoparticle crystals with a diamond-like lattice. *Science* **2006**, *312* (5772), 420-424. DOI: 10.1126/science.1125124 From NLM PubMed-not-MEDLINE.
- (34) Ni, W.; Mosquera, R. A.; Pérez-Juste, J.; Liz-Marzán, L. M. Evidence for Hydrogen-Bonding-Directed Assembly of Gold Nanorods in Aqueous Solution. *The Journal of Physical Chemistry Letters* **2010**, *1* (8), 1181-1185. DOI: 10.1021/jz1002154.
- (35) Klajn, R.; Bishop, K. J.; Grzybowski, B. A. Light-controlled self-assembly of reversible and irreversible nanoparticle suprastructures. *Proc Natl Acad Sci U S A* **2007**, *104* (25), 10305-10309. DOI: 10.1073/pnas.0611371104 From NLM Medline.
- (36) Klajn, R.; Bishop, K. J.; Fialkowski, M.; Paszewski, M.; Campbell, C. J.; Gray, T. P.; Grzybowski, B. A. Plastic and moldable metals by self-assembly of sticky nanoparticle aggregates. *Science* **2007**, *316* (5822), 261-264. DOI: 10.1126/science.1139131 From NLM PubMed-not-MEDLINE.
- (37) Kress, R. N.; Jones, M. R. Colloidal interactions get patchy and directional. *Proc Natl Acad Sci U S A* **2020**, *117* (27), 15382-15384. DOI: 10.1073/pnas.2006330117 From NLM PubMed-not-MEDLINE.

- (38) Walker, D. A.; Leitsch, E. K.; Nap, R. J.; Szleifer, I.; Grzybowski, B. A. Geometric curvature controls the chemical patchiness and self-assembly of nanoparticles. *Nature nanotechnology* **2013**, *8* (9), 676-681. DOI: 10.1038/nnano.2013.158 From NLM PubMed-not-MEDLINE.
- (39) Jin, R.; Wu, G.; Li, Z.; Mirkin, C. A.; Schatz, G. C. What controls the melting properties of DNA-linked gold nanoparticle assemblies? *Journal of the American Chemical Society* **2003**, *125* (6), 1643-1654.
- (40) Moaseri, E.; Bollinger, J. A.; Changalvaie, B.; Johnson, L.; Schroer, J.; Johnston, K. P.; Truskett, T. M. Reversible Self-Assembly of Glutathione-Coated Gold Nanoparticle Clusters via pH-Tunable Interactions. *Langmuir* **2017**, *33* (43), 12244-12253. DOI: 10.1021/acs.langmuir.7b02446 From NLM PubMed-not-MEDLINE.
- (41) Bian, T.; Gardin, A.; Gemen, J.; Houben, L.; Perego, C.; Lee, B.; Elad, N.; Chu, Z.; Pavan, G. M.; Klajn, R. Electrostatic co-assembly of nanoparticles with oppositely charged small molecules into static and dynamic superstructures. *Nature chemistry* **2021**, *13* (10), 940-949. DOI: 10.1038/s41557-021-00752-9 From NLM PubMed-not-MEDLINE.
- (42) Grzelczak, M.; Liz-Marzan, L. M.; Klajn, R. Stimuli-responsive self-assembly of nanoparticles. *Chem Soc Rev* **2019**, *48* (5), 1342-1361, 10.1039/C8CS00787J. DOI: 10.1039/c8cs00787j From NLM PubMed-not-MEDLINE.
- (43) Zubair Iqbal, M.; Ali, I.; Khan, W. S.; Kong, X.; Dempsey, E. Reversible self-assembly of gold nanoparticles in response to external stimuli. *Materials & Design* **2021**, *205*, 109694. DOI: 10.1016/j.matdes.2021.109694.
- (44) Zhao, H.; Sen, S.; Udayabhaskararao, T.; Sawczyk, M.; Kucanda, K.; Manna, D.; Kundu, P. K.; Lee, J. W.; Kral, P.; Klajn, R. Reversible trapping and reaction acceleration within dynamically self-assembling nanoflasks. *Nature nanotechnology* **2016**, *11* (1), 82-88. DOI: 10.1038/nnano.2015.256 From NLM PubMed-not-MEDLINE.
- (45) Hamon, C.; Liz-Marzan, L. M. Hierarchical Assembly of Plasmonic Nanoparticles. *Chemistry* **2015**, *21* (28), 9956-9963. DOI: 10.1002/chem.201500149 From NLM PubMed-not-MEDLINE.
- (46) Alberts, B.; Johnson, A.; Lewis, J.; Morgan, D.; Raff, M. C.; Roberts, K.; Walter, P.; Wilson, J. H.; Hunt, T. *Molecular biology of the cell*; Garland Science, Taylor and Francis Group New York, NY, 2015.
- (47) Yan, B.; Thubagere, A.; Premasiri, W. R.; Ziegler, L. D.; Dal Negro, L.; Reinhard, B. M. Engineered SERS substrates with multiscale signal enhancement: nanoparticle cluster arrays. *ACS nano* **2009**, *3* (5), 1190-1202. DOI: 10.1021/nn800836f From NLM Medline.
- (48) van Rossum, S. A. P.; Tena-Solsona, M.; van Esch, J. H.; Eelkema, R.; Boekhoven, J. Dissipative out-of-equilibrium assembly of man-made supramolecular materials. *Chem Soc Rev* **2017**, *46* (18), 5519-5535. DOI: 10.1039/c7cs00246g From NLM PubMed-not-MEDLINE.
- (49) Fialkowski, M.; Bishop, K. J.; Klajn, R.; Smoukov, S. K.; Campbell, C. J.; Grzybowski, B. A. Principles and implementations of dissipative (dynamic) self-

assembly. *The journal of physical chemistry. B* **2006**, *110* (6), 2482-2496. DOI: 10.1021/jp054153q From NLM Medline.

(50) Marolf, D. M.; Jones, M. R. Measurement Challenges in Dynamic and Nonequilibrium Nanoscale Systems. *Anal Chem* **2019**, *91* (21), 13324-13336. DOI: 10.1021/acs.analchem.9b02702 From NLM PubMed-not-MEDLINE.

(51) Takahata, R.; Yamazoe, S.; Koyasu, K.; Tsukuda, T. Surface plasmon resonance in gold ultrathin nanorods and nanowires. *Journal of the American Chemical Society* **2014**, *136* (24), 8489-8491. DOI: 10.1021/ja503558c From NLM PubMed-not-MEDLINE.

(52) Gong, S.; Schwalb, W.; Wang, Y.; Chen, Y.; Tang, Y.; Si, J.; Shirinzadeh, B.; Cheng, W. A wearable and highly sensitive pressure sensor with ultrathin gold nanowires. *Nat Commun* **2014**, *5*, 3132. DOI: 10.1038/ncomms4132 From NLM PubMed-not-MEDLINE.

(53) Halder, A.; Ravishankar, N. Ultrafine Single-Crystalline Gold Nanowire Arrays by Oriented Attachment. *Advanced Materials* **2007**, *19* (14), 1854-1858. DOI: 10.1002/adma.200602325.

(54) Lu, X.; Yavuz, M. S.; Tuan, H. Y.; Korgel, B. A.; Xia, Y. Ultrathin gold nanowires can be obtained by reducing polymeric strands of oleylamine-AuCl complexes formed via aurophilic interaction. *Journal of the American Chemical Society* **2008**, *130* (28), 8900-8901. DOI: 10.1021/ja803343m From NLM Medline.

(55) Pazos-Perez, N.; Baranov, D.; Irsen, S.; Hilgendorff, M.; Liz-Marzan, L. M.; Giersig, M. Synthesis of flexible, ultrathin gold nanowires in organic media. *Langmuir* **2008**, *24* (17), 9855-9860. DOI: 10.1021/la801675d From NLM PubMed-not-MEDLINE.

(56) Feng, H.; Yang, Y.; You, Y.; Li, G.; Guo, J.; Yu, T.; Shen, Z.; Wu, T.; Xing, B. Simple and rapid synthesis of ultrathin gold nanowires, their self-assembly and application in surface-enhanced Raman scattering. *Chem Commun (Camb)* **2009**, (15), 1984-1986, 10.1039/B822507A. DOI: 10.1039/b822507a From NLM PubMed-not-MEDLINE.

(57) Pschunder, F.; Puig, J.; Giovanetti, L. J.; Huck-Iriart, C.; Requejo, F. G.; Buceta, D.; Hoppe, C. E.; Ramallo-López, J. M. New Insights into the Growth Mechanism of Ultrathin Au Nanowires from Combined in Situ EXAFS and SAXS Studies. *The Journal of Physical Chemistry C* **2018**, *122* (50), 29051-29061. DOI: 10.1021/acs.jpcc.8b10449.

(58) Vargas, J. A.; Petkov, V.; Nouh, E. S. A.; Ramamoorthy, R. K.; Lacroix, L. M.; Poteau, R.; Viau, G.; Lecante, P.; Arenal, R. Ultrathin Gold Nanowires with the Polytetrahedral Structure of Bulk Manganese. *ACS nano* **2018**, *12* (9), 9521-9531. DOI: 10.1021/acs.nano.8b05036 From NLM PubMed-not-MEDLINE.

(59) Bettscheider, S.; Kuttich, B.; Engel, L. F.; González-García, L.; Kraus, T. Bundling of Nanowires Induced by Unbound Ligand. *The Journal of Physical Chemistry C* **2021**, *125* (6), 3590-3598. DOI: 10.1021/acs.jpcc.0c10919.

- (60) Chen, Y.; Wang, Y.; Peng, J.; Xu, Q.; Weng, J.; Xu, J. Assembly of Ultrathin Gold Nanowires: From Polymer Analogue to Colloidal Block. *ACS nano* **2017**, *11* (3), 2756-2763. DOI: 10.1021/acsnano.6b07777 From NLM PubMed-not-MEDLINE.
- (61) Maurer, J. H.; Gonzalez-Garcia, L.; Reiser, B.; Kanelidis, I.; Kraus, T. Templated Self-Assembly of Ultrathin Gold Nanowires by Nanoimprinting for Transparent Flexible Electronics. *Nano letters* **2016**, *16* (5), 2921-2925. DOI: 10.1021/acs.nanolett.5b04319 From NLM PubMed-not-MEDLINE.
- (62) Gong, S.; Zhao, Y.; Shi, Q.; Wang, Y.; Yap, L. W.; Cheng, W. Self-assembled Ultrathin Gold Nanowires as Highly Transparent, Conductive and Stretchable Supercapacitor. *Electroanalysis* **2016**, *28* (6), 1298-1304. DOI: 10.1002/elan.201600081.
- (63) Zhao, Y.; Dong, D.; Wang, Y.; Gong, S.; An, T.; Yap, L. W.; Cheng, W. Highly Stretchable Fiber-Shaped Supercapacitors Based on Ultrathin Gold Nanowires with Double-Helix Winding Design. *ACS applied materials & interfaces* **2018**, *10* (49), 42612-42620. DOI: 10.1021/acsmi.8b14769 From NLM PubMed-not-MEDLINE.
- (64) Chen, Y.; Ouyang, Z.; Gu, M.; Cheng, W. Mechanically strong, optically transparent, giant metal superlattice nanomembranes from ultrathin gold nanowires. *Adv Mater* **2013**, *25* (1), 80-85. DOI: 10.1002/adma.201202241 From NLM PubMed-not-MEDLINE.
- (65) Reiser, B.; Gerstner, D.; Gonzalez-Garcia, L.; Maurer, J. H.; Kanelidis, I.; Kraus, T. Multivalent bonds in self-assembled bundles of ultrathin gold nanowires. *Physical chemistry chemical physics : PCCP* **2016**, *18* (39), 27165-27169, 10.1039/C6CP05181B. DOI: 10.1039/c6cp05181b From NLM PubMed-not-MEDLINE.
- (66) Nough, E. S. A.; Baquero, E. A.; Lacroix, L. M.; Delpech, F.; Poteau, R.; Viau, G. Surface-Engineering of Ultrathin Gold Nanowires: Tailored Self-Assembly and Enhanced Stability. *Langmuir* **2017**, *33* (22), 5456-5463. DOI: 10.1021/acs.langmuir.7b00477 From NLM PubMed-not-MEDLINE.
- (67) Xu, S.; Li, P.; Lu, Y. In situ atomic-scale analysis of Rayleigh instability in ultrathin gold nanowires. *Nano Research* **2017**, *11* (2), 625-632. DOI: 10.1007/s12274-017-1667-3.
- (68) Jiang, J.; Zhang, Y.; Zhou, J.; Jiang, Y.; Li, Y. Facile Surface Modification of Ultrathin Gold Nanowires Film with Hydrogen Sulfide for Improvement of Stability. *Advanced Engineering Materials* **2022**, *24* (10), 2200509. DOI: 10.1002/adem.202200509.
- (69) Takahata, R.; Yamazoe, S.; Warakulwit, C.; Limtrakul, J.; Tsukuda, T. Rayleigh Instability and Surfactant-Mediated Stabilization of Ultrathin Gold Nanorods. *The Journal of Physical Chemistry C* **2016**, *120* (30), 17006-17010. DOI: 10.1021/acs.jpcc.6b03113.
- (70) Maturi, M.; Buratti, V. V.; Casula, G.; Locatelli, E.; Sambri, L.; Bonfiglio, A.; Comes Franchini, M. Surface-Stabilization of Ultrathin Gold Nanowires for Capacitive Sensors in Flexible Electronics. *ACS Applied Nano Materials* **2021**, *4* (9), 8668-8673. DOI: 10.1021/acsanm.1c01849.



- (71) Cormier, S.; Ding, T.; Turek, V.; Baumberg, J. J. Dynamic- and Light-Switchable Self-Assembled Plasmonic Metafilms. *Advanced Optical Materials* **2018**, *6* (14), 1800208. DOI: 10.1002/adom.201800208.
- (72) Santos, P. J.; Gabrys, P. A.; Zornberg, L. Z.; Lee, M. S.; Macfarlane, R. J. Macroscopic materials assembled from nanoparticle superlattices. *Nature* **2021**, *591* (7851), 586-591. DOI: 10.1038/s41586-021-03355-z From NLM PubMed-not-MEDLINE.
- (73) Chen, F.; Li, X.; Hihath, J.; Huang, Z.; Tao, N. Effect of anchoring groups on single-molecule conductance: comparative study of thiol-, amine-, and carboxylic-acid-terminated molecules. *Journal of the American Chemical Society* **2006**, *128* (49), 15874-15881. DOI: 10.1021/ja065864k From NLM PubMed-not-MEDLINE.
- (74) Bazin, H.; Descotes, G.; Bouchu, A.; Petit-Ramel, M. Comparison of calcium complexation of some carboxylic acids derived from D-glucose and D-fructose. *Canadian Journal of Chemistry* **1995**, *73* (8), 1338-1347. DOI: 10.1139/v95-165.
- (75) Russo, R.; Malinconico, M.; Santagata, G. Effect of cross-linking with calcium ions on the physical properties of alginate films. *Biomacromolecules* **2007**, *8* (10), 3193-3197. DOI: 10.1021/bm700565h From NLM Medline.
- (76) Dudev, T.; Lim, C. Monodentate versus Bidentate Carboxylate Binding in Magnesium and Calcium Proteins: What Are the Basic Principles? *The Journal of Physical Chemistry B* **2004**, *108* (14), 4546-4557. DOI: 10.1021/jp0310347.
- (77) Loubat, A.; Imperor-Clerc, M.; Pansu, B.; Meneau, F.; Raquet, B.; Viau, G.; Lacroix, L. M. Growth and self-assembly of ultrathin Au nanowires into expanded hexagonal superlattice studied by in situ SAXS. *Langmuir* **2014**, *30* (14), 4005-4012. DOI: 10.1021/la500549z From NLM PubMed-not-MEDLINE.
- (78) Clare Speakman, J. Acid salts of carboxylic acids, crystals with some 'very short' hydrogen bonds. Berlin, Heidelberg, 1972; Springer Berlin Heidelberg: pp 141-199.
- (79) Socha, O.; Dracinsky, M. Dimerization of Acetic Acid in the Gas Phase-NMR Experiments and Quantum-Chemical Calculations. *Molecules* **2020**, *25* (9), 2150. DOI: 10.3390/molecules25092150 From NLM Medline.
- (80) Takamuku, T.; Kyoshoin, Y.; Noguchi, H.; Kusano, S.; Yamaguchi, T. Liquid structure of acetic acid-water and trifluoroacetic acid-water mixtures studied by large-angle X-ray scattering and NMR. *The journal of physical chemistry. B* **2007**, *111* (31), 9270-9280. DOI: 10.1021/jp0724976 From NLM Medline.
- (81) Ferreira, G. A.; Loh, W. Structural Parameters of Lamellar Phases Formed by the Self-Assembly of Dialkyldimethylammonium Bromides in Aqueous Solution. *Journal of the Brazilian Chemical Society* **2016**, *27*.
- (82) Hamley, I. W. Diffuse scattering from lamellar structures. *Soft matter* **2022**, *18* (4), 711-721, 10.1039/D1SM01758F. DOI: 10.1039/d1sm01758f From NLM PubMed-not-MEDLINE.
- (83) Behabtu, N.; Young, C. C.; Tsentalovich, D. E.; Kleiner, O.; Wang, X.; Ma, A. W.; Bengio, E. A.; ter Waarbeek, R. F.; de Jong, J. J.; Hoogerwerf, R. E.; et al. Strong, light, multifunctional fibers of carbon nanotubes with ultrahigh conductivity. *Science*

**2013**, 339 (6116), 182-186. DOI: 10.1126/science.1228061 From NLM PubMed-not-MEDLINE.

(84) Tsentalovich, D. E.; Headrick, R. J.; Mirri, F.; Hao, J.; Behabtu, N.; Young, C. C.; Pasquali, M. Influence of Carbon Nanotube Characteristics on Macroscopic Fiber Properties. *ACS applied materials & interfaces* **2017**, 9 (41), 36189-36198. DOI: 10.1021/acsami.7b10968 From NLM PubMed-not-MEDLINE.

(85) Kelly, K. L.; Coronado, E.; Zhao, L. L.; Schatz, G. C. The Optical Properties of Metal Nanoparticles: The Influence of Size, Shape, and Dielectric Environment. *The Journal of Physical Chemistry B* **2002**, 107 (3), 668-677. DOI: 10.1021/jp026731y.

(86) Halas, N. J.; Lal, S.; Chang, W. S.; Link, S.; Nordlander, P. Plasmons in strongly coupled metallic nanostructures. *Chem Rev* **2011**, 111 (6), 3913-3961. DOI: 10.1021/cr200061k From NLM PubMed-not-MEDLINE.

(87) Whitty, A. Cooperativity and biological complexity. *Nat Chem Biol* **2008**, 4 (8), 435-439. DOI: 10.1038/nchembio0808-435 From NLM Medline.

(88) Hunter, C. A.; Anderson, H. L. What is Cooperativity? *Angew Chem Int Edit* **2009**, 48 (41), 7488-7499.

(89) von Krbek, L. K. S.; Schalley, C. A.; Thordarson, P. Assessing cooperativity in supramolecular systems. *Chem Soc Rev* **2017**, 46 (9), 2622-2637. DOI: 10.1039/c7cs00063d From NLM PubMed-not-MEDLINE.

(90) Bohr, C.; Hasselbalch, K.; Krogh, A. Ueber einen in biologischer Beziehung wichtigen Einfluss, den die Kohlensäurespannung des Blutes auf dessen Sauerstoffbindung übt 1. *Skandinavisches Archiv für Physiologie* **1904**, 16 (2), 402-412.

(91) Hill, A. V. The possible effects of the aggregation of the molecules of haemoglobin on its dissociation curves. *j. physiol.* **1910**, 40, 4-7.

(92) Pfeil, A.; Lehn, J.-M. Helicate self-organisation: positive cooperativity in the self-assembly of double-helical metal complexes. *Journal of the Chemical Society, Chemical Communications* **1992**, (11), 838-840.

(93) Taylor, P. N.; Anderson, H. L. Cooperative self-assembly of double-strand conjugated porphyrin ladders. *Journal of the American Chemical Society* **1999**, 121 (49), 11538-11545.

(94) Ercolani, G. Assessment of cooperativity in self-assembly. *Journal of the American Chemical Society* **2003**, 125 (51), 16097-16103. DOI: 10.1021/ja038396c From NLM PubMed-not-MEDLINE.

(95) Bloomfield, V. A.; Crothers, D. M.; Hearst, J. E.; Tinoco, I. *Nucleic acids : structures, properties, and functions*; Univ. Science Books, 2000.

(96) Laramy, C. R.; Lopez-Rios, H.; O'Brien, M. N.; Girard, M.; Stawicki, R. J.; Lee, B.; de la Cruz, M. O.; Mirkin, C. A. Controlled Symmetry Breaking in Colloidal Crystal Engineering with DNA. *ACS nano* **2019**, 13 (2), 1412-1420. DOI: 10.1021/acsnano.8b07027 From NLM Medline.

(97) Mirkin, C. A.; Letsinger, R. L.; Mucic, R. C.; Storhoff, J. J. A DNA-based method for rationally assembling nanoparticles into macroscopic materials. *Nature* **1996**, 382 (6592), 607.

- (98) Love, J. C.; Estroff, L. A.; Kriebel, J. K.; Nuzzo, R. G.; Whitesides, G. M. Self-assembled monolayers of thiolates on metals as a form of nanotechnology. *Chemical Reviews* **2005**, *105* (4), 1103-1169.
- (99) Nykypanchuk, D.; Maye, M. M.; van der Lelie, D.; Gang, O. DNA-guided crystallization of colloidal nanoparticles. *Nature* **2008**, *451* (7178), 549-552. DOI: 10.1038/nature06560 From NLM Medline.
- (100) Park, S. Y.; Lytton-Jean, A. K.; Lee, B.; Weigand, S.; Schatz, G. C.; Mirkin, C. A. DNA-programmable nanoparticle crystallization. *Nature* **2008**, *451* (7178), 553-556. DOI: 10.1038/nature06508 From NLM Medline.
- (101) Macfarlane, R. J.; Lee, B.; Jones, M. R.; Harris, N.; Schatz, G. C.; Mirkin, C. A. Nanoparticle superlattice engineering with DNA. *Science* **2011**, *334* (6053), 204-208. DOI: 10.1126/science.1210493 From NLM Medline.
- (102) Auyeung, E.; Cutler, J. I.; Macfarlane, R. J.; Jones, M. R.; Wu, J.; Liu, G.; Zhang, K.; Osberg, K. D.; Mirkin, C. A. Synthetically programmable nanoparticle superlattices using a hollow three-dimensional spacer approach. *Nature nanotechnology* **2012**, *7* (1), 24.
- (103) Macfarlane, R. J.; O'Brien, M. N.; Petrosko, S. H.; Mirkin, C. A. Nucleic acid-modified nanostructures as programmable atom equivalents: forging a new "table of elements". *Angewandte Chemie International Edition* **2013**, *52* (22), 5688-5698.
- (104) Auyeung, E.; Li, T. I.; Senesi, A. J.; Schmucker, A. L.; Pals, B. C.; de La Cruz, M. O.; Mirkin, C. A. DNA-mediated nanoparticle crystallization into Wulff polyhedra. *Nature* **2014**, *505* (7481), 73.
- (105) Park, D. J.; Zhang, C.; Ku, J. C.; Zhou, Y.; Schatz, G. C.; Mirkin, C. A. Plasmonic photonic crystals realized through DNA-programmable assembly. *Proceedings of the National Academy of Sciences* **2015**, *112* (4), 977-981.
- (106) Lytton-Jean, A. K.; Gibbs-Davis, J. M.; Long, H.; Schatz, G. C.; Mirkin, C. A.; Nguyen, S. T. Highly Cooperative Behavior of Peptide Nucleic Acid-Linked DNA-Modified Gold-Nanoparticle and Comb-Polymer Aggregates. *Advanced Materials* **2009**, *21* (6), 706-709.
- (107) Randeria, P. S.; Jones, M. R.; Kohlstedt, K. L.; Banga, R. J.; Olvera de la Cruz, M.; Schatz, G. C.; Mirkin, C. A. What controls the hybridization thermodynamics of spherical nucleic acids? *Journal of the American Chemical Society* **2015**, *137* (10), 3486-3489.
- (108) Wang, Y.; Wang, Y.; Zheng, X.; Ducrot, E.; Yodh, J. S.; Weck, M.; Pine, D. J. Crystallization of DNA-coated colloids. *Nat Commun* **2015**, *6*, 7253. DOI: 10.1038/ncomms8253 From NLM Medline.
- (109) Xiong, H.; van der Lelie, D.; Gang, O. Phase behavior of nanoparticles assembled by DNA linkers. *Physical review letters* **2009**, *102* (1), 015504.
- (110) Manning, G. S. Limiting laws and counterion condensation in polyelectrolyte solutions I. Colligative properties. *The journal of chemical Physics* **1969**, *51* (3), 924-933.
- (111) Dreyfus, R.; Leunissen, M. E.; Sha, R.; Tkachenko, A.; Seeman, N. C.; Pine, D. J.; Chaikin, P. M. Aggregation-disaggregation transition of DNA-coated colloids:

experiments and theory. *Physical review. E, Statistical, nonlinear, and soft matter physics* **2010**, *81* (4 Pt 1), 041404. DOI: 10.1103/PhysRevE.81.041404 From NLM Medline.

(112) Lim, C. W.; Kim, T. W. Dynamic [2]Catenation of Pd(II) Self-assembled Macrocycles in Water. *Chemistry Letters* **2012**, *41* (1), 70-72. DOI: 10.1246/cl.2012.70.

(113) Santos, P. J.; Cao, Z.; Zhang, J.; Alexander-Katz, A.; Macfarlane, R. J. Dictating Nanoparticle Assembly via Systems-Level Control of Molecular Multivalency. *Journal of the American Chemical Society* **2019**, *141* (37), 14624-14632. DOI: 10.1021/jacs.9b04999 From NLM PubMed-not-MEDLINE.

(114) Jones, M. R.; Mirkin, C. A. Bypassing the limitations of classical chemical purification with DNA-programmable nanoparticle recrystallization. *Angewandte Chemie* **2013**, *52* (10), 2886-2891. DOI: 10.1002/anie.201209504 From NLM Medline.

(115) Mammen, M.; Choi, S. K.; Whitesides, G. M. Polyvalent Interactions in Biological Systems: Implications for Design and Use of Multivalent Ligands and Inhibitors. *Angewandte Chemie* **1998**, *37* (20), 2754-2794. DOI: 10.1002/(SICI)1521-3773(19981102)37:20<2754::AID-ANIE2754>3.0.CO;2-3 From NLM PubMed-not-MEDLINE.

(116) Koshland, D. E., Jr.; Hamadani, K. Proteomics and models for enzyme cooperativity. *J Biol Chem* **2002**, *277* (49), 46841-46844. DOI: 10.1074/jbc.R200014200 From NLM Medline.

(117) Cattoni, D. I.; Chara, O.; Kaufman, S. B.; Gonzalez Flecha, F. L. Cooperativity in Binding Processes: New Insights from Phenomenological Modeling. *Plos One* **2015**, *10* (12), e0146043. DOI: 10.1371/journal.pone.0146043 From NLM Medline.

(118) Anderson, P. W. More is different. *Science* **1972**, *177* (4047), 393-396. DOI: 10.1126/science.177.4047.393 From NLM PubMed-not-MEDLINE.

(119) Whitesides, G. M.; Ismagilov, R. F. Complexity in chemistry. *Science* **1999**, *284* (5411), 89-92. DOI: 10.1126/science.284.5411.89 From NLM Medline.

(120) Mattia, E.; Otto, S. Supramolecular systems chemistry. *Nature nanotechnology* **2015**, *10* (2), 111-119. DOI: 10.1038/nnano.2014.337 From NLM Medline.

(121) Lopez, U.; Gautrais, J.; Couzin, I. D.; Theraulaz, G. From behavioural analyses to models of collective motion in fish schools. *Interface Focus* **2012**, *2* (6), 693-707. DOI: 10.1098/rsfs.2012.0033 From NLM PubMed-not-MEDLINE.

(122) Vicsek, T.; Czirok, A.; Ben-Jacob, E.; Cohen, I. I.; Shochet, O. Novel type of phase transition in a system of self-driven particles. *Physical review letters* **1995**, *75* (6), 1226-1229. DOI: 10.1103/PhysRevLett.75.1226 From NLM Publisher.

(123) Phillips, R.; Quake, S. R. The Biological Frontier of Physics. *Phys Today* **2006**, *59* (5), 38-43. DOI: 10.1063/1.2216960.

(124) Grzybowski, B. A.; Huck, W. T. The nanotechnology of life-inspired systems. *Nature nanotechnology* **2016**, *11* (7), 585-592. DOI: 10.1038/nnano.2016.116 From NLM Medline.

- (125) Ludlow, R. F.; Otto, S. Systems chemistry. *Chem Soc Rev* **2008**, 37 (1), 101-108. DOI: 10.1039/b611921m From NLM PubMed-not-MEDLINE.
- (126) Ragazzon, G.; Prins, L. J. Energy consumption in chemical fuel-driven self-assembly. *Nature nanotechnology* **2018**, 13 (10), 882-889. DOI: 10.1038/s41565-018-0250-8 From NLM PubMed-not-MEDLINE.
- (127) Boekhoven, J.; Hendriksen, W. E.; Koper, G. J.; Eelkema, R.; van Esch, J. H. Transient assembly of active materials fueled by a chemical reaction. *Science* **2015**, 349 (6252), 1075-1079. DOI: 10.1126/science.aac6103 From NLM PubMed-not-MEDLINE.
- (128) Boekhoven, J.; Brizard, A. M.; Kowlgi, K. N.; Koper, G. J.; Eelkema, R.; van Esch, J. H. Dissipative self-assembly of a molecular gelator by using a chemical fuel. *Angewandte Chemie* **2010**, 49 (28), 4825-4828. DOI: 10.1002/anie.201001511 From NLM PubMed-not-MEDLINE.
- (129) Leira-Iglesias, J.; Sorrenti, A.; Sato, A.; Dunne, P. A.; Hermans, T. M. Supramolecular pathway selection of perylenediimides mediated by chemical fuels. *Chem Commun (Camb)* **2016**, 52 (58), 9009-9012. DOI: 10.1039/c6cc01192f From NLM PubMed-not-MEDLINE.
- (130) Rakotondradany, F.; Whitehead, M. A.; Lehuis, A. M.; Sleiman, H. F. Photoresponsive supramolecular systems: self-assembly of azodibenzoic acid linear tapes and cyclic tetramers. *Chemistry* **2003**, 9 (19), 4771-4780. DOI: 10.1002/chem.200304864 From NLM PubMed-not-MEDLINE.
- (131) Wang, G.; Tang, B.; Liu, Y.; Gao, Q.; Wang, Z.; Zhang, X. The fabrication of a supra-amphiphile for dissipative self-assembly. *Chem Sci* **2016**, 7 (2), 1151-1155. DOI: 10.1039/c5sc03907j From NLM PubMed-not-MEDLINE.
- (132) Zhang, J.; Luijten, E.; Grzybowski, B. A.; Granick, S. Active colloids with collective mobility status and research opportunities. *Chem Soc Rev* **2017**, 46 (18), 5551-5569. DOI: 10.1039/c7cs00461c From NLM PubMed-not-MEDLINE.
- (133) Wang, W.; Duan, W.; Ahmed, S.; Sen, A.; Mallouk, T. E. From one to many: dynamic assembly and collective behavior of self-propelled colloidal motors. *Acc Chem Res* **2015**, 48 (7), 1938-1946. DOI: 10.1021/acs.accounts.5b00025 From NLM PubMed-not-MEDLINE.
- (134) Yan, J.; Han, M.; Zhang, J.; Xu, C.; Luijten, E.; Granick, S. Reconfiguring active particles by electrostatic imbalance. *Nature materials* **2016**, 15 (10), 1095-1099. DOI: 10.1038/nmat4696 From NLM PubMed-not-MEDLINE.
- (135) Ibele, M.; Mallouk, T. E.; Sen, A. Schooling behavior of light-powered autonomous micromotors in water. *Angewandte Chemie* **2009**, 48 (18), 3308-3312. DOI: 10.1002/anie.200804704 From NLM Medline.
- (136) Zhang, J.; Yan, J.; Granick, S. Directed Self-Assembly Pathways of Active Colloidal Clusters. *Angewandte Chemie* **2016**, 55 (17), 5166-5169. DOI: 10.1002/anie.201509978 From NLM PubMed-not-MEDLINE.
- (137) Jiang, H.; Ding, H.; Pu, M.; Hou, Z. Emergence of collective dynamical chirality for achiral active particles. *Soft matter* **2017**, 13 (4), 836-841. DOI: 10.1039/c6sm02335e From NLM PubMed-not-MEDLINE.

- (138) Zhang, J.; Granick, S. Natural selection in the colloid world: active chiral spirals. *Faraday Discuss* **2016**, *191*, 35-46. DOI: 10.1039/c6fd00077k From NLM PubMed-not-MEDLINE.
- (139) Palacci, J.; Sacanna, S.; Steinberg, A. P.; Pine, D. J.; Chaikin, P. M. Living crystals of light-activated colloidal surfers. *Science* **2013**, *339* (6122), 936-940. DOI: 10.1126/science.1230020 From NLM PubMed-not-MEDLINE.
- (140) Yan, J.; Bloom, M.; Bae, S. C.; Luijten, E.; Granick, S. Linking synchronization to self-assembly using magnetic Janus colloids. *Nature* **2012**, *491* (7425), 578-581. DOI: 10.1038/nature11619 From NLM PubMed-not-MEDLINE.
- (141) Tagliazucchi, M.; Weiss, E. A.; Szleifer, I. Dissipative self-assembly of particles interacting through time-oscillatory potentials. *Proc Natl Acad Sci U S A* **2014**, *111* (27), 9751-9756. DOI: 10.1073/pnas.1406122111 From NLM Medline.
- (142) Sanchez, T.; Chen, D. T.; DeCamp, S. J.; Heymann, M.; Dogic, Z. Spontaneous motion in hierarchically assembled active matter. *Nature* **2012**, *491* (7424), 431-434. DOI: 10.1038/nature11591 From NLM PubMed-not-MEDLINE.
- (143) Keber, F. C.; Loiseau, E.; Sanchez, T.; DeCamp, S. J.; Giomi, L.; Bowick, M. J.; Marchetti, M. C.; Dogic, Z.; Bausch, A. R. Topology and dynamics of active nematic vesicles. *Science* **2014**, *345* (6201), 1135-1139. DOI: 10.1126/science.1254784 From NLM PubMed-not-MEDLINE.
- (144) DeCamp, S. J.; Redner, G. S.; Baskaran, A.; Hagan, M. F.; Dogic, Z. Orientational order of motile defects in active nematics. *Nature materials* **2015**, *14* (11), 1110-1115. DOI: 10.1038/nmat4387 From NLM PubMed-not-MEDLINE.
- (145) Paxton, W. F.; Kistler, K. C.; Olmeda, C. C.; Sen, A.; St Angelo, S. K.; Cao, Y.; Mallouk, T. E.; Lammert, P. E.; Crespi, V. H. Catalytic nanomotors: autonomous movement of striped nanorods. *Journal of the American Chemical Society* **2004**, *126* (41), 13424-13431. DOI: 10.1021/ja047697z From NLM PubMed-not-MEDLINE.
- (146) Kline, T. R.; Paxton, W. F.; Mallouk, T. E.; Sen, A. Catalytic nanomotors: remote-controlled autonomous movement of striped metallic nanorods. *Angewandte Chemie* **2005**, *44* (5), 744-746. DOI: 10.1002/anie.200461890 From NLM PubMed-not-MEDLINE.
- (147) Paxton, W. F.; Baker, P. T.; Kline, T. R.; Wang, Y.; Mallouk, T. E.; Sen, A. Catalytically induced electrokinetics for motors and micropumps. *Journal of the American Chemical Society* **2006**, *128* (46), 14881-14888. DOI: 10.1021/ja0643164 From NLM Medline.
- (148) Wang, W.; Castro, L. A.; Hoyos, M.; Mallouk, T. E. Autonomous motion of metallic microrods propelled by ultrasound. *ACS nano* **2012**, *6* (7), 6122-6132. DOI: 10.1021/nn301312z From NLM Medline.
- (149) Sundararajan, S.; Lammert, P. E.; Zudans, A. W.; Crespi, V. H.; Sen, A. Catalytic motors for transport of colloidal cargo. *Nano letters* **2008**, *8* (5), 1271-1276. DOI: 10.1021/nl072275j From NLM Medline.
- (150) Boles, M. A.; Ling, D.; Hyeon, T.; Talapin, D. V. Erratum: The surface science of nanocrystals. *Nature materials* **2016**, *15* (3), 364. DOI: 10.1038/nmat4578 From NLM PubMed-not-MEDLINE.

- (151) Alivisatos, A. P. Semiconductor clusters, nanocrystals, and quantum dots. *Science* **1996**, 271 (5251), 933-937.
- (152) Bell, A. T. The impact of nanoscience on heterogeneous catalysis. *Science* **2003**, 299 (5613), 1688-1691. DOI: 10.1126/science.1083671 From NLM PubMed-not-MEDLINE.
- (153) Sun, J.; Ma, D.; Zhang, H.; Liu, X.; Han, X.; Bao, X.; Weinberg, G.; Pfander, N.; Su, D. Toward monodispersed silver nanoparticles with unusual thermal stability. *Journal of the American Chemical Society* **2006**, 128 (49), 15756-15764. DOI: 10.1021/ja064884j From NLM PubMed-not-MEDLINE.
- (154) Ding, T.; Valev, V. K.; Salmon, A. R.; Forman, C. J.; Smoukov, S. K.; Scherman, O. A.; Frenkel, D.; Baumberg, J. J. Light-induced actuating nanotransducers. *Proc Natl Acad Sci U S A* **2016**, 113 (20), 5503-5507. DOI: 10.1073/pnas.1524209113 From NLM PubMed-not-MEDLINE.
- (155) Li, R.; Bian, K.; Hanrath, T.; Bassett, W. A.; Wang, Z. Decoding the superlattice and interface structure of truncate PbS nanocrystal-assembled supercrystal and associated interaction forces. *Journal of the American Chemical Society* **2014**, 136 (34), 12047-12055. DOI: 10.1021/ja5057032 From NLM PubMed-not-MEDLINE.
- (156) Li, T.; Senesi, A. J.; Lee, B. Small Angle X-ray Scattering for Nanoparticle Research. *Chem Rev* **2016**, 116 (18), 11128-11180. DOI: 10.1021/acs.chemrev.5b00690 From NLM PubMed-not-MEDLINE.
- (157) Jain, P. K.; Huang, X.; El-Sayed, I. H.; El-Sayed, M. A. Noble metals on the nanoscale: optical and photothermal properties and some applications in imaging, sensing, biology, and medicine. *Accounts Chem Res* **2008**, 41 (12), 1578-1586.
- (158) Stolarczyk, J. K.; Deak, A.; Brougham, D. F. Nanoparticle clusters: assembly and control over internal order, current capabilities, and future potential. *Advanced materials* **2016**, 28 (27), 5400-5424.
- (159) Vicidomini, G.; Bianchini, P.; Diaspro, A. STED super-resolved microscopy. *Nat Methods* **2018**, 15 (3), 173-182. DOI: 10.1038/nmeth.4593 From NLM Medline.
- (160) Sikora, A.; Bednarz, L. Dynamic speed control in atomic force microscopy to improve imaging time and quality. *Measurement Science and Technology* **2014**, 25 (4), 044005.
- (161) Guo, Y.; Li, D.; Zhang, S.; Yang, Y.; Liu, J. J.; Wang, X.; Liu, C.; Milkie, D. E.; Moore, R. P.; Tulu, U. S.; et al. Visualizing Intracellular Organelle and Cytoskeletal Interactions at Nanoscale Resolution on Millisecond Timescales. *Cell* **2018**, 175 (5), 1430-1442 e1417. DOI: 10.1016/j.cell.2018.09.057 From NLM Medline.
- (162) Fritzsche, M.; Li, D.; Colin-York, H.; Chang, V. T.; Moeendarbary, E.; Felce, J. H.; Sezgin, E.; Charras, G.; Betzig, E.; Eggeling, C. Self-organizing actin patterns shape membrane architecture but not cell mechanics. *Nat Commun* **2017**, 8, 14347. DOI: 10.1038/ncomms14347 From NLM Medline.
- (163) Fritzsche, M.; Fernandes, R. A.; Chang, V. T.; Colin-York, H.; Clausen, M. P.; Felce, J. H.; Galiani, S.; Erlenkamper, C.; Santos, A. M.; Heddlestone, J. M.; et al. Cytoskeletal actin dynamics shape a ramifying actin network underpinning

immunological synapse formation. *Sci Adv* **2017**, 3 (6), e1603032. DOI:

10.1126/sciadv.1603032 From NLM Medline.

(164) Beach, J. R.; Bruun, K. S.; Shao, L.; Li, D.; Swider, Z.; Remmert, K.; Zhang, Y.; Conti, M. A.; Adelstein, R. S.; Rusan, N. M.; et al. Actin dynamics and competition for myosin monomer govern the sequential amplification of myosin filaments. *Nat Cell Biol* **2017**, 19 (2), 85-93. DOI: 10.1038/ncb3463 From NLM Medline.

(165) Saurabh, S.; Perez, A. M.; Commerci, C. J.; Shapiro, L.; Moerner, W. E. Super-resolution Imaging of Live Bacteria Cells Using a Genetically Directed, Highly Photostable Fluoromodule. *Journal of the American Chemical Society* **2016**, 138 (33), 10398-10401. DOI: 10.1021/jacs.6b05943 From NLM Medline.

(166) Nixon-Abell, J.; Obara, C. J.; Weigel, A. V.; Li, D.; Legant, W. R.; Xu, C. S.; Pasolli, H. A.; Harvey, K.; Hess, H. F.; Betzig, E.; et al. Increased spatiotemporal resolution reveals highly dynamic dense tubular matrices in the peripheral ER. *Science* **2016**, 354 (6311), aaf3928. DOI: 10.1126/science.aaf3928 From NLM Medline.

(167) Li, L.; Liu, H.; Dong, P.; Li, D.; Legant, W. R.; Grimm, J. B.; Lavis, L. D.; Betzig, E.; Tjian, R.; Liu, Z. Real-time imaging of Huntingtin aggregates diverting target search and gene transcription. *Elife* **2016**, 5, e17056. DOI: 10.7554/eLife.17056 From NLM Medline.

(168) Andrade, D. M.; Clausen, M. P.; Keller, J.; Mueller, V.; Wu, C.; Bear, J. E.; Hell, S. W.; Lagerholm, B. C.; Eggeling, C. Cortical actin networks induce spatio-temporal confinement of phospholipids in the plasma membrane--a minimally invasive investigation by STED-FCS. *Sci Rep* **2015**, 5, 11454. DOI: 10.1038/srep11454 From NLM Medline.

(169) Chen, B. C.; Legant, W. R.; Wang, K.; Shao, L.; Milkie, D. E.; Davidson, M. W.; Janetopoulos, C.; Wu, X. S.; Hammer, J. A., 3rd; Liu, Z.; et al. Lattice light-sheet microscopy: imaging molecules to embryos at high spatiotemporal resolution. *Science* **2014**, 346 (6208), 1257998. DOI: 10.1126/science.1257998 From NLM Medline.

(170) Casolari, J. M.; Thompson, M. A.; Salzman, J.; Champion, L. M.; Moerner, W. E.; Brown, P. O. Widespread mRNA association with cytoskeletal motor proteins and identification and dynamics of myosin-associated mRNAs in *S. cerevisiae*. *Plos One* **2012**, 7 (2), e31912. DOI: 10.1371/journal.pone.0031912 From NLM Medline.

(171) Urban, N. T.; Willig, K. I.; Hell, S. W.; Nagerl, U. V. STED nanoscopy of actin dynamics in synapses deep inside living brain slices. *Biophys J* **2011**, 101 (5), 1277-1284. DOI: 10.1016/j.bpj.2011.07.027 From NLM Medline.

(172) Ptacin, J. L.; Lee, S. F.; Garner, E. C.; Toro, E.; Eckart, M.; Comolli, L. R.; Moerner, W. E.; Shapiro, L. A spindle-like apparatus guides bacterial chromosome segregation. *Nat Cell Biol* **2010**, 12 (8), 791-798. DOI: 10.1038/ncb2083 From NLM Medline.

(173) Lauterbach, M. A.; Ullal, C. K.; Westphal, V.; Hell, S. W. Dynamic imaging of colloidal-crystal nanostructures at 200 frames per second. *Langmuir* **2010**, 26 (18), 14400-14404. DOI: 10.1021/la102474p From NLM Medline.

(174) Frost, N. A.; Shroff, H.; Kong, H.; Betzig, E.; Blanpied, T. A. Single-molecule discrimination of discrete perisynaptic and distributed sites of actin filament



- assembly within dendritic spines. *Neuron* **2010**, 67 (1), 86-99. DOI: 10.1016/j.neuron.2010.05.026 From NLM Medline.
- (175) Eggeling, C.; Ringemann, C.; Medda, R.; Schwarzmann, G.; Sandhoff, K.; Polyakova, S.; Belov, V. N.; Hein, B.; von Middendorff, C.; Schonle, A.; et al. Direct observation of the nanoscale dynamics of membrane lipids in a living cell. *Nature* **2009**, 457 (7233), 1159-1162. DOI: 10.1038/nature07596 From NLM Medline.
- (176) Ye, X.; Jones, M. R.; Frechette, L. B.; Chen, Q.; Powers, A. S.; Ercius, P.; Dunn, G.; Rotskoff, G. M.; Nguyen, S. C.; Adiga, V. P. Single-particle mapping of nonequilibrium nanocrystal transformations. *Science* **2016**, 354 (6314), 874-877.
- (177) Shin, D.; Park, J. B.; Kim, Y. J.; Kim, S. J.; Kang, J. H.; Lee, B.; Cho, S. P.; Hong, B. H.; Novoselov, K. S. Growth dynamics and gas transport mechanism of nanobubbles in graphene liquid cells. *Nat Commun* **2015**, 6, 6068. DOI: 10.1038/ncomms7068 From NLM PubMed-not-MEDLINE.
- (178) Park, J.; Elmlund, H.; Ercius, P.; Yuk, J. M.; Limmer, D. T.; Chen, Q.; Kim, K.; Han, S. H.; Weitz, D. A.; Zettl, A.; et al. Nanoparticle imaging. 3D structure of individual nanocrystals in solution by electron microscopy. *Science* **2015**, 349 (6245), 290-295. DOI: 10.1126/science.aab1343 From NLM PubMed-not-MEDLINE.
- (179) Jeong, M.; Yuk, J. M.; Lee, J. Y. Observation of Surface Atoms during Platinum Nanocrystal Growth by Monomer Attachment. *Chem Mater* **2015**, 27 (9), 3200-3202. DOI: 10.1021/acs.chemmater.5b00334.
- (180) Yuk, J. M.; Park, J.; Ercius, P.; Kim, K.; Hellebusch, D. J.; Crommie, M. F.; Lee, J. Y.; Zettl, A.; Alivisatos, A. P. High-resolution EM of colloidal nanocrystal growth using graphene liquid cells. *Science* **2012**, 336 (6077), 61-64. DOI: 10.1126/science.1217654 From NLM PubMed-not-MEDLINE.
- (181) Shekhirev, M.; Sutter, E.; Sutter, P. In Situ Atomic Force Microscopy of the Reconfiguration of On-Surface Self-Assembled DNA-Nanoparticle Superlattices. *Advanced Functional Materials* **2019**, 1806924.
- (182) Hosono, N.; Terashima, A.; Kusaka, S.; Matsuda, R.; Kitagawa, S. Highly responsive nature of porous coordination polymer surfaces imaged by in situ atomic force microscopy. *Nature chemistry* **2019**, 11 (2), 109-116. DOI: 10.1038/s41557-018-0170-0 From NLM PubMed-not-MEDLINE.
- (183) Cho, K. R.; Kulshreshtha, P.; Wu, K. J. J.; Seto, J.; Qiu, S. R.; De Yoreo, J. J. The effects of different types of additives on growth of biomineral phases investigated by in situ atomic force microscopy. *Journal of Crystal Growth* **2019**, 509, 8-16.
- (184) Ravula, T.; Ishikuro, D.; Kodera, N.; Ando, T.; Anantharamaiah, G. M.; Ramamoorthy, A. Real-Time Monitoring of Lipid Exchange via Fusion of Peptide Based Lipid-Nanodiscs. *Chem Mater* **2018**, 30 (10), 3204-3207. DOI: 10.1021/acs.chemmater.8b00946.
- (185) Kumar, M.; Choudhary, M. K.; Rimer, J. D. Transient modes of zeolite surface growth from 3D gel-like islands to 2D single layers. *Nat Commun* **2018**, 9 (1), 2129. DOI: 10.1038/s41467-018-04296-4 From NLM PubMed-not-MEDLINE.

- (186) Tian, Y.; Li, J.; Cai, M.; Zhao, W.; Xu, H.; Liu, Y.; Wang, H. High resolution imaging of mitochondrial membranes by in situ atomic force microscopy. *RSC Adv.* **2013**, *3* (3), 708-712. DOI: 10.1039/c2ra22166g.
- (187) Filipe, V.; Hawe, A.; Jiskoot, W. Critical evaluation of Nanoparticle Tracking Analysis (NTA) by NanoSight for the measurement of nanoparticles and protein aggregates. *Pharm Res* **2010**, *27* (5), 796-810. DOI: 10.1007/s11095-010-0073-2 From NLM Medline.
- (188) Jalili, N.; Laxminarayana, K. A review of atomic force microscopy imaging systems: application to molecular metrology and biological sciences. *Mechatronics* **2004**, *14* (8), 907-945. DOI: 10.1016/j.mechatronics.2004.04.005.
- (189) Ando, T. High-speed atomic force microscopy and its future prospects. *Biophys Rev* **2018**, *10* (2), 285-292. DOI: 10.1007/s12551-017-0356-5 From NLM PubMed-not-MEDLINE.
- (190) Uchihashi, T.; Iino, R.; Ando, T.; Noji, H. High-speed atomic force microscopy reveals rotary catalysis of rotorless F(1)-ATPase. *Science* **2011**, *333* (6043), 755-758. DOI: 10.1126/science.1205510 From NLM Medline.
- (191) Shakesheff, K. M.; Davies, M. C.; Roberts, C. J.; Tendler, S. J. B.; Shard, A. G.; Domb, A. In situ Atomic Force Microscopy Imaging of Polymer Degradation in an Aqueous Environment. *Langmuir* **2002**, *10* (12), 4417-4419. DOI: 10.1021/la00024a005.
- (192) Santos, N. C.; Castanho, M. A. An overview of the biophysical applications of atomic force microscopy. *Biophysical chemistry* **2004**, *107* (2), 133-149.
- (193) Yang, Y.; Goetzfried, M. A.; Hidaka, K.; You, M.; Tan, W.; Sugiyama, H.; Endo, M. Direct Visualization of Walking Motions of Photocontrolled Nanomachine on the DNA Nanostructure. *Nano letters* **2015**, *15* (10), 6672-6676. DOI: 10.1021/acs.nanolett.5b02502 From NLM Medline.
- (194) Miyagi, A.; Chipot, C.; Rangl, M.; Scheuring, S. High-speed atomic force microscopy shows that annexin V stabilizes membranes on the second timescale. *Nature nanotechnology* **2016**, *11* (9), 783.
- (195) Lupulescu, A. I.; Rimer, J. D. In situ imaging of silicalite-1 surface growth reveals the mechanism of crystallization. *Science* **2014**, *344* (6185), 729-732. DOI: 10.1126/science.1250984 From NLM Medline.
- (196) Yamashita, H.; Taoka, A.; Uchihashi, T.; Asano, T.; Ando, T.; Fukumori, Y. Single-molecule imaging on living bacterial cell surface by high-speed AFM. *J Mol Biol* **2012**, *422* (2), 300-309. DOI: 10.1016/j.jmb.2012.05.018 From NLM Medline.
- (197) Brown, R. Absorption and scattering of light by small particles. **1984**.
- (198) Gillespie, C.; Halling, P.; Edwards, D. Monitoring of particle growth at a low concentration of a poorly water soluble drug using the NanoSight LM20. *Colloids and Surfaces A: Physicochemical and Engineering Aspects* **2011**, *384* (1-3), 233-239. DOI: 10.1016/j.colsurfa.2011.03.052.
- (199) Arancon, R. A. D.; Lin, S. H. T.; Chen, G.; Lin, C. S. K.; Lai, J.; Xu, G.; Luque, R. Nanoparticle tracking analysis of gold nanomaterials stabilized by various capping agents. *RSC Advances* **2014**, *4* (33), 17114-17119. DOI: 10.1039/c4ra00208c.

- (200) Chaudhari, K.; Pradeep, T. Spatiotemporal mapping of three dimensional rotational dynamics of single ultrasmall gold nanorods. *Sci Rep* **2014**, *4*, 5948. DOI: 10.1038/srep05948 From NLM PubMed-not-MEDLINE.
- (201) Andres-Arroyo, A.; Reece, P. J. Using light scattering to resolve Brownian rotation dynamics of optically trapped Au nanorods. *Journal of Applied Physics* **2018**, *123* (5), 054302.
- (202) Steimel, J. P.; Aragonés, J. L.; Hu, H.; Qureshi, N.; Alexander-Katz, A. Emergent ultra-long-range interactions between active particles in hybrid active-inactive systems. *Proceedings of the National Academy of Sciences* **2016**, *113* (17), 4652-4657.
- (203) Nikonova, O. A.; Nedelec, J. M.; Kessler, V. G.; Seisenbaeva, G. A. Precursor-directed assembly of complex oxide nanobeads: the role of strongly coordinated inorganic anions. *Langmuir* **2011**, *27* (18), 11622-11628. DOI: 10.1021/la2028719 From NLM Medline.
- (204) Otsuka, I.; Osaka, M.; Sakai, Y.; Travelet, C.; Putaux, J.-L.; Borsali, R. Self-assembly of maltoheptaose-block-polystyrene into micellar nanoparticles and encapsulation of gold nanoparticles. *Langmuir* **2013**, *29* (49), 15224-15230.
- (205) Shen, H.; Tauzin, L. J.; Baiyasi, R.; Wang, W.; Moringo, N.; Shuang, B.; Landes, C. F. Single Particle Tracking: From Theory to Biophysical Applications. *Chem Rev* **2017**, *117* (11), 7331-7376. DOI: 10.1021/acs.chemrev.6b00815 From NLM Medline.
- (206) Sahl, S. J.; Leutenegger, M.; Hilbert, M.; Hell, S. W.; Eggeling, C. Fast molecular tracking maps nanoscale dynamics of plasma membrane lipids. *Proc Natl Acad Sci U S A* **2010**, *107* (15), 6829-6834. DOI: 10.1073/pnas.0912894107 From NLM Medline.
- (207) Harke, B.; Ullal, C. K.; Keller, J.; Hell, S. W. Three-dimensional nanoscopy of colloidal crystals. *Nano letters* **2008**, *8* (5), 1309-1313. DOI: 10.1021/nl073164n From NLM Medline.
- (208) Sun, S.; Murray, C. B.; Weller, D.; Folks, L.; Moser, A. Monodisperse FePt nanoparticles and ferromagnetic FePt nanocrystal superlattices. *Science* **2000**, *287* (5460), 1989-1992. DOI: 10.1126/science.287.5460.1989 From NLM PubMed-not-MEDLINE.
- (209) Zhang, J.; Santos, P. J.; Gabrys, P. A.; Lee, S.; Liu, C.; Macfarlane, R. J. Self-Assembling Nanocomposite Tectons. *Journal of the American Chemical Society* **2016**, *138* (50), 16228-16231. DOI: 10.1021/jacs.6b11052 From NLM PubMed-not-MEDLINE.
- (210) Smith, A. M.; Nie, S. Semiconductor nanocrystals: structure, properties, and band gap engineering. *Accounts Chem Res* **2009**, *43* (2), 190-200.
- (211) Peng, X.; Manna, L.; Yang, W.; Wickham, J.; Scher, E.; Kadavanich, A.; Alivisatos, A. P. Shape control of CdSe nanocrystals. *Nature* **2000**, *404* (6773), 59-61. DOI: 10.1038/35003535 From NLM Publisher.
- (212) Ithurria, S.; Tessier, M. D.; Mahler, B.; Lobo, R. P.; Dubertret, B.; Efros, A. L. Colloidal nanoplatelets with two-dimensional electronic structure. *Nature materials*

**2011**, *10* (12), 936-941. DOI: 10.1038/nmat3145 From NLM PubMed-not-MEDLINE.

(213) Dulkeith, E.; Ringler, M.; Klar, T. A.; Feldmann, J.; Munoz Javier, A.; Parak, W. J. Gold nanoparticles quench fluorescence by phase induced radiative rate suppression. *Nano letters* **2005**, *5* (4), 585-589. DOI: 10.1021/nl0480969 From NLM Medline.

(214) Singh, M. P.; Strouse, G. F. Involvement of the LSPR spectral overlap for energy transfer between a dye and Au nanoparticle. *Journal of the American Chemical Society* **2010**, *132* (27), 9383-9391. DOI: 10.1021/ja1022128 From NLM Medline.

(215) Waldchen, S.; Lehmann, J.; Klein, T.; van de Linde, S.; Sauer, M. Light-induced cell damage in live-cell super-resolution microscopy. *Sci Rep* **2015**, *5*, 15348. DOI: 10.1038/srep15348 From NLM Medline.

(216) Guo, Y.; Li, D.; Zhang, S.; Yang, Y.; Liu, J.-J.; Wang, X.; Liu, C.; Milkie, D. E.; Moore, R. P.; Tulu, U. S.; et al. Visualizing Intracellular Organelle and Cytoskeletal Interactions at Nanoscale Resolution on Millisecond Timescales. *Cell* **2018**, *175* (5), 1430-1442.e1417. DOI: 10.1016/j.cell.2018.09.057.

(217) Williams, D. B.; Carter, C. B. The transmission electron microscope. In *Transmission electron microscopy*, Springer, 1996; pp 3-17.

(218) Urban, K. W. Studying atomic structures by aberration-corrected transmission electron microscopy. *Science* **2008**, *321* (5888), 506-510. DOI: 10.1126/science.1152800 From NLM PubMed-not-MEDLINE.

(219) Ross, F. M. Opportunities and challenges in liquid cell electron microscopy. *Science* **2015**, *350* (6267), aaa9886. DOI: 10.1126/science.aaa9886 From NLM PubMed-not-MEDLINE.

(220) de Jonge, N.; Ross, F. M. Electron microscopy of specimens in liquid. *Nature nanotechnology* **2011**, *6* (11), 695-704. DOI: 10.1038/nnano.2011.161 From NLM Medline.

(221) Kim, J.; Ou, Z.; Jones, M. R.; Song, X.; Chen, Q. Imaging the polymerization of multivalent nanoparticles in solution. *Nat Commun* **2017**, *8* (1), 761. DOI: 10.1038/s41467-017-00857-1 From NLM PubMed-not-MEDLINE.

(222) Luo, B.; Smith, J. W.; Wu, Z.; Kim, J.; Ou, Z.; Chen, Q. Polymerization-Like Co-Assembly of Silver Nanoplates and Patchy Spheres. *ACS nano* **2017**, *11* (8), 7626-7633. DOI: 10.1021/acsnano.7b02059 From NLM PubMed-not-MEDLINE.

(223) Jin, B.; Sushko, M. L.; Liu, Z.; Jin, C.; Tang, R. In Situ Liquid Cell TEM Reveals Bridge-Induced Contact and Fusion of Au Nanocrystals in Aqueous Solution. *Nano letters* **2018**, *18* (10), 6551-6556. DOI: 10.1021/acs.nanolett.8b03139 From NLM PubMed-not-MEDLINE.

(224) Smeets, P. J.; Cho, K. R.; Kempen, R. G.; Sommerdijk, N. A.; De Yoreo, J. J. Calcium carbonate nucleation driven by ion binding in a biomimetic matrix revealed by in situ electron microscopy. *Nature materials* **2015**, *14* (4), 394-399. DOI: 10.1038/nmat4193 From NLM Medline.

(225) Nielsen, M. H.; Aloni, S.; De Yoreo, J. J. In situ TEM imaging of CaCO<sub>3</sub> nucleation reveals coexistence of direct and indirect pathways. *Science* **2014**, *345*

- (6201), 1158-1162. DOI: 10.1126/science.1254051 From NLM PubMed-not-MEDLINE.
- (226) Zheng, H.; Smith, R. K.; Jun, Y. W.; Kisielowski, C.; Dahmen, U.; Alivisatos, A. P. Observation of single colloidal platinum nanocrystal growth trajectories. *Science* **2009**, *324* (5932), 1309-1312. DOI: 10.1126/science.1172104 From NLM PubMed-not-MEDLINE.
- (227) Chen, Q.; Cho, H.; Manthiram, K.; Yoshida, M.; Ye, X.; Alivisatos, A. P. Interaction Potentials of Anisotropic Nanocrystals from the Trajectory Sampling of Particle Motion using in Situ Liquid Phase Transmission Electron Microscopy. *ACS Cent Sci* **2015**, *1* (1), 33-39. DOI: 10.1021/acscentsci.5b00001 From NLM PubMed-not-MEDLINE.
- (228) Tan, S. F.; Chee, S. W.; Lin, G.; Mirsaidov, U. Direct observation of interactions between nanoparticles and nanoparticle self-assembly in solution. *Accounts Chem Res* **2017**, *50* (6), 1303-1312.
- (229) Tan, S. F.; Anand, U.; Mirsaidov, U. Interactions and attachment pathways between functionalized gold nanorods. *ACS nano* **2017**, *11* (2), 1633-1640.
- (230) Nagamanasa, K. H.; Wang, H.; Granick, S. Liquid-Cell Electron Microscopy of Adsorbed Polymers. *Adv Mater* **2017**, *29* (41), 1703555. DOI: 10.1002/adma.201703555 From NLM PubMed-not-MEDLINE.
- (231) Parent, L. R.; Bakalis, E.; Ramirez-Hernandez, A.; Kammeyer, J. K.; Park, C.; de Pablo, J.; Zerbetto, F.; Patterson, J. P.; Gianneschi, N. C. Directly Observing Micelle Fusion and Growth in Solution by Liquid-Cell Transmission Electron Microscopy. *Journal of the American Chemical Society* **2017**, *139* (47), 17140-17151. DOI: 10.1021/jacs.7b09060 From NLM Medline.
- (232) Lyumkis, D. Challenges and opportunities in cryo-EM single-particle analysis. *J Biol Chem* **2019**, *294* (13), 5181-5197. DOI: 10.1074/jbc.REV118.005602 From NLM Medline.
- (233) Panciera, F.; Chou, Y. C.; Reuter, M. C.; Zakharov, D.; Stach, E. A.; Hofmann, S.; Ross, F. M. Synthesis of nanostructures in nanowires using sequential catalyst reactions. *Nature materials* **2015**, *14* (8), 820-825. DOI: 10.1038/nmat4352 From NLM PubMed-not-MEDLINE.
- (234) Klein, K. L.; Anderson, I. M.; de Jonge, N. Transmission electron microscopy with a liquid flow cell. *J Microsc* **2011**, *242* (2), 117-123. DOI: 10.1111/j.1365-2818.2010.03484.x From NLM Medline.
- (235) Le Caër, S. Water radiolysis: influence of oxide surfaces on H<sub>2</sub> production under ionizing radiation. *Water* **2011**, *3* (1), 235-253.
- (236) Schneider, N. M.; Norton, M. M.; Mendel, B. J.; Grogan, J. M.; Ross, F. M.; Bau, H. H. Electron-Water Interactions and Implications for Liquid Cell Electron Microscopy. *The Journal of Physical Chemistry C* **2014**, *118* (38), 22373-22382. DOI: 10.1021/jp507400n.
- (237) Woehl, T. J.; Jungjohann, K. L.; Evans, J. E.; Arslan, I.; Ristenpart, W. D.; Browning, N. D. Experimental procedures to mitigate electron beam induced

- artifacts during in situ fluid imaging of nanomaterials. *Ultramicroscopy* **2013**, 127, 53-63. DOI: 10.1016/j.ultramic.2012.07.018 From NLM Medline.
- (238) Kim, J.; Jones, M. R.; Ou, Z.; Chen, Q. In Situ Electron Microscopy Imaging and Quantitative Structural Modulation of Nanoparticle Superlattices. *ACS nano* **2016**, 10 (11), 9801-9808. DOI: 10.1021/acsnano.6b05270 From NLM PubMed-not-MEDLINE.
- (239) Rehn, S. M.; Jones, M. R. New Strategies for Probing Energy Systems with In Situ Liquid-Phase Transmission Electron Microscopy. *Acs Energy Lett* **2018**, 3 (6), 1269-1278. DOI: 10.1021/acsenergylett.8b00527.
- (240) Zheng, H.; Meng, Y. S.; Zhu, Y. Frontiers of in situ electron microscopy. *MRS Bulletin* **2015**, 40 (1), 12-18. DOI: 10.1557/mrs.2014.305.
- (241) Alberdi, A.; Gómez Fernández, J.; Collaboration, E. H. T. First M87 Event Horizon Telescope Results. III. Data Processing and Calibration. **2019**.
- (242) Crocker, J. C.; Grier, D. G. Methods of digital video microscopy for colloidal studies. *Journal of colloid and interface science* **1996**, 179 (1), 298-310.
- (243) Mino, G.; Mallouk, T. E.; Darnige, T.; Hoyos, M.; Dauchet, J.; Dunstan, J.; Soto, R.; Wang, Y.; Rousselet, A.; Clement, E. Enhanced diffusion due to active swimmers at a solid surface. *Physical review letters* **2011**, 106 (4), 048102. DOI: 10.1103/PhysRevLett.106.048102 From NLM PubMed-not-MEDLINE.
- (244) Anthony, S.; Carroll-Portillo, A.; Timlin, J. Dynamics and Interactions of Individual Proteins in the Membrane of Single, Living Cells. In *Single Cell Protein Analysis*, Springer, 2015; pp 185-207.
- (245) Chee, S. W.; Anand, U.; Bisht, G.; Tan, S. F.; Mirsaidov, U. Direct Observations of the Rotation and Translation of Anisotropic Nanoparticles Adsorbed at a Liquid-Solid Interface. *Nano letters* **2019**.
- (246) Stevens, A.; Yang, H.; Carin, L.; Arslan, I.; Browning, N. D. The potential for Bayesian compressive sensing to significantly reduce electron dose in high-resolution STEM images. *Microscopy-Jpn* **2013**, 63 (1), 41-51.
- (247) Bayles, A. V.; Squires, T. M.; Helgeson, M. E. Probe microrheology without particle tracking by differential dynamic microscopy. *Rheologica Acta* **2017**, 56 (11), 863-869.
- (248) LeCun, Y.; Bengio, Y.; Hinton, G. Deep learning. *Nature* **2015**, 521 (7553), 436-444. DOI: 10.1038/nature14539 From NLM Medline.
- (249) Schmidhuber, J. Deep learning in neural networks: an overview. *Neural Netw* **2015**, 61, 85-117. DOI: 10.1016/j.neunet.2014.09.003 From NLM Medline.
- (250) Belianinov, A.; Vasudevan, R.; Strelcov, E.; Steed, C.; Yang, S. M.; Tselev, A.; Jesse, S.; Biegalski, M.; Shipman, G.; Symons, C.; et al. Big data and deep data in scanning and electron microscopies: deriving functionality from multidimensional data sets. *Adv Struct Chem Imaging* **2015**, 1 (1), 6. DOI: 10.1186/s40679-015-0006-6 From NLM PubMed-not-MEDLINE.
- (251) Orth, A.; Schaak, D.; Schonbrun, E. Microscopy, Meet Big Data. *Cell Syst* **2017**, 4 (3), 260-261. DOI: 10.1016/j.cels.2017.03.009 From NLM Medline.

- (252) Huang, B.; Esfahani, E. N.; Li, J. Mapping intrinsic electromechanical responses at the nanoscale via sequential excitation scanning probe microscopy empowered by deep data. *National Science Review* **2018**, 6 (1), 55-63.
- (253) Madsen, J.; Liu, P.; Kling, J.; Wagner, J. B.; Hansen, T. W.; Winther, O.; Schiøtz, J. A Deep Learning Approach to Identify Local Structures in Atomic-Resolution Transmission Electron Microscopy Images. *Advanced Theory and Simulations* **2018**, 1 (8).
- (254) Ouyang, W.; Aristov, A.; Lelek, M.; Hao, X.; Zimmer, C. Deep learning massively accelerates super-resolution localization microscopy. *Nat Biotechnol* **2018**, 36 (5), 460-468. DOI: 10.1038/nbt.4106 From NLM Medline.
- (255) Huang, B.; Li, Z.; Li, J. An artificial intelligence atomic force microscope enabled by machine learning. *Nanoscale* **2018**, 10 (45), 21320-21326. DOI: 10.1039/c8nr06734a From NLM PubMed-not-MEDLINE.
- (256) Phillips, R.; Rob, P. *Crystals, defects and microstructures: modeling across scales*; Cambridge University Press, 2001.
- (257) Murtola, T.; Bunker, A.; Vattulainen, I.; Deserno, M.; Karttunen, M. Multiscale modeling of emergent materials: biological and soft matter. *Physical Chemistry Chemical Physics* **2009**, 11 (12), 1869-1892.
- (258) Vlachos, D. G. Multiscale modeling for emergent behavior, complexity, and combinatorial explosion. *AIChE Journal* **2012**, 58 (5), 1314-1325.
- (259) Hansgen, D. A.; Vlachos, D. G.; Chen, J. G. Using first principles to predict bimetallic catalysts for the ammonia decomposition reaction. *Nature chemistry* **2010**, 2 (6), 484-489. DOI: 10.1038/nchem.626 From NLM Medline.
- (260) Chatterjee, A.; Vlachos, D. G. Systems tasks in nanotechnology via hierarchical multiscale modeling: Nanopattern formation in heteroepitaxy. *Chemical Engineering Science* **2007**, 62 (18-20), 4852-4863.
- (261) Vvedensky, D. D. Multiscale modelling of nanostructures. *Journal of Physics: Condensed Matter* **2004**, 16 (50), R1537.
- (262) Elliott, J. A. Novel approaches to multiscale modelling in materials science. *International Materials Reviews* **2011**, 56 (4), 207-225.
- (263) Saliccioli, M.; Stamatakis, M.; Caratzoulas, S.; Vlachos, D. G. A review of multiscale modeling of metal-catalyzed reactions: Mechanism development for complexity and emergent behavior. *Chemical Engineering Science* **2011**, 66 (19), 4319-4355.